Hydraulic stability of a living breakwater

Wave flume experiments

MSc Thesis
Pieter Geenen

reefy
Innovation for nature
TU Delft

Hydraulic stability of a living breakwater

Wave flume experiments

by

Pieter Geenen

To obtain the degree of Master of Science
at the Delft University of Technology.
To be defended publicly on May 22th, 2024 at 16:00.

Student number:	4579933	
Project duration:	May 2023 – May 2024	
Thesis committee:	Prof. dr. ir. Marcel van Gent,	TU Delft (Chair)
	Dr. ir. Bas Hofland,	TU Delft
	Ir. Daan Houtzager,	Reefy
	Ir. Jaime Ascencio,	Reefy

This thesis is confidential and cannot be made public until May 2025.

Cover: Photo of the Reef Enhancing Breakwater model in the wave flume.

reefy
Innovation for nature

TU Delft

Preface

This thesis is the final part of my master's degree in Hydraulic Engineering and marks the end of my academic career. I was given the opportunity to do my graduation internship at the startup Reefy, for which I am extremely grateful. Over the past year, I have been working on the stability of the Reef Enhancing Breakwater. Not only was this research educational, interesting, and challenging, but conducting wave flume experiments is also super cool.

First and foremost, I would like to thank my daily supervisor Daan Houtzager for his help and support throughout this journey. During the numerous meetings, he provided guidance, answered many of my questions and steered me in the right direction. Secondly, I would like to express my gratitude towards my other supervisors Marcel van Gent, Bas Hofland and Jaime Ascencio for their valuable advice, feedback and the time they have invested in me.

Completion of my thesis was of course not possible without the other members of the Reefy team. I would like to extend a special shoutout to Arthur Pinkse, Leon Haines and the other interns for the great times at the office. I really enjoyed being part of the Reefy team.

Now that my time as a student has come to an end, I can look back on an amazing period. I want to thank all the people that made this possible.

Pieter Geenen
Delft, May 2024

Summary

Coastal structures such as breakwaters can mitigate the erosive effects of sea level rise by protecting the shoreline from wave impact. The Reef Enhancing Breakwater (REB) is a modular and permeable structure that can dissipate wave energy and on the other hand aims to boost marine biodiversity by providing the required habitat conditions. This research investigates the hydraulic stability of the REB under wave loading, using a physical model.

Experiments have been conducted in the Scheldt flume of Deltares, using a 1:20 scale model. Both 2 and 3 level structures with simple and complex forms have been tested on top of gravel underlayers with different roughnesses. Mainly irregular waves were used with significant wave heights up to 12.5 cm. The wave steepness ranged from 2% to 4% and the water depth was varied as well. As failure was not reached on the horizontal foreshore (main location), the structure was relocated closer towards the transition slope (alternative location) where plunging breakers can emerge. Furthermore, smart ReefBlocks with integrated mobility sensor were used to measure accelerations and angular velocities of the blocks induced by the wave motion.

There were 5 main types of movements observed: sliding, rocking, shaking, tilting and lifting. This research provides an explanation for the relation between these movements and the configuration type. Sliding was the most common type of movement, observed in all configurations, and happened mainly in the top layer. The maximum number of observed sliding events in one test was equal to 4 movements/block/1000 waves.

Three limit states are defined: start of motion, start of damage and failure. Start of motion is the moment at which one or multiple blocks within the structure move for the very first time. Damage is defined as a block losing its interlocking with another block. Failure is defined to be reached for a damage level $N_{od} = 0.4$. For each setup, the expected and characteristic values of the stability number ($H_{m0}/\Delta D_n$) have been determined per limit state. Only one displacement occurred at the main location, while on the alternative location, near the transition slope, failures were reached due to the violent impacts of plunging breakers. Because the wave height is limited by the water depth in front of the structure, the 2 level simple, 2 level complex and 3 level complex form structures are stable for bed slopes that do not allow for plunging waves. For the situation without the plunging breakers, the characteristic values of the start of movement limit state ($N_{s,m}$) range from 0.39 to 0.51. When the site conditions are such that plunging waves can emerge, different design criteria apply, because plunging waves hitting directly on the structure can lead to damage and failure of the REB. For that situation, the characteristic value of the start of damage limit state ($N_{s,d}$) is 0.94. The characteristic values of the failure limit state ($N_{s,f}$) range from 0.94 to 1.11. The start of motion was not determined for the setups on the alternative location.

For the setups on the main location, the most common type of movement, sliding, was further analysed and compared to various hydraulic and structural variables. It was found that the number of sliding movements is influenced by the wave height, wave steepness, water level and structure height. Increasing the water level allows for higher waves and can lead to more instabilities, but when the water level becomes too high, the structure becomes too submerged and

the number of movements decreases again. A wave steepness of 2% results in more movements than a steepness of 4%, as longer waves contain more energy. Other influencing variables such as underlayer irregularity and increased drag by epifauna were considered as well. Most sliding movements were observed for $H_{m0}/\Delta D_n > 0.8$. The model is conservative for sliding movements since the PLA model blocks have a lower friction coefficient than concrete and start sliding for smaller forces.

The impact of the sliding movements on the structural performance of the ReefBlock is investigated by estimating the sliding induced stresses in the protrusions. The data from the smart ReefBlocks was used to determine the impact velocity. A model based on conservative assumptions was used to calculate the resulting impact force and check for rupture of the protrusion. It appears that the resulting tensile stresses exceed the concrete strength. However, it is questionable to what extent this approach is representative, as the model differs considerably from the actual protrusion. Further research is necessary to provide a definitive answer.

Contents

Symbols

a	Acceleration
A	Area of a cross-section
b	Width of a cross-section
c	Wave propagation speed
d	Water depth
d_0	Offshore water depth
d_s	Water depth at the toe of the structure
D	Diameter
D_{50}	Median diameter
D_n	Nominal diameter
D_{n50}	Median nominal diameter
E	Expected value
E	Young's modulus
f_c	Static concrete strength
$f_{c,impact}$	Concrete impact strength
F	Force
g	Gravitational acceleration
h	Height of a cross-section
h_s	Structure height
H	Wave height
$H_{1/3}$	Mean of the highest one-third of the waves
$H_{1/50}$	Mean of the highest $1/50$ of the waves
$H_{1/150}$	Mean of the highest $1/150$ of the waves
H_b	Breaking wave height
H_{m0}	Significant wave height, calculated from zeroth order of the spectrum
H_s	Significant wave height
I	Mass moment of inertia
k	Spring stiffness
k	Wave number
K_{sh}	Shoaling factor
L	Length
L	Wavelength
L_0	Deep water wavelength
$L_{0,p}$	Deep water wavelength corresponding to the peak period
L_{block}	Length of a ReefBlock
L_m	Length dimension of the model
L_p	Length dimension of the prototype
L_p	Wave length corresponding to the peak period
m	Mass
m	Metre
M	Bending moment
n	Ratio between group velocity and phase velocity
n_l	Geometric scale factor

n_{dis}	Number of displaced units
N	Number of waves
N_{od}	Relative damage level
N_s	Stability number
N_s^*	Spectral stability number
$N_{s,d}$	Stability number corresponding to the start of damage
$N_{s,f}$	Stability number corresponding to failure
$N_{s,m}$	Stability number corresponding to the start of movement
P	Permeability parameter
R_c	Freeboard
Re	Reynolds number
s	Second
s	Wave steepness
s_0	Deep water wave steepness
$s_{0,p}$	Deep water wave steepness corresponding to the peak period
s_p	Local wave steepness corresponding to the peak period
S	Damage level
t	Time
T	Wave period
T_p	Peak period
T_{m01}	Mean spectral wave period
$T_{m-1,0}$	Mean spectral energy period
v	Kinematic viscosity
v_i	Impact velocity
V	Volume
w	Width of the flume
W	Moment of resistance
α	Slope angle
δ	Deflection
Δ	Relative density
Δ_m	Relative density of the model
Δ_p	Relative density of the prototype
γ_b	Breaker index
θ_r	Angle of repose
μ	Mean value
ξ	Iribarren parameter
ξ_m	Iribarren number corresponding to the mean wave period
$\xi_{0,p}$	Iribarren number calculated with $s_{0,p}$
ρ_b	Density of the block
ρ_w	Density of water
σ	Standard deviation
σ_c	Compressive stress
σ_t	Tensile stress
σ_{max}	Maximum stress
σ_{shear}	Shear stress
ϕ	Angle of wave incidence
ω	Angular frequency
ω	Angular velocity

Abbreviations

ARC	Active Reflection Compensation
CFD	Computational fluid dynamics
IMU	Inertial measurement unit
REB	Reef Enhancing Breakwater
PLA	Polylactic acid
WG	Wave gauge
Z&S	Zelt & Skjelbreia
2D	2-dimensional
3D	3-dimensional

1 Introduction

1.1 Context

The climate is changing rapidly, resulting in an accelerating sea level rise and more extreme weather events. Severe storms with higher intensities will occur on a more frequent basis and are already leading to erosion of coasts in alarming proportions (IPCC, 2021). Most sea-connected countries are vulnerable for coastal erosion and are facing the threats of land loss, which negatively affects the local communities and economic activity (Saengsupavanich et al., 2022). Since roughly 40 percent of the world population lives in coastal regions, coastal erosion can have a significant impact on society (Pörtner et al., 2022). These densely populated areas exhibit population growth together with urbanization, and this trend is expected to continue in the future (Neumann et al., 2015). Therefore, it is crucial to protect these places from the negative consequences of climate change.

Figure 1.1: Coastline erosion as a consequence of climate change (Dronen, 2018).

Implementation of hard coastal structures like breakwaters can mitigate these erosive effects by protecting the shoreline from wave impact. They absorb and dissipate wave energy and reduce its erosive power (Na'Im et al., 2018). It forces high waves to break before reaching the shoreline and gives sediments the opportunity to accumulate behind the structure, resulting in stable beaches. However, these conventional structures often act as a barrier and interrupt the nearshore hydrodynamics and sediment transport, affecting surroundings and nearby marine habitats. Besides that, these type of structures may have a negative influence on the aesthetics by blocking the horizon view (Saengsupavanich et al., 2022).

Reefs can also protect shorelines and are among nature's strongest coastal defences. A reef is a shallow ridge of material on the seabed, containing a hard substrate that is ideal for organisms to attach to. In addition, it creates sheltered and turbulent zones, leading to complex abiotic

conditions, which attracts a variety of species. Reefs act as important barriers to mitigate flooding and shoreline erosion and can reduce wave energy up to 97 percent (Ferrario et al., 2014; Toth et al., 2023). Coral reef is the most famous type and is known for its high biodiversity. Even though they only make up 1 percent of the earth's surface, they are home to more than 25 percent of all marine species (UNEP and WWF, 2003). Moreover, they are resilient and have the ability to recover, to some extent, after storms, but also accrete vertically in order to adjust to a rising sea level. (Perry et al., 2012). On the other hand are coral reefs one of the most fragile and endangered ecosystems in the world, and human activities, causing for rising temperatures and pollution, have harmed or destroyed many of them (Vittal Hegde, 2010).

Figure 1.2: Difference between living (left) and dead (right) coral (Lobo, 2020).

So, it is not surprising that engineers have been trying to develop artificial reefs. An artificial reef can be defined as a man-made submerged structure that mimics some of the characteristics of natural reefs. Their purposes range from increasing marine life and recreational diving to surf-wave generation and coastline protection (Baine, 2001). The concept of an artificial reef, used as a fish production enhancing structure, was already successfully applied three centuries ago in Japan (Thierry, 1988). It should be noted that artificial reefs must be stable enough to survive heavy storm events and prevent it from being lifted and displaced, destroying the surrounding corals or losing its functionality.

Nowadays, engineers strive to develop multipurpose designs, whereby engineering requirements are met while enhancing the natural habitat value (Firth et al., 2013). A good example for such a multipurpose design is the Reef Enhancing Breakwater (REB) from the company Reefy. They have been developing patented modular ReefBlocks, that can dissipate wave energy to protect the coastline, and on the other hand boost marine biodiversity on several scales by providing the required habitat conditions. The holes, crevices and tunnels are creating sheltered and high turbulent zones that provide habitat for marine life. The permeability of the blocks with the interconnected system of tunnels not only makes the element more stable, but it also allows water flow from one side to the other. This improves water quality, facilitates passage for underwater life, and reduces the concentrated return currents near the edges of the blocks. The design also includes surface textures that adds rugosity and small variations, targeted to specific species. Hence, it can be considered as a living breakwater. When combined, these big LEGO-like concrete blocks form a permeable structure that requires relatively few

materials and little space compared to a conventional breakwater. An interlocking mechanism is created by the holes and protrusions, so the blocks can function as one big modular structure. Previously, Reefy conducted both physical and numerical studies on the wave transmission of a REB (Van den Brekel, 2021; Kadoglou, 2023). An initial study on the stability of the REB was performed as well during these prior experiments. However, the design of the blocks has changed and more insights into its stability is required for the development of design guidelines and quantification of movements. Gaining more knowledge about the behaviour of the REB will help Reefy with their mission to rewild the ocean.

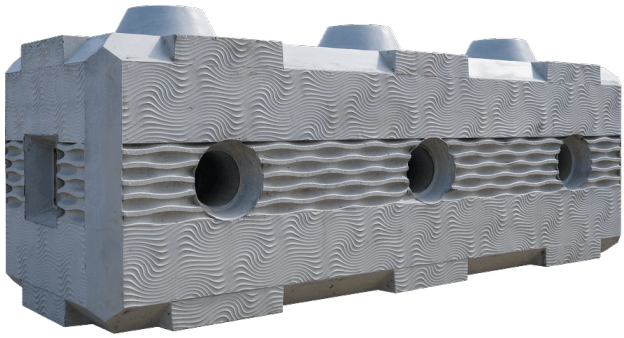

Figure 1.3: ReefBlock, developed by Reefy.

1.2 Research objective and questions

The objective of this research can be formulated as follows:

"Provide insight into the hydraulic stability of a Reef Enhancing Breakwater under wave loading, using a physical model."

The following research questions are defined to achieve this goal:

1. What type of movements occur within the REB?
2. What are the limit states of the REB?
3. How do hydraulic and structural variables influence the number of sliding movements within the structure?
4. Can the sliding induced stresses lead to rupture of a protrusion?

Answering these questions will help to clarify how the REB behaves regarding its stability under wave loading.

1.3 Scope

In this research, the hydraulic stability of the REB is studied using a physical model. The experiments are performed in the Eastern Scheldt wave flume at Deltares using a flat foreshore. Different configurations up to 3 layers high will be checked under 2D normal incident wave conditions. Both regular and irregular waves are used, ranging from daily to storm conditions. For the majority of the tests, the structure is submerged. The influence of configuration type, bed irregularity and increased drag by epifauna are considered as well as hydraulic variables like wave height, wave steepness and water depth. The ecological value of the REB is not considered in this study.

1.4 Approach and outline

This research is carried out using a physical model. For 12 days, the Eastern Scheldt flume of Deltares was used. The research starts with a literature study to find out what variables are likely to influence the stability of the REB. This theoretical study delivers the input for the experiments so that suitable configurations, loading conditions and a flume set up can be determined. At the same time, blocks are produced and optimized during the prototyping phase. Then, the actual tests are performed in the wave flume. Afterwards the data, gathered with various sensors, is processed and analysed.

Chapter 1 provides an introduction to the thesis. Chapter 2 contains the theoretical framework based on a literature study. In Chapter 3, the methodology is described. How the data is processed is explained in Chapter 4. The results are presented and analysed in Chapter 5, followed by the discussion and conclusions in Chapter 6 and 7 respectively. Finally, recommendations are listed in Chapter 8.

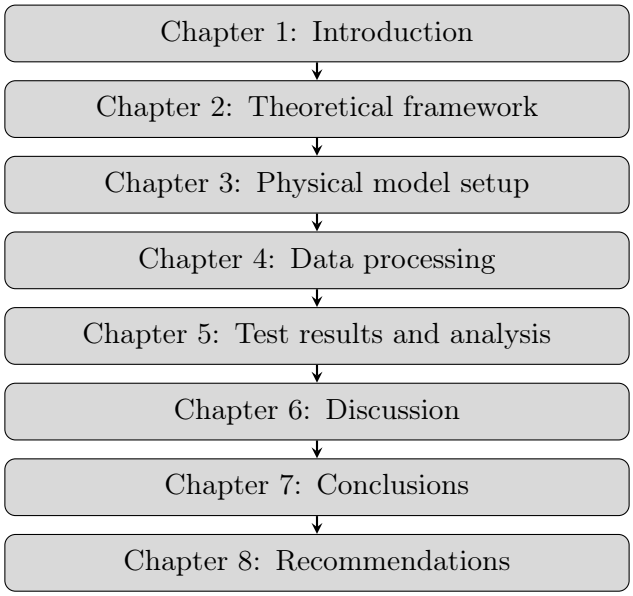

Figure 1.4: Thesis outline.

2
Theoretical framework

This chapter summarizes some necessary insights and background knowledge in order to fully understand this report. Also, it functions as a starting point and proves input for the experimental setup of the physical model.

2.1 Previous Reefy experiments

Previous research on wave dissipation of the REB was conducted by Van den Brekel (2021). 15 different setups were tested in combination with 35 different loading conditions. The main purpose was to determine wave transmission, so most setups were not loaded to failure. In some of the tests, the blocks were even fastened together with interlocking tubes, as this is a possibility in the field as well. The structures were tested under both normal conditions and storm conditions. Even though the majority of the tests were intended for other purposes, a small stability study was performed as well. However, the amount of useful data was limited. Besides that, it was chosen to give the model blocks a density of about 1900 kg/m^3, which is significantly lower than the density of concrete. Therefore, it is questionable whether the outcomes are representative, especially now the design of the ReefBlock has been changed as well. However, from this study it was found that:

- The frontmost blocks of the top layer are the first to start moving.
- The first movements of the 1:15 scale blocks occurred at 0.12 m regular wave heights.
- The structure seems more stable for steeper waves.
- A structure with a gentler front slope will be more stable.
- A narrow stack of blocks is less stable than a structure covering the entire width of the flume.
- The more submerged structures remained stable throughout the experiments
- The effect of permeability on the stability was not observed.
- Waves start breaking over the structure when the submergence is equal or smaller than the wave height.

Even though the design of the ReefBlocks have changed since the previous experiments, the data is still useful and serves as input for the model setup of this research.

2.2 Breakwater types

A breakwater is a structure in a water body that protects an area against waves and currents. They are designed to dissipate energy by forcing the incoming waves to break, reduce wave transmission and creating a sheltered area. A breakwater's structural design has a wide range

of alternatives, each varying in terms of stability, permeability, cost, and aesthetics, etc. The most common breakwater is a multi-layered heap of loose material and is called rubble mound. Sand or gravel is frequently used as core, while heavier components like rocks or concrete units are used for the armour layer. Sometimes, features like berms or crown walls are added to these breakwaters. Another conventional breakwater type is the monolithic breakwater, consisting of one big element, functioning as a single block. Examples of monolithic structures are caissons and block walls. A monolithic structure combined with some loose material is known as a composite breakwater. These are the three main types, but there are other unique breakwater varieties, such as the floating, pneumatic, hydraulic and piles breakwaters. (Verhagen and d'Angremond, 2009; Van den Bos and Verhagen, 2018)

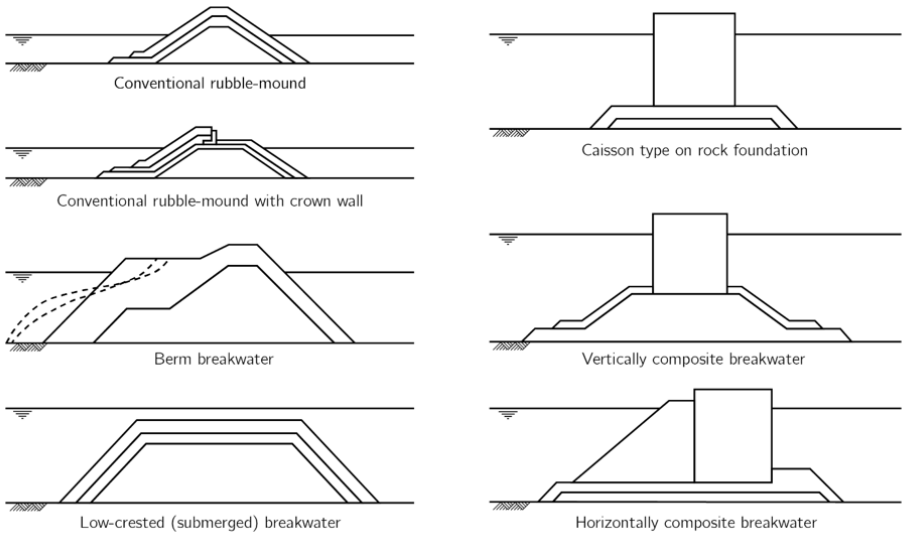

Figure 2.1: Cross-sections of multiple breakwater types (Rock Manual, 2007).

A structure can be defined as low-crested when it is overtopped by waves and has its crest level roughly around the still water level. Van der Meer and Pilarczyk (1990) suggest that the low-crested rubble mound breakwaters can be subdivided into three categories: dynamically stable reef breakwaters, statically stable emerged breakwaters and the statically stable submerged breakwaters. The reef breakwater, not to be confused with a REB, simply is low-crested rubble mound, but without the typical multi-layered cross-section and is allowed to reshape during storm events. An emerged breakwater has a crest above the still water level and that of a submerged breakwater is below the still water level. The freeboard of a breakwater, indicated with R_c, is the difference between the still water level and the crest level of the structure. For an emerged structure the freeboard is positive, while for a submerged structure the freeboard is negative.

It is hard to classify the REB as one of the aforementioned breakwater types due to its unique geometry and the significant size of the blocks. That implies that it is likely to behave somewhat differently regarding stability as well. The REB is a low-crested structure that can be both emerged and submerged, due to tidal variations. Therefore, both submerged and emerged states will be included in this research. However, in the majority of the tests the structure will be submerged, as storm conditions often induce higher water levels.

2.3 Wave breaking

To understand the process of wave breaking, basic knowledge about near shore transformation of waves is requisite. Waves change as they approach shallower waters. There are three different zones that can be distinguished, based on the water depth to wavelength ratio, in which the waves behave different:

1. Deep water ($\frac{d}{L} > 0.5$)
2. Intermediate water ($0.05 < \frac{d}{L} < 0.5$)
3. Shallow water ($\frac{d}{L} < 0.05$)

Height, length and direction changes when a wave is propagating out of the deep water zone. The reason for this transformation is that the wave starts to feel the bottom, leading to processes like refraction, shoaling and breaking. The propagation speed of a wave is dependent on the depth as listed in equation 2.1 & 2.2.

$$c = \frac{gT}{2\pi} \tanh(kd) \tag{2.1}$$

The propagation speed of waves that enter shallower water will decrease, meaning that the wave length decreases as well, since the wave period is remains constant.

$$c = \frac{L}{T} = \frac{\omega}{k} \tag{2.2}$$

With:

$$\omega = \frac{2\pi}{T} \tag{2.3}$$

$$k = \frac{2\pi}{L} \tag{2.4}$$

A combination of Equation 2.1 & 2.2 results in the so-called dispersion relation:

$$L = \frac{gT^2}{2\pi} \tanh(kd) \tag{2.5}$$

With a decreasing wavelength, the energy of the waves becomes more concentrated, leading to an increase in wave height. This phenomenon is known as shoaling. The shoaling factor can be calculated with:

$$K_{sh} = \frac{H_2}{H_1} = \sqrt{\frac{c_1 * n_1}{c_2 * n_2}} \tag{2.6}$$

With:

$$n = 0.5\left(1 + \frac{2kd}{\sinh(2kd)}\right)$$

A similar process happens for the propagation of obliquely incident waves. When waves move towards shallower water, they bend towards the shore normal and the wave height increases. This is called refraction. The wave steepness, which is a ratio of the height and the length of the wave (equation 2.7), changes due to these processes as well.

$$s = \frac{H}{L} \tag{2.7}$$

At some point, the waves will start to break as a result of instability caused by a certain water depth, steepness or a combination of them. For regular waves this can be described with Miche's criterion:

$$H_b = 0.142\ L\ \tanh\left(\frac{2\pi d}{L}\right) \tag{2.8}$$

For deep water conditions this results in $H_b/L = 0.142$. In shallow water this leads to $H_b/d = 0.88$. From solitary wave theory it follows that waves already break when $H/d = 0.78$. Meaning that a wave cannot be greater than a certain fraction of the local water depth. When the wave reaches this critical depth, it breaks and it is therefore called depth induced wave breaking. This ratio between maximum wave height and water depth, also called the breaker index γ_b (equation 2.9), typically has a value of 0.78 for regular waves. The ratio between significant wave height and local water depth is in the range of 0.4-0.5. (Holthuijsen, 2007; Schiereck, 2019)

$$\gamma_b = \frac{H}{d} \tag{2.9}$$

Waves can break in various ways, each with its own properties. Four types of wave breaking can be distinguished (figure 2.2). The breaker type depends on the ratio between bed slope steepness and wave steepness, expressed in ξ and known as the Iribarren number or the surf similarity parameter.

$$\xi = \frac{tan(\alpha)}{\sqrt{s}} \tag{2.10}$$

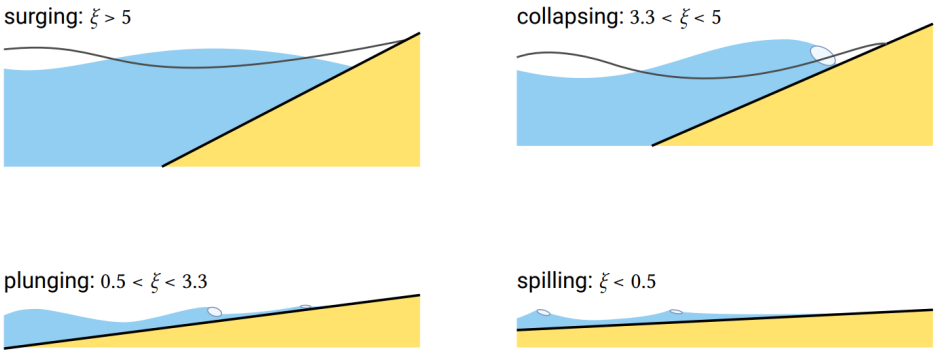

Figure 2.2: Four breaker types, depending on the Iribarren number (ξ) (Bosboom and Stive, 2022).

According to Camenen and Larson (2007), the breaker type not only depends on the Iribarren number, but on the breaker index as well. (Figure 2.3)

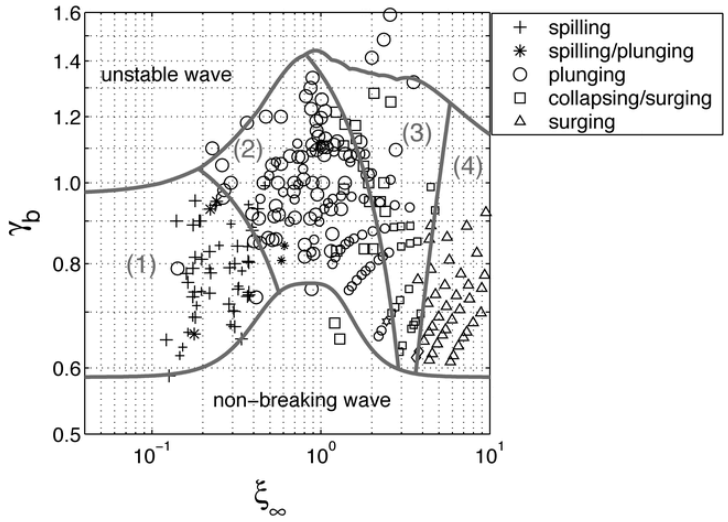

Figure 2.3: Observation of different breaker types with respect to the Iribarren number and the breaker depth index (1: spilling breaker area, 2: plunging breaker area, 3: collapsing breaker area, 4: surging area). (Camenen and Larson, 2007)

From these four breaker types, especially plunging waves can be violent to coastal structures as they release a lot of their energy within a short time and relatively small area, resulting in heavy impacts.

2.4 Failure mechanisms of a breakwater

In order to understand the stability behaviour of a hydraulic structure, it must be clear what the possible failure mechanisms are. A lot is known about failure mechanisms of conventional breakwaters (Figure 2.4). It is questionable whether this is applicable on the REB, because it cannot be classified as a conventional breakwater type. This means the critical failure mechanisms are possibly different as well.

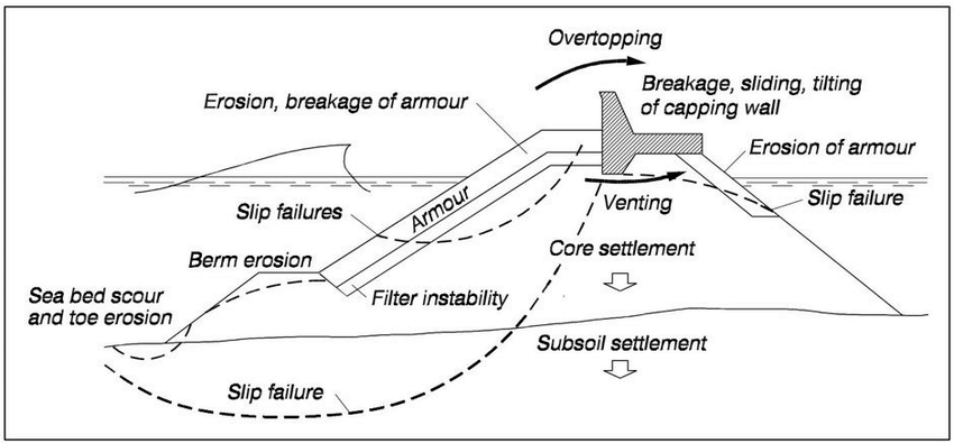

Figure 2.4: Possible failure mechanisms of a rubble mound breakwater (Burcharth, 1997).

Several potential mechanisms that can lead to failure can be distinguished:

Rocking

Wave loading can cause a block to rotate back and forth in an arbitrary direction, this is known as rocking. The block experiences numerous minor collisions, which lead to tensile stresses in the block. All those collisions can eventually result into abrasion or breakage of the blocks as brittle materials like concrete are not very resistant to tensile stresses. But, it should be noted that the strength of concrete cannot be scaled, so the failure of the blocks in the scale model tests is not representative for the real scale model (Rock Manual, 2007). This implies that even if the scale model does not break, the real model possibly still can. Therefore, it is important to monitor for what conditions the blocks start rocking and to what extent. The challenging aspect of rocking is that it is difficult to observe visually in physical models (Houtzager et al., 2023). Often, rocking happens at the moment of impact and the breaking wave will obstruct the view. Rocking is an important mechanism since it can happen rather quickly, especially when the blocks are not perfectly placed on top of each other. In that situation, the block has a narrow base of support, which makes it very unstable and it can start moving already under moderate wave loads. Rocking is expected to be one of the first movements to occur during the experiments.

Sliding

When the horizontal wave forces exceed the frictional resistance of a block, sliding can occur and the block starts moving horizontally. The interlocking feature of the blocks does counteract this process to a certain extent, but it could happen that the protrusions break. It is also possible that a block is not properly interlocked due to installation errors. In those cases a block can slide out of the structure, creating a gap in the breakwater and possibly leading to failure. It could also happen that the interlocked blocks from several layers start sliding together at once. This was observed in the previous Reefy experiments, but it is uncertain to what extent this was caused by the interlocking tubes that were used to make the construction function as a whole. Also, the structure was placed directly on the foreshore instead of a gravel layer, which have different friction characteristics.

Lifting

When the uplift force caused by orbital velocities is greater than the downforce from the block's submerged weight, lifting may occur. In that situation, the block will be elevated vertically and will no longer be interlocked. This can have serious consequences when the block is also displaced horizontally at the same time. This will cause it to settle in a new position and make it more susceptible for sliding and rocking, or it can be completely removed from the structure. Lifting can happen with single elements at the top of the stack, but theoretically multiple elements from different layers can be lifted simultaneously as well.

Tilting

Tilting is comparable with lifting, but in this case it is only one side of the block that is moving upwards, while the other side is functioning as a hinge. The block at the top layer of the stack flips over and falls down. During the experiments, tilting of top blocks is likely to happen as this type of motion was also observed during previous Reefy experiments.

Scour

A common failure mechanism of hydraulic structures is scour. The layer under the structure itself, which is made out of finer material, can be eroded by currents and wave motion. When this material under the structure is disappearing, the structure will lose its support, becomes unstable and will eventually fail. A proper scour protection can prevent this transport of finer material. In case the differences in diameters are too big, filter layers should be applied. Within this research, scour is not the main mechanism of interest as it could be countered by improving the scour protection. The focus will be more on the interaction between the waves and the blocks.

Differential movement and settlements

Irregularities and settlements in the underlayer can lead to uneven vertical displacements. As a result, the interlocking may be reduced or lost and blocks are more exposed and susceptible to rocking. This increases the chance of failure. Settlement of the subsoil is not expected to occur during the experiments, as there will be no soft subsoil in the flume.

2.5 Stability number

Stability can be expressed in terms of a stability number N_s (equation 2.11), which represents a ratio between load and strength: The significant wave height (H_{m0}) versus the relative density (Δ) and nominal diameter (D_n) of the unit.

$$N_s = \frac{H_{m0}}{\Delta D_n} \tag{2.11}$$

In which:

$$\Delta = \frac{\rho_b - \rho_w}{\rho_w} \tag{2.12}$$

Using this load to strength ratio, it is possible to define several limit states. For example:

- $N_{s,m}$ = Start of motion
- $N_{s,d}$ = Start of damage
- $N_{s,f}$ = Failure of the structure

The stability of most breakwaters is based on damage, quantified in terms of displaced blocks or rocks. For the REB, damage can be defined as a displacement of a block such that it loses its interlocking with another block. Failure corresponds to a certain damage level but is not fixed and can differ between structures, based on the requirements. Often, a breakwater is said to have failed when it is unable to fulfil its function any longer, for instance when the cross-section has been changed due to a certain number of displaced units. In a design is determined what level of damage is acceptable and what level corresponds to failure.

The damage can be expressed with the relative damage level (N_{od}). This parameter can be calculated by counting all displaced units within a certain area (n_{dis}), multiply it with the nominal diameter and divide it by the considered width (w). Dividing this parameter by the number of units within a cross-section of one diameter wide results in damage percentage level S.

$$N_{od} = \frac{n_{dis} * D_n}{w} \tag{2.13}$$

With these limit states, a stability range can be determined, which is already done for some conventional armour unit types (Figure 2.5). The range is determined based on a certain acceptable damage level, which for some of the units goes up to $S = 5\%$ (Rock Manual, 2007).

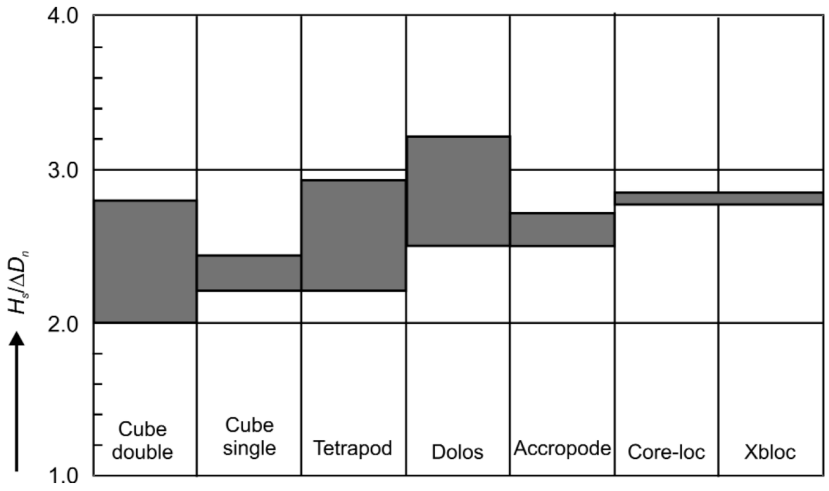

Figure 2.5: Suggested stability ranges of conventional armour units. The lower bound corresponds with 0% damage (Rock Manual, 2007).

Nominal diameter

For most armour elements in breakwaters, the nominal diameter D_n is used as input for the characteristic size in equation 2.11. This parameter was introduced because it can represent elements with different shapes in the same way. Its value can be determined by taking the cube root of the material volume (equation 2.14). An object's volume can be derived from its mass and density. For a ReefBlock with a weight of 5716 kg and a density of 2400 kg/m^3, the nominal diameter is equal to 1.34 m.

$$D_n = \sqrt[3]{V} \tag{2.14}$$

2.6 Stability of submerged breakwaters

Stability depends on multiple variables. For conventional (submerged) breakwaters, most of those variables have already been described. However, it is uncertain which of these variables have an influence on the REB stability as well.

Relative freeboard

As described by Van der Meer et al. (1996) are low-crested structures often more stable than high-crested structures, because some of the wave energy passes over it. The level of submergence can be expressed with the relative crest freeboard, which is defined as R_c/D_{n50}. This value is positive for emerged structures and negative for submerged structures. When the relative crest freeboard of a submerged structure decreases, it is evident that the stability increases.

Vidal et al. (1992) divided the structure into segments: the crest, the front slope and the

rear-side slope (figure 2.6). For a submerged structure, stability of the crest and rear-side slope play a more important role than for non-overtopping structures.

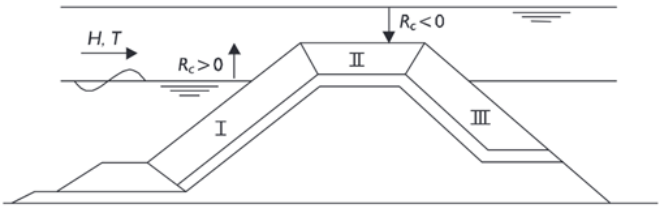

Figure 2.6: Segments of a breakwater: I = front slope, II = crest, III = rear-side slope (Rock Manual, 2007).

This was used by Van der Meer et al. (1996) to make a graph of the stability of a low-crested rubble mound structure (figure 2.7). It was concluded that the crest is the least stable segment of a submerged structure and the highest instabilities occur when the freeboard is 0. Stability numbers of about 1.5 were found for start of damage. It was stated that stability is more influenced by the freeboard than by the wave period. Also, longer waves appeared to be predominant over shorter waves.

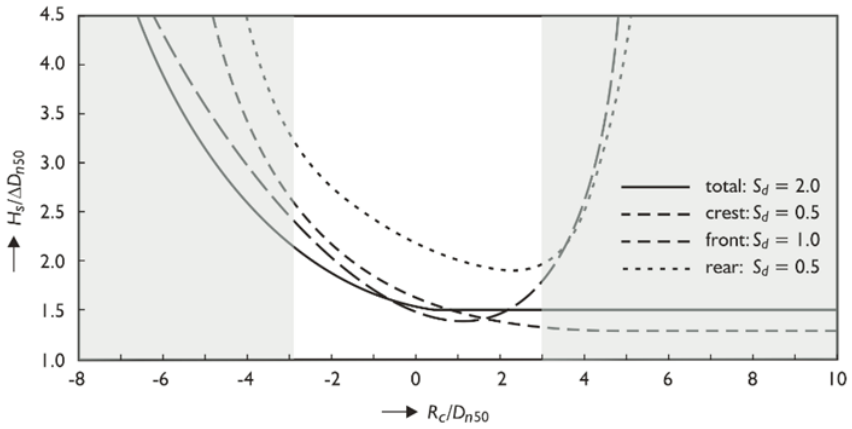

Figure 2.7: Stability for starting damage of a low-crested rubble mound structure. Note that the graphs outside range $-2.9 < R_c/D_{n50} < 3.0$ are extrapolated (Van der Meer et al., 1996).

The stability of the crest of a submerged rubble mound breakwater depends mainly on the freeboard and the nominal diameter. This can be represented by equation (2.15). (Rock Manual, 2007)

$$\frac{H_s}{\Delta D_{n50}} = A + B\left(\frac{R_c}{D_{n50}}\right) + C\left(\frac{R_c}{D_{n50}}\right)^2 \tag{2.15}$$

Values for A, B and C were determined by multiple researchers, but the results are not deviating a lot. Therefore, the following rule of thumb can be used for first estimates of designs.

$$D_{50} \geq 0.3D \quad \text{for} \quad \frac{H_s}{d} = 0.6 \quad \& \quad \cot\alpha_s \geq 100 \quad \& \quad \Delta \approx 1.6 \tag{2.16}$$

Spectral stability number

During his studies on reef breakwaters, Ahrens (1987) discovered that the wave period has a significant influence on the stability. Therefore, he modified the stability number into the spectral stability number (equation 2.17).

$$N_s^* = N_s * s_p^{-1/3} \tag{2.17}$$

With the local wave steepness $s_p = H_s/L_p$. In which L_p represents the airy wave length, calculated from the peak period and the water depth at the toe of the structure. Compared to the traditional stability number, the spectral stability number shows less scatter when plotted against the damage trends. When the spectral stability value is less than 6, there is little to no damage. In later studies, Ahrens and Member (1989) came with an approximate threshold for stone movement of $N_s^* = 7$

Van der Meer and Pilarczyk (1990) stated that it might be better to describe the stability of statically stable submerged structures with the spectral stability number as well. Furthermore, it says that a submerged breakwaters' stability is a function of the spectral stability number, damage level and relative crest height only as shown in equation 2.18.

$$\frac{h_s}{d} = (2.1 + 0.1\ S)\ exp(-0.14\ N_s^*) \tag{2.18}$$

It seems that the wave period definitely influences the stability of low crested structures and so it is likely to be the case for the REB as well.

Permeability

The influence of permeability on the stability of the REB was not observed during the experiments of Van den Brekel (2021). For rubble mound structures, the permeability does have an effect on the stability. A breakwater with a permeable core proves to be more stable. Therefore, Van der Meer (1988) added a permeability factor to his stability equations for rubble mound structures (equations 2.19 & 2.20). Wave period, damage and the number of waves were included as well.

$$\frac{H_s}{\Delta D_{n50}} = 6.2P^{0.18}\left(\frac{S}{\sqrt{N}}\right)^{0.2}\xi_m^{-0.5} \qquad \text{(plunging breakers)} \tag{2.19}$$

$$\frac{H_s}{\Delta D_{n50}} = 1.0P^{-0.13}\left(\frac{S}{\sqrt{N}}\right)^{0.2}\xi_m^{P}\sqrt{\cot(\alpha)} \qquad \text{(surging breakers)} \tag{2.20}$$

The influence of permeability on the stability of a REB is still unclear.

2.7 Methods to test stability

To evaluate a structure's hydrodynamic performance, several techniques can be applied. The two main types are physical models and numerical models.

Hydrodynamics can be simulated with CFD (computational fluid dynamics) modelling. Computers can predict the behaviour of fluids by solving equations based on the principles of fluid dynamics. OpenFOAM is an example of an open-source CFD software that is available for these

kinds of computations. However, these methods have some limiting factors like the required computational power and time. Besides, the combination of wave breaking and the complex geometry of the ReefBlock makes it very complicated to determine stability.

A more preferred alternative is to use a physical model, which is a physical representation of the real-world prototype. A physical model has proven to be accurate and reliable and is therefore a commonly used tool for obtaining knowledge about breakwater stability. For large structures like breakwaters, scale models are often used due to practical considerations. It is required that the scale model's behaviour is consistent with that of the real scale prototype. A number of scale rules have been derived for this and will be treated in section 2.8. (Schiereck, 2019)

While using a physical model, there are various ways to gather data. The simplest way of collecting data is by visual observation. This can be done with the eyes or with the help of a camera. But, as stated in section 2.4, this will not always lead to correct results, because not all processes and movements are visible. One can use more sophisticated measurement methods, such as with sensors. Nowadays, a wide variety of sensors is available like mobility, velocity and pressure sensors.

Mobility sensor

Measuring the motion of breakwater armour units with motion sensors, as described by Hofland et al. (2018), is proven to be a successful method in studies on rocking. This method makes it possible to measure accelerations and angular velocities inside the units at a sampling frequency of 100 Hz, without any wires attached to them during the tests. This technique is used to determine the impact velocities and can give more insight in the stability and behaviour of the blocks. The sensor measures the x, y, z components of the acceleration and the angular velocity. The total angular velocity and acceleration can be calculated with:

$$\mid \omega \mid = \sqrt{\omega_x^2 + \omega_y^2 + \omega_z^2} \tag{2.21}$$

$$\mid a_{tot} \mid = \sqrt{a_x^2 + a_y^2 + a_z^2} \tag{2.22}$$

2.8 Scaling rules

The use of scale models is only valid if the model and the prototype behave in the same manner. Scaling all properties, using the same ratio, will lead to scale effects and incorrect results. Appropriate scaling relations have been derived for this and are based on three principles:

1. Geometric similarity
This means that all the shapes are similar. Lengths, areas and volumes are scaled with ratios n, n^2, n^3 respectively.

2. Kinematic similarity
In addition to geometric similarity, the ratios of time between the model and prototype must be equal as well. This creates similarity of motion. This applies to terms like velocities and accelerations.

3. Dynamic similarity
This requires not only geometric and kinematic similarity, but also constant force ratios. For

example inertial, gravitational, surface tension and viscous forces. It is extremely difficult to achieve a perfect dynamic similarity since some forces or properties cannot be changed. Therefore, the most relevant force should be scaled, while the scale effects of the other forces are kept negligible (Heller, 2011).

Inertia and gravitation are the dominating forces in hydraulic models with waves. These forces are both represented in the Froude number. The prototype and the model should have the same Froude number to achieve similarity. It must hold that:

$$\frac{u_m}{\sqrt{g_m L_m}} = \frac{u_p}{\sqrt{g_p L_p}} \tag{2.23}$$

To simplify, a scale factor can be introduced. This is the geometrical scale factor and is just the ratio between the length scales of the model and the prototype.

$$n_L = \frac{L_p}{L_m} \tag{2.24}$$

With this length scale factor, the other scale factors can be found as well and it follows that not all properties are scaled linearly (table 2.1). Every quantity can be scaled easily, using these scale factors. It should be noted that this is based on the assumption of equal gravitational forces in the model and prototype.

Variable	**Unit**	**Froude scale**
Length	L	n_L
Area	L^2	n_L^2
Volume	L^3	n_L^3
Time	T	$n_L^{0.5}$
Frequency	T^{-1}	$n_L^{-0.5}$
Velocity	L/T	$n_L^{0.5}$
Acceleration	L/T^2	1
Discharge	L^3/T	$n_L^{2.5}$

Table 2.1: Scale factors according to Froude scaling.

In order to neglect viscous force terms, the flow must be turbulent enough. According to Hughes (1993), this can be checked with the following condition:

$$Re = \frac{\sqrt{gH_s}D_n}{\nu} > 3 * 10^4 \tag{2.25}$$

The effect caused by surface tension can be described with the Weber number. For very small waves, this force term should be taken into account. The Weber similitude in the model can be disregarded as long as the following requirements listed by Wolters et al. (2010) are met:

- The water depth should be greater than 5 cm.
- The significant wave height should be greater than 5 cm.

- The wave steepness must be realistic

Scaling the stability of rock or concrete units, can be done with the stability number. Again, this value should be the same for both the model and the prototype:

$$\frac{H_m}{\Delta_m D_m} = \frac{H_p}{\Delta_p D_p} \tag{2.26}$$

The stability number contains the relative density, which is depending on the material density and the water density. Because fresh water is often used during the experiments, while the prototype will be placed in salt water, the relative density of the model and prototype can be different. It could also happen that other material densities are used. This can be compensated by adjusting the diameter of the material or using a correction factor in such a way that the stability numbers match.

3
Physical model setup

3.1 Scale of the model

For the determination of the scale, there are two restrictions. The upper limit is confined by the highest waves that the flume can handle. The lower limit is determined by scale effects, mentioned in Section 2.8, which should be negligible. To neglect the surface tension forces, a minimum significant wave height of 5 cm is required.

Based on previous experiments, the stability range is expected to be $1 < N_s < 2$. In the flume, 0.2 m is the highest significant wave height that can be generated. By combining these values, a scale of 1:20 is found to meet the requirements. This scale corresponds with significant wave heights up to 0.18 m within the expected stability range.

After checking equation 2.25, it can be concluded that the viscous scale effects are negligible for this scale. Even the lowest waves create enough turbulence to disregard viscous force terms.

$$Re = \frac{\sqrt{gH_s}D_n}{\nu} = 4.7 * 10^4 > 3 * 10^4 \tag{3.1}$$

3.2 Block design

The design of the ReefBlock, patented by the company Reefy, has been changing considerably over the past years. In this research, the latest iteration of the design (August 2023) is used. The blocks that are used in these experiments are made from 3D printed PLA moulds, which are filled with a concrete/steel mixture. Due to practical limitations, the complex surface textures, that are present on the real ReefBlocks, are not included in the scaled blocks. It is expected that this will not have a significant influence on stability of the blocks because of the limited size of the textures.

Block geometry

The core of the model block has a length, height and width of 50mm, 50mm and 150mm respectively (Figure 3.1). In addition, it contains three protrusions and multiple holes. When placing two blocks on top of each other, the protrusions of the lower block can be fitted into the bottom holes of the upper block, creating an interlocking mechanism. The volume of the block was extracted from the 3D model and is equal to $2.977 * 10^{-4}\ m^3$. Subsequently, the nominal diameter can be calculated with Equation 2.14:

$$D_n = \sqrt[3]{2.977 * 10^{-4}} = 0.06677\ m \tag{3.2}$$

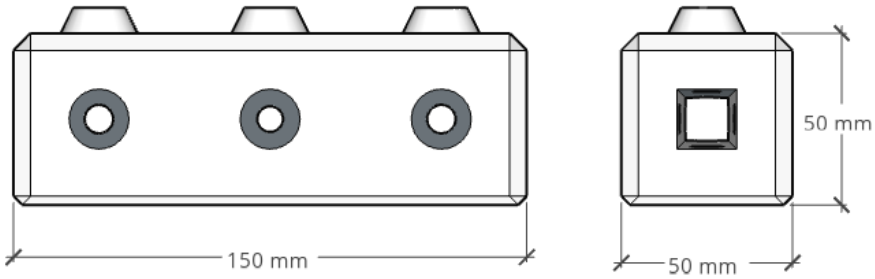

Figure 3.1: Main block dimensions of the 1:20 block.

Block weight

The plastic moulds are filled with concrete. Steel flakes are added to this concrete mixture in order to compensate for the low density of the plastic and increase the weight even further, as the used concrete for the model is lighter than that of the prototype (See section 3.2 Block density). After production, one block was cracked open and the steel flakes were discovered to be evenly distributed throughout the block.

Human errors and construction errors caused the blocks to differ slightly in weight from each other. In total 120 blocks were made. The block weights appear to approach a normal distribution (Figure 3.2b).

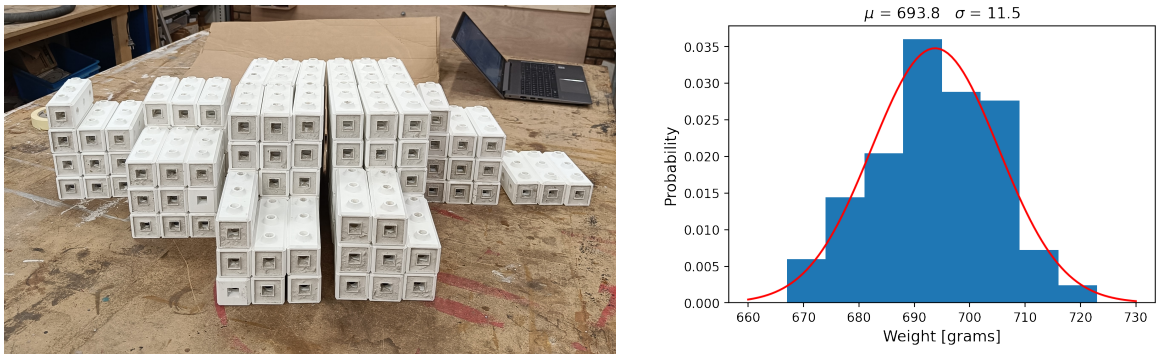

(a) Model blocks grouped by weight.

(b) Normal distribution fitted to block weight.

Figure 3.2: Distribution of the model ReefBlock weights.

The top 14 outliers were removed in order to narrow the distribution. The characteristic values of this adjusted dataset are listed in Table 3.1. The standard deviation is equal to 1.3% of the mean block weight, which is assumed to be sufficiently accurate.

Mean	695.1
Standard deviation	8.8
min. value	677.5
max. value	714.5

Table 3.1: Characteristic values (saturated) block weight distribution in grams.

When blocks are submerged, water is able to get in the pores of the concrete and slightly increases the block weight. This creates a difference between a wet and a dry block. The weights

are measured for both situations. As the blocks are placed in water during the experiments, it is the saturated weight that is used. More insight into the production process of the blocks can be found in appendix 8

Block density

Real scale ReefBlocks are made of concrete with a density of 2400 kg/m3. The REB will mainly be applied in coastal areas, at which the structure is placed in salt water, leading to a relative density (Equation 2.12) of:

$$\Delta_p = \frac{2400 - 1025}{1025} = 1.34 \tag{3.3}$$

The average density of the model blocks is 2335 kg/m3. Placing these in fresh water results in a relative density of:

$$\Delta_m = \frac{2335 - 1000}{1000} = 1.335 \tag{3.4}$$

The small difference between these two values can be compensated by a correction factor. This factor is equal to $\Delta_p/\Delta_m = 1.005$, implicating that a 0.5% smaller nominal diameter or 0.5% higher wave should be used. It would also be an option to use this difference as part of a built-in safety factor.

Interlocking system

Every block has three holes at the bottom and three protrusions on top. This makes it possible to interlock the blocks and build a modular structure. Connected blocks can work together and hold one another in place. Due to installation considerations, the diameter of the holes is slightly larger than the diameter of the protrusions (see Figure 3.3). It allows blocks that are not perfectly placed to still interlock. On the other hand it results in more freedom of movement. This tolerance is 4.5 mm for the model blocks.

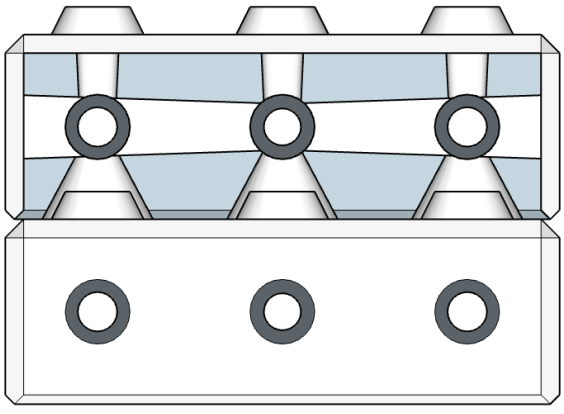

Figure 3.3: Cross-section showing the tolerance of the interlocking system.

3.3 Flume setup

For the experiments, the eastern part of the Scheldt Flume from Deltares is used. The flume is 55 m long, 1 m wide and has a height of 1.2 m. The flume is able to generate waves, currents, or a combination of the two. A pumping system in the flume allows it to regulate the water

level. Figure 3.4 shows an overview of the flume with its components. Each component will be discussed below.

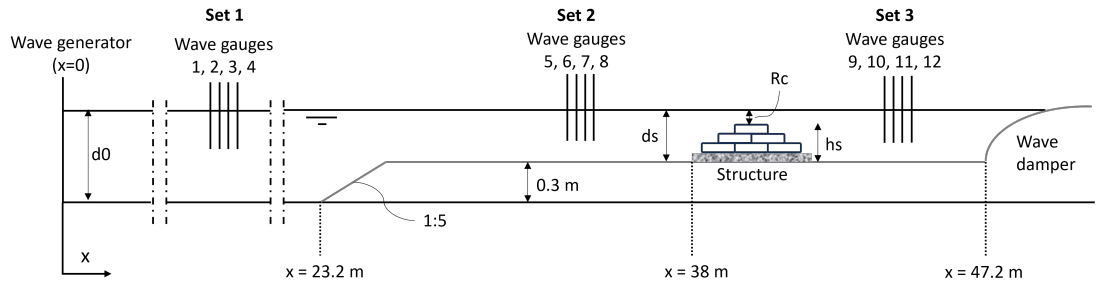

(a) Structure at main location.

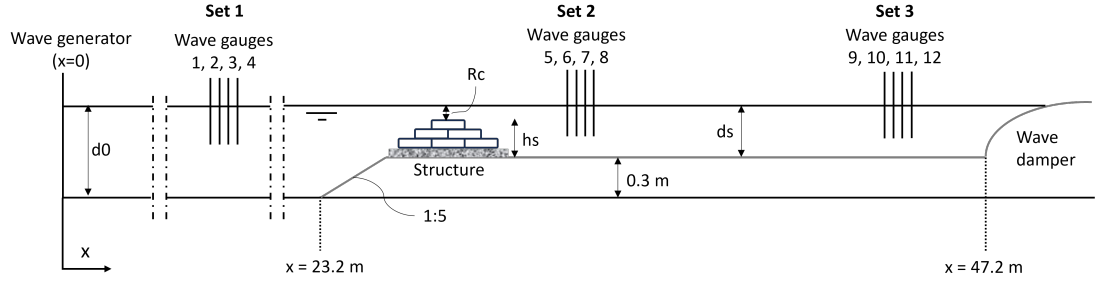

(b) Structure at alternative location.

Figure 3.4: Layout of the flume, including the main components and locations.

With parameters:

- d_0 = Offshore water depth [m]
- d_s = Water depth at structure [m]
- h_s = Height of the structure [m]
- $R_c = h_s - d_s$ = Freeboard of the structure [m]

Wave generator

The wave generator is a piston-type translatory wave board that is equipped with Active Reflection Compensation (ARC), which is a system that is able to compensate for the reflected waves. This system was active during all the tests. The maximum significant wave height that the wave generator can produce is 0.25 m and it has a frequency range of 0.01 - 2 Hz. The location of the wave maker is set to $x = 0$.

Wave damper

On the other side of the flume, a parabolic wave damper is installed. It dampens the waves and limits the reflection back to the wave gauges and structure. The damper is attached to a lifting cable and can be adjusted to the suitable height every time the water level in the flume is lowered or raised to absorb most of the wave energy. The location of the front of the wave damper is $x = 47.2\ m$

Foreshore

The wave maker can generate significant wave heights up to one third of the water depth. So, in order to have relatively higher waves compared to the local water depth at the location of the structure, a foreshore is installed. The front part of this 0.3 m high foreshore has a slope of 1:5. This slope was selected, since steeper slopes are more likely to be found in coastal areas with natural reefs. The length of the foreshore is chosen to be 24 m, because there needs to be enough space between the slope, the structure, the damper and the wave gauges for them to not interfere with one another. The part of the flume between the wave generator and the foreshore is called the offshore part.

Location of the structure

The location of the structure is chosen such that it corresponds with the location of the flume that contains the widest glass window (Figure 3.5). This makes it possible to properly film and observe the front- and backside of the structure under an angle without being blocked by the steel frames.

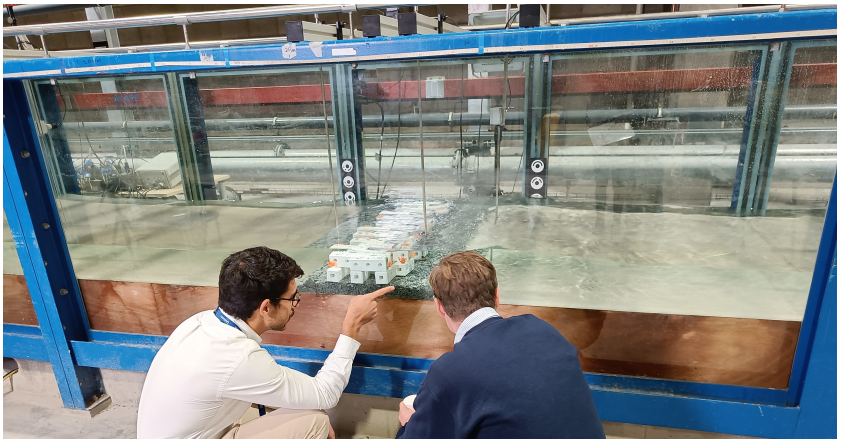

Figure 3.5: Part of the flume wall with the wider glass window.

The toe of the structure is kept constant for the majority of the tests at the location $x = 38\ m$. However, for some tests it was decided to move the structure more forward and closer to the toe of the foreshore (Figure 3.6). At this location ($x = 25\ m$), it was possible to achieve wave breaking, caused by the slope instead of the REB, resulting in higher impacts on the structure.

Figure 3.6: Alternative location of the structure, close to the slope.

Wave gauges

A wave gauge (WG) is a sensor that can measure wave heights based on electrical conductivity. The wave gauges are put in sets of four, as this is needed for the wave decomposition method. In total 3 sets are installed in the flume. One in the offshore part, the second set just before the structure and another set behind the structure. In this way, the wave transformation between the offshore and nearshore can be determined, as well as the wave transmission over the structure. In addition, a movable wave gauge was installed as well. All wave gauges were calibrated by Deltares before the experiments.

Set	Wave gauge	Location
1	1	$x = 14.65$
	2	$x = 15.45$
	3	$x = 15.9$
	4	$x = 16.2$
2	5	$x = 35.15$
	6	$x = 35.75$
	7	$x = 36.05$
	8	$x = 36.3$
3	9	$x = 40.28$
	10	$x = 40.88$
	11	$x = 41.18$
	12	$x = 41.45$
Moveable	13	Variable

Table 3.2: List of all wave gauges and their locations. All x values are in [m].

Flow velocity sensors

Electromagnetic liquid velocity meters are sensors that can measure flow velocity along a probe in two perpendicular directions based on electromagnetic conductivity. During the experiments, three of these sensors are used at variable locations. They are zeroed out at the start of each day when there is no flow in the flume.

Video cameras

The structure was filmed with video cameras from three different positions. Two cameras next to the flume, one filming the front and the other filming the rear side of the structure (Figure 3.7). The third video camera was mounted on top of the flume and filmed the top view of the structure.

(a) Front view. **(b)** Rear view. **(c)** Top view.

Figure 3.7: Video camera footage from different angles.

Underlayer

In reality, the REB is likely to be placed on a scour protection layer. Placing the blocks on the flat foreshore, like happened during the previous experiments, would not be a representative situation. In order to imitate reality as closely as possible, an underlayer is constructed. The thickness of the underlayer is equal to one block height and made out of gravel with a grading of 8-11 mm. This underlayer is on both sides protected by a gravel armour layer with a grading of 22-40 mm.

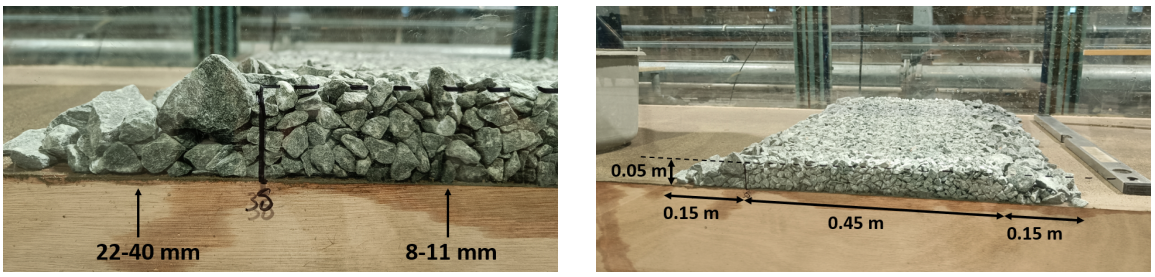

(a) Close-up of the underlayer toe. **(b)** Entire underlayer.

Figure 3.8: Dimensions and gradings of the underlayer.

For the tests with the structure on the alternative location near the slope of the foreshore, the armour layer was strengthened with rocks of grading 40-80 mm.

For most tests, irregularities in the underlayer within a range of +/- 1 cm were created by hand to mimic realistic construction accuracy. This value is based on practical values from the Rock Manual (2007), which suggests that the placing tolerance of a side stone dumping vessel is +/- 20 cm. This is named underlayer 1.

During one of the testing days, the irregularity of the underlayer was increased to see how that affects the stability of the structure. It was chosen to make it quite extreme, expecting to observe a noticeable difference. This unevenness of the gravel layer can clearly be seen when the REB is placed on top of it (Figure 3.9). The blocks were barely tamped when placed on top of the underlayer. This is named underlayer 2.

(a) Underlayer 1. **(b)** Underlayer 2.

Figure 3.9: Setups with different underlayer irregularities.

3.4 REB configurations

There are various possibilities when it comes to the configuration of the REB. This includes for example the number of layers, the complexity, orientation, and the efficiency in terms of

number of blocks per unit length.

It was chosen by Reefy to limit the maximum number of levels to 3 and also to mainly focus on 2 levels structures during these experiments.

From previous experiments that Reefy conducted, it was concluded that the blocks in the top layer are the first to start moving. A clear difference in behaviour was observed between the two possible orientations of these top blocks. Blocks with an orientation in the wave direction are significantly more stable than blocks with an orientation perpendicular to the wave direction. This can be explained by the difference in frontal area and the distance to the pivot point. Therefore, the majority of the setups has this favourable top block orientation (Figure 3.10). In reality, it is likely that waves are obliquely incident and coming from different directions, but that is not comparable with the unfavourable orientation as all top layer blocks are supported by neighbouring blocks and prevent one another from being pushed off. Because of the used production method, each block has one open and one closed outer end (see Appendix 8). During the tests, the outer end that is in front, facing the waves, is always the closed one (see Figure 3.7).

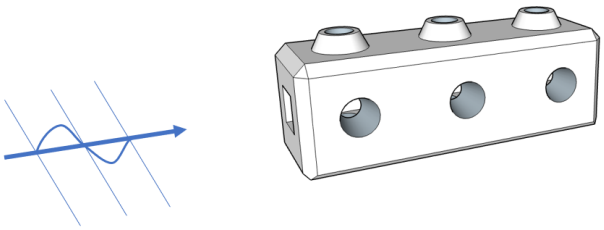

Figure 3.10: Smart block orientation with respect to wave direction.

The most straightforward configuration is the 'simple form'. It is robust and its shape is comparable with a conventional rubble mound breakwater. Therefore, it is expected to be more stable with respect to other variations.

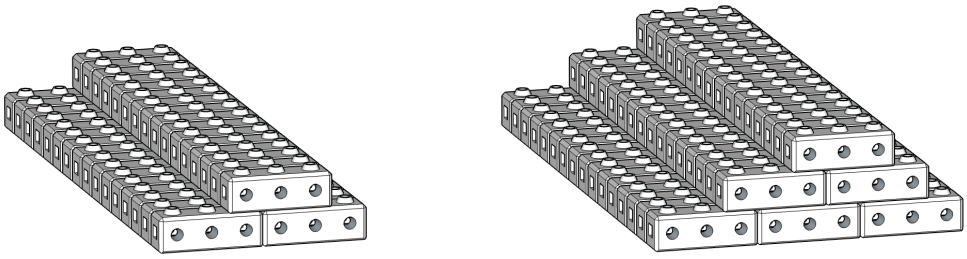

(a) 2 level structure. **(b)** 3 level structure.

Figure 3.11: REB configurations with simple form.

Regarding ecology, adding complexity to the structure by creating a variation of holes, overhangs and tunnels is favourable. This requires even less blocks than for the simple form. However, due to the complexity, blocks are more exposed and might be more susceptible for wave impacts and currents.

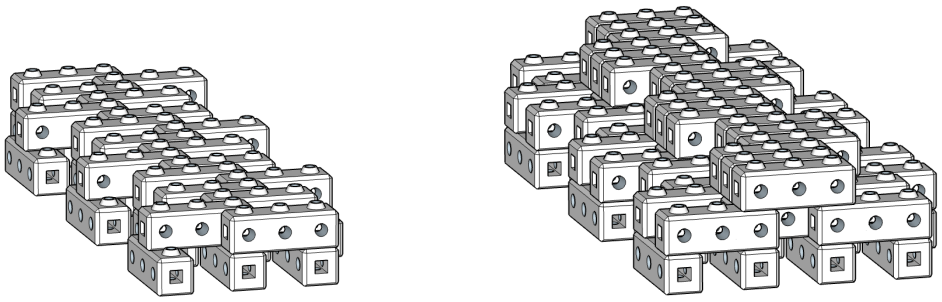

(a) 2 level structure. **(b)** 3 level structure.

Figure 3.12: REB configurations with complex form.

In total, 22 different setups are tested during the experiments. Images of all setups can be found in Appendix 8. However, some of the setups were used for different purposes and are not relevant for this research. The setups that are relevant for this research are listed in (Table 3.3)

Setup	Height	Description
Setup 1	2 levels	REB combination of variations including unfavourable orientated top blocks
Setup 2	2 levels	REB combination of simple and complex form
Setup 3	3 levels	REB combination of simple and complex form
Setup 4	2 levels	REB with simple form
Setup 5	3 levels	REB with simple form
Setup 6	3 levels	REB with complex form
Setup 7	2 levels	REB with complex form
Setup 8	2 levels	REB with complex form including epifauna
Setup 9	2 levels	REB made out of randomly placed blocks
Setup 10	3 levels	REB combination of simple and complex form
Setup 12	3 levels	REB with complex form
Setup 13	2 levels	REB with complex form
Setup 14	2 levels	REB with simple form, placed on very irregular underlayer
Setup 15	2 levels	REB with complex form, placed on very irregular underlayer
Setup 16	2 levels	REB with simple form, placed near foreshore slope
Setup 17	2 levels	REB with simple form, placed near foreshore slope
Setup 18	2 levels	REB with complex form, placed near foreshore slope

Table 3.3: Overview of the relevant setups. Setup 11 was removed from list set as it served a different purpose

In setup 8, two top block variations are tested (Figure 3.13). One block variation has rounded edges and no protrusions. As no other blocks will be stacked on top of these blocks, the protrusions are deemed unnecessary and can be left out. The idea behind this variation is to find out how the smoothness of the block may influence the behaviour of the block. Because the protrusions are missing, this block variation has a slightly lower volume and weight than a standard ReefBlock. The other variation in this setup contains additional roughness on top,

mimicking marine growth on the structure. These blocks have a slightly higher volume and weight than the standard ReefBlock. To mimic the presence of marine life even more, some holes of the top blocks are sealed with clay. Also, plastic corals are glued to the base blocks. These features increase the pressure and drag forces on the blocks.

Figure 3.13: Setup 8, two top block variations and marine growth. Rounded top blocks on the left, additional roughness top blocks on the right.

Setup 9 consists of blocks that are dropped in different orientations until a REB with height of about 2 levels is formed (Figure 3.14). There is a large difference in how individual blocks are interlocked or supported by others. It also causes some blocks to have an unfavourable orientation or be in a more exposed position. The goal of this setup is to get a qualitative understanding of such an unstructured configuration and find out if it could be a serious alternative for the other REB configurations in places where advanced placement methods are limited.

Figure 3.14: Setup with randomly placed blocks.

3.5 Test conditions

Both regular and irregular waves are used for the experiments. For stability research it is common to use irregular waves as they give a better representation for real life wave conditions. A JONSWAP wave spectrum with a peak enhancement factor of 3.3 was used for the majority of the tests. This spectrum is often used for physical modelling of coastal areas. Tests with irregular waves require about 1000 waves to obtain a representative spectrum. While for regular waves, all waves are equal, so that does not require a minimum number of waves and this can save some time. Therefore, it was chosen to use regular waves on the first testing day. This gave the opportunity to determine critical values relatively quickly by fast iteration. Moreover,

on some of the testing days there were other experiments that took place in the offshore part of the flume simultaneously, which required regular waves as well.

The considered hydraulic variables in this study are water depth, wave height and steepness. Offshore water depths ranged between 0.47 m and 0.62 m for the tests with regular waves and between 0.42 m and 0.62 m for the irregular wave tests. Generated regular wave heights varied between 0.05 m and 0.15 m. For the irregular wave tests, significant wave heights varied between 0.05 m and 0.16 m. It was tried to find the highest depth limited wave height for each water level. The water level was raised when the waves started breaking before reaching the structure. The steepness ranged mainly between 0.02 and 0.04. Water depth, wave height and steepness were chosen and the corresponding wave period was calculated using linear wave theory (Equation 2.5). Wave signals corresponding to the target wave height and period were made and uploaded to the wave generator. All files were given names that had all important values included in their name. For example: D1d47H05T0903s4IA, which is an abbreviation for Day 1, water depth 0.47 m, wave height 0.05 m, wave period 0.903 s, wave steepness 0.04, irregular waves, first run.

An overview of all the test conditions, with regular and irregular waves, can be found in Table 3.4 & Table 3.5 respectively. Note that these are input values and not necessarily match with the actual conditions that are produced by the wave generator.

Condition	d_0 $[m]$	H $[m]$	T $[s]$	s $[-]$
R1	0.47	0.05	0.903	0.04
R2	0.47	0.05	1.391	0.02
R3	0.47	0.05	2.457	0.01
R4	0.47	0.06	0.802	0.06
R5	0.47	0.07	0.870	0.06
R6	0.47	0.08	0.860	0.07
R7	0.47	0.08	0.935	0.06
R8	0.47	0.08	1.192	0.04
R9	0.47	0.08	2.020	0.02
R10	0.47	0.10	1.063	0.06
R11	0.47	0.10	1.391	0.04
R12	0.47	0.10	2.457	0.02
R13	0.47	0.11	2.679	0.02
R14	0.47	0.12	2.020	0.03
R15	0.47	0.13	1.431	0.05
R16	0.47	0.13	1.700	0.04
R17	0.47	0.14	1.805	0.04
R18	0.47	0.15	1.912	0.04
R19	0.52	0.08	1.176	0.04
R20	0.52	0.08	1.951	0.02
R21	0.52	0.10	1.362	0.04
R22	0.52	0.10	2.362	0.02
R23	0.52	0.12	1.071	0.07
R24	0.52	0.12	1.176	0.06
R25	0.52	0.12	1.553	0.04
R26	0.57	0.12	1.520	0.04
R27	0.57	0.12	2.681	0.02
R28	0.57	0.14	1.281	0.06
R29	0.57	0.15	1.340	0.06

Table 3.4: Overview input values of all the regular wave conditions.

Condition	d_0 $[m]$	H_{m0} $[m]$	T_p $[s]$	$s_{0,p}$ $[-]$
I1	0.42	0.06	1.010	0.04
I2	0.42	0.07	1.875	0.02
I3	0.47	0.05	0.903	0.04
I4	0.47	0.08	1.192	0.04
I5	0.47	0.08	1.458	0.03
I6	0.47	0.08	2.020	0.02
I7	0.47	0.10	1.391	0.04
I8	0.47	0.10	1.735	0.03
I9	0.47	0.10	2.457	0.02
I10	0.47	0.12	2.020	0.03
I11	0.47	0.15	2.457	0.03
I12	0.52	0.10	1.054	0.06
I13	0.52	0.10	1.362	0.04
I14	0.52	0.10	1.684	0.03
I15	0.52	0.10	2.362	0.02
I16	0.52	0.11	2.571	0.02
I17	0.52	0.12	1.176	0.06
I18	0.52	0.12	1.553	0.04
I19	0.52	0.12	1.951	0.03
I20	0.52	0.12	2.782	0.02
I21	0.57	0.12	1.520	0.04
I22	0.57	0.12	2.681	0.02
I23	0.57	0.14	1.705	0.04
I24	0.57	0.14	2.152	0.03
I25	0.57	0.14	3.085	0.02
I26	0.57	0.16	1.894	0.04
I27	0.57	0.16	3.493	0.02
I28	0.62	0.16	1.848	0.04
I29	0.62	0.16	3.368	0.02

Table 3.5: Overview input values of all the irregular wave conditions.

Table 3.6 shows the applied conditions per setup.

Setup	Conditions
Setup 1	R1, R2, R4, R6, R8, R9, R11, R19, R20, R21, R22, R23, R24, R25
Setup 2	R7, R8, R9, R10, R20, R22, R24, R26, R27, R28, R29
Setup 3	R26, R27, R28
Setup 4	I3, I4, I5, I13, I16, I21, I22
Setup 5	I21
Setup 6	I21
Setup 7	I3, I4, I5, I8, I12, I13, I16, I17, I18, I20
Setup 8	I3, I4, I5, I9, I16
Setup 9	R1, R3, R5, R9, R11, R12, R13, R14, R15, R18
Setup 10	R11, R14, R15, R16, R17, R18
Setup 12	I3, I4, I5, I6, I13, I14, I15, I18, I19, I20, I23, I24, I25, I26, I27, I28, I29
Setup 13	I1, I2, I6, I14, I15
Setup 14	I3, I4, I6, I13, I15, I18, I20
Setup 15	I4, I6, I13, I15, I18, I20
Setup 16	I5, I7, I10, I11
Setup 17	I7, I10, I11
Setup 18	I7, I10, I11

Table 3.6: Overview of the conditions per setup.

Online record sheets were used to note visual observations.

3.6 Mobility sensor

Two smart ReefBlocks have been made that are able to measure motion. These specially designed blocks are equipped with small compartments that contain a 9-axis inertial measurement unit. This sensor, comparable with the one in your smartphone, is able to measure 3 components of acceleration, rotation rate and magnetic field. The sensor is connected to a tiny processor board, micro SD card board and external battery. It is able to log and save data without being wired to a computer, making it a fully stand-alone sensor. A micro SD card 32GB type V30 is used. The sensor is made fully waterproof so it can function while the block is submerged. After drying, the sensor can be connected to a laptop to retrieve the stored data from it and to recharge the battery. The compartment clamps itself into the block and can be removed from the block easily. Two reed switches, that can be controlled with magnets, have been integrated in the system to control the battery and USB port connection. This prevents short circuits from occurring and makes it possible to turn the sensor on and off. Extra steel was added to the concrete mixture to obtain the same weight as the regular blocks. An overview of the production process of these sensor blocks can be found in Appendix 8. These smart ReefBlocks are based on and created similarly as the previously developed smart rocking armour units described by Hofland et al. (2018), Caldera (2019), Houtzager (2020) & Hofland et al. (2023). The blocks are placed in the flume when movements were observed. The signal of the sensor could be reset after each test by placing a magnet near the reed switch. The locations of these switches are marked with black dots.

(a) Internal structure of the compartment.

(b) Sensor compartments wired to laptop.

(c) Sensor compartments placed in blocks.

Figure 3.15: Smart ReefBlocks.

The sensor has a sampling frequency of 100 Hz and logs the data after 50 samples. When the thresholds $\mid \omega \mid = 0.05$ and $\mid a_{tot} \mid = 1.03$ are not exceeded, it only saves a data point every 0.5 second.

3.7 Photogrammetry

To determine the irregularities in the underlayer, photogrammetry is used. This technique combines photos from different angles to generate a 3D model. Before a REB configuration was placed on top of the layer of gravel, 60 to 100 photos were taken of this underlayer from different positions and angles. This quantity of photos provides sufficient overlap for an object of this size. Plates with circular markers are placed on all sides around the underlayer to increase the accuracy. These markers can serve as reference points for a coordinate system as well. Two marker plates are glued to the flume wall and have a permanent position throughout all tests.

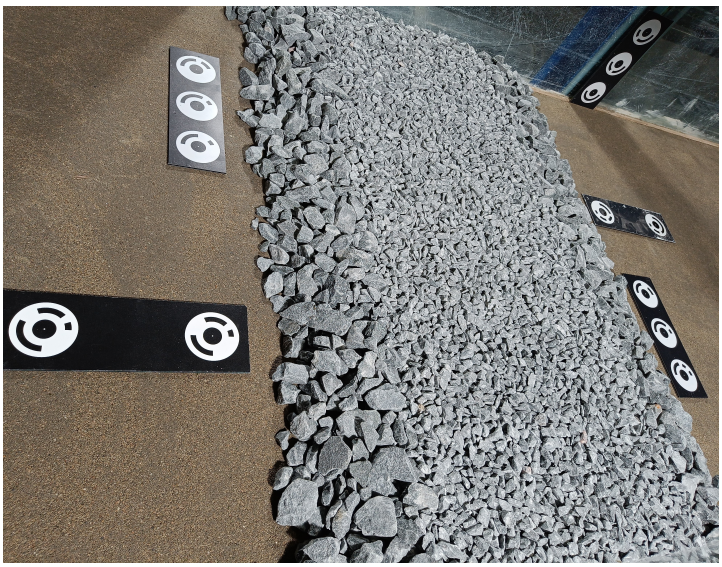

Figure 3.16: Photo of the underlayer with surrounding markers plates.

4
Data processing

Data has been collected by the wave gauges, cameras and mobility sensors. For further analysis, some of the data requires processing. This processing includes decomposition of wave data, quantifying movements and photogrammetry.

4.1 Data selection

A distinction was made how the data of each setup is used for answering each research question. This selection is based on the wave type, the location of the structure, and the available dataset. An overview is given in Table 4.1.

Setup	**Research question 1**	**Research question 2**	**Research question 3**	**Research question 4**
Setup 1	x			
Setup 2	x			
Setup 3	x			
Setup 4	x	x	x	
Setup 5	x		x	
Setup 6	x		x	x
Setup 7	x	x	x	x
Setup 8	x	x	x	x
Setup 9	x			
Setup 10	x			x
Setup 12	x	x	x	
Setup 13	x	x	x	
Setup 14	x	x	x	x
Setup 15	x	x	x	x
Setup 16	x	x		x
Setup 17	x	x		x
Setup 18	x	x		x

Table 4.1: Used data for answering each research question. Setup 11 is disregarded as it served for a different purpose.

4.2 Wave decomposition

During wave flume experiments reflection occurs, caused by the flume boundaries, the foreshore and by the structure. Even with a parabolic wave damper and ARC in the wave paddle, there still is some reflection. This causes the wave gauges to measure wave signals that are

coming from both directions. Therefore, the wave signal must be decomposed into incoming and reflected waves. In this research, the method of Zelt and Skjelbreia (1992) is used for the wave decomposition. This is a common method to decompose one-dimensional wave fields and is based on linear wave theory. Spin up and spin down times were removed from the signal. The script for wave decomposition was provided by Deltares, generating a variance density spectrum from which the following parameters were derived:

- H_{m0} - Spectral significant wave height
- $H_{1/3}$ - Mean of the highest one-third of the waves
- $H_{1/50}$ - Mean of the highest 1/50 of the waves
- $H_{1/150}$ - Mean of the highest 1/150 of the waves
- T_p - Peak period
- $T_{m-1,0}$ - Mean spectral energy period
- T_{m01} - Mean spectral wave period

For the data analysis, it was chosen to work with the significant wave height H_{m0} and peak period T_p.

4.3 Video data

The videos of all tests are processed. Together with the record sheet notes, it was qualitatively described for each test what happened by answering the following questions:

1. Are there movements?
2. Which blocks are moving?
3. What type of movement is it?
4. In what direction does it move?
5. Are there displacements?

These observations led to some first outcomes:

- Mainly top blocks are moving
- Sliding in the wave direction is the most occurring type of movement
- 2 level structures move less than 3 level structures
- 2 level simple form moves less than 2 level complex form
- 3 level complex form moves less than 3 level simple form

Based on these outcomes, it was decided that, for the quantitative analysis, the focus should be on the sliding movements in the top layer. As determined in Table 4.1, setups 4, 7, 8, 12, 13, 14, 15 are suitable for such an analysis, therefore they were reanalysed to quantify the movements. The procedure was as follows:

1. Only consider top layer
2. Disregard blocks of the outer rows because of wall influence
3. Scrolling through video frames instead of playing entire video
4. Back and forth movements are counted as separate movements
5. Divide by the number of blocks that are considered

6. Divide by the total number of waves

The method of going through video frames instead of watching the entire video is chosen because it makes it easier to spot individual movements. Particularly when several blocks have to be watched simultaneously. The method is substantially faster than watching the entire video as well. An alternative would be to count all movements within a small timespan and divide it by the number of waves within that period of time. But for an irregular wave series, this time span should be rather long to get an average value that is a good representative for the entire test. To validate the used method, it was checked that there is sufficient time between two consecutive movements, so that no movements were missed. Also, it was compared with the other method in which the entire video was watched, resulting in matching values.

The counted sliding movements are further analysed using python (version 3.8.8).

4.4 Photogrammetry

Photogrammetry is used to determine the irregularity of the gravel bed. The photos of underlayer 1 and underlayer 2 are loaded into Agisoft Metashape (version 2.1.0). This software combines images and converts them into a 3D model. It starts with rating the quality of the uploaded images and assigns a value to it between 0 and 1. The higher this value, the better the quality of the image. The Agisoft manual recommends excluding images with a value lower than 0.5. Most photos were rated above 0.8, which implies sufficient quality. The software automatically recognises the marker plates that were used. These markers improve the alignment of the images and are used for the orientation and scaling of the model. After the photos are aligned, point clouds of over 2 million points were generated. The point clouds were then exported and have been further analysed in python.

The point clouds of both underlayers are displayed in Figures 4.1 & 4.3. The irregularity of the underlayer is determined by only considering the top part of the underlayer, on which the structure is placed (Figures 4.2 & 4.4).

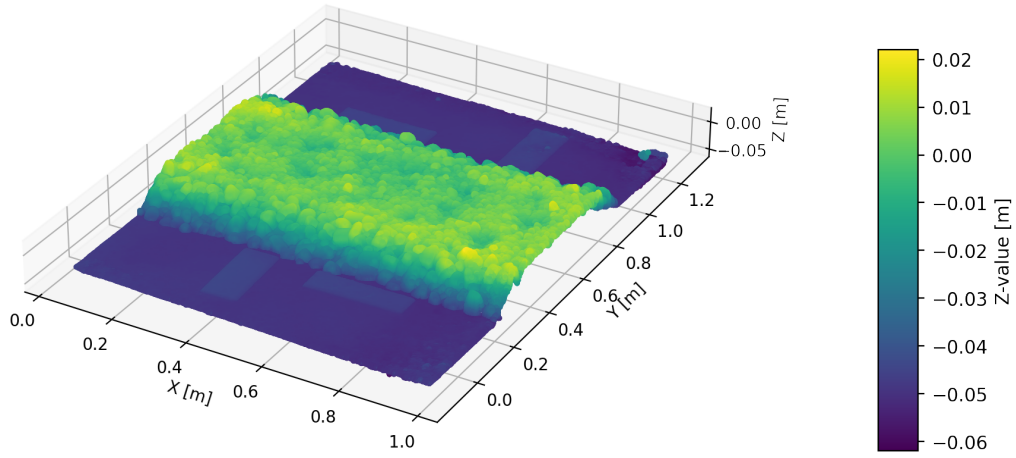

Figure 4.1: Point cloud of entire underlayer 1.

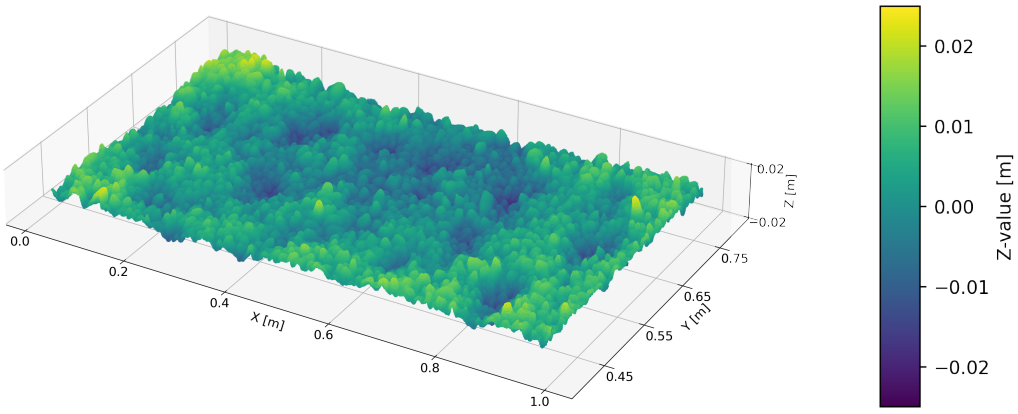

Figure 4.2: Point cloud of the top part of underlayer 1.

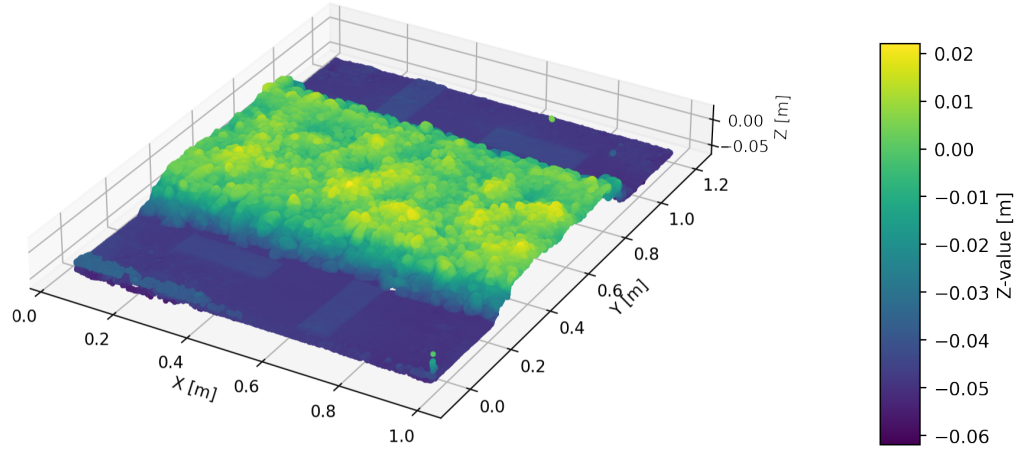

Figure 4.3: Point cloud of entire underlayer 2.

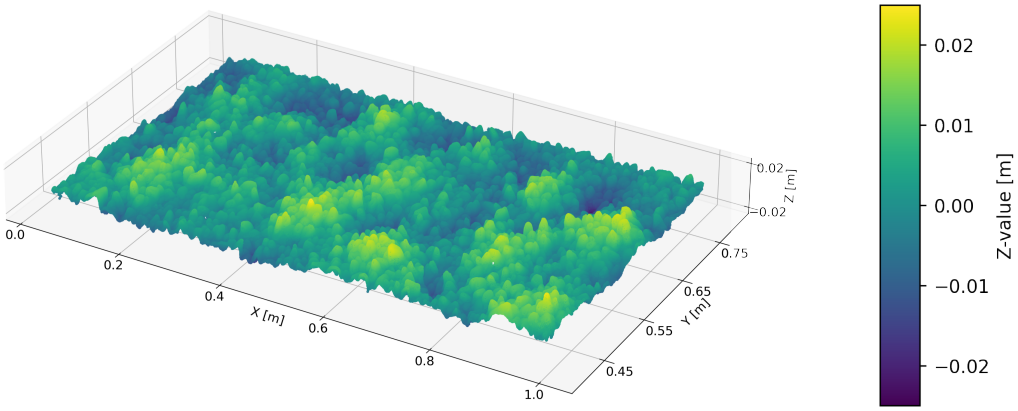

Figure 4.4: Point cloud of the top part of underlayer 2.

The irregularity of the underlayer can be expressed in terms of standard deviation and the height difference between highest and lowest point. These values are calculated for both underlayer and presented in Table 4.2

	Standard deviation [mm]	Lowest [mm]	Highest [mm]	Height difference [mm]
Underlayer 1	4.0	-15.8	16.1	31.8 (± 1.5 D_{n50})
Underlayer 2	5.8	22.4	21.6	44.0 (± 2 D_{n50})

Table 4.2: Values representing the irregularity of the underlayers.

It can be seen that underlayer 2 has a higher standard deviation and maximum height difference, and is therefore more irregular than underlayer 1. Both underlayers exceed the placing tolerance stated in the Rock Manual (2007), which is ± 1 D_{n50} for light gradings and ± 0.2 m (= 10 mm for 1:20 scale model) for coarse gradings.

4.5 Mobility sensor data

After drying, the sensor blocks were connected to a laptop. The data was retrieved from the SD with a serial port terminal application called CoolTerm (version 2.0.1) and saved as .txt file. This text file contains columns with the x, y, z values of the acceleration and the angular velocity. This has been further analysed using python. The data is used to determine the impact velocities of both sliding and rocking movements. A test was performed to determine the directions of the sensor axes (Figure 4.5).

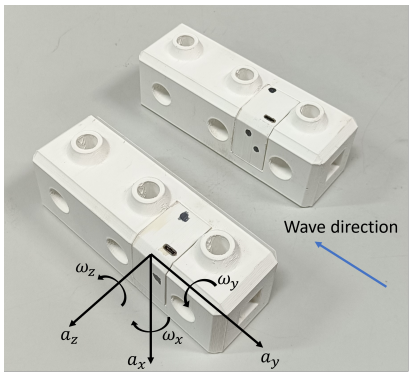

Figure 4.5: Sensor orientation in the block. a_x, a_y, a_z correspond to the acceleration. $\omega_x, \omega_y, \omega_z$ are the directions of the angular velocity.

Within this research, the emphasis lies on the extreme events only. The data is plotted against the time and by zooming in on the graph, single extreme events become visible. The timescale of single movements is in the order of tenths of a second.

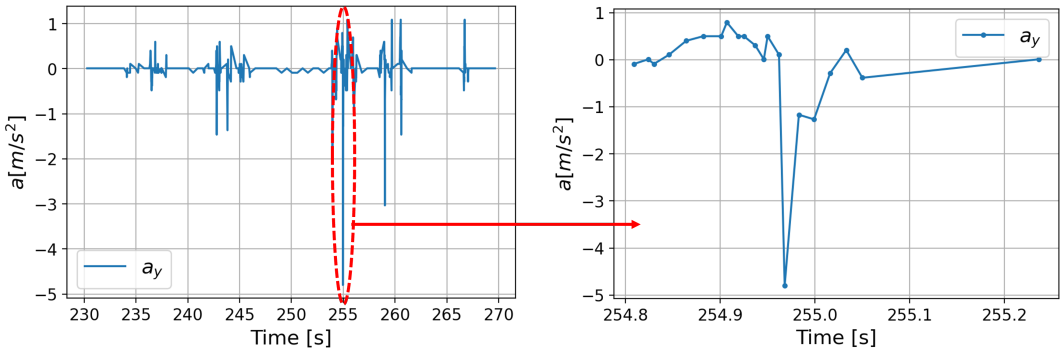

Figure 4.6: Zooming in on the extreme event of the dataset (test D4d52H12T1176s6IA, setup 7).

Rocking impact velocity

As rocking is a rotational movement, the impact velocity can be deducted from the measured angular velocity, by multiplying the peak value by the length of the block.

$$v_i = |\omega_z|_{max} * L_{block} \tag{4.1}$$

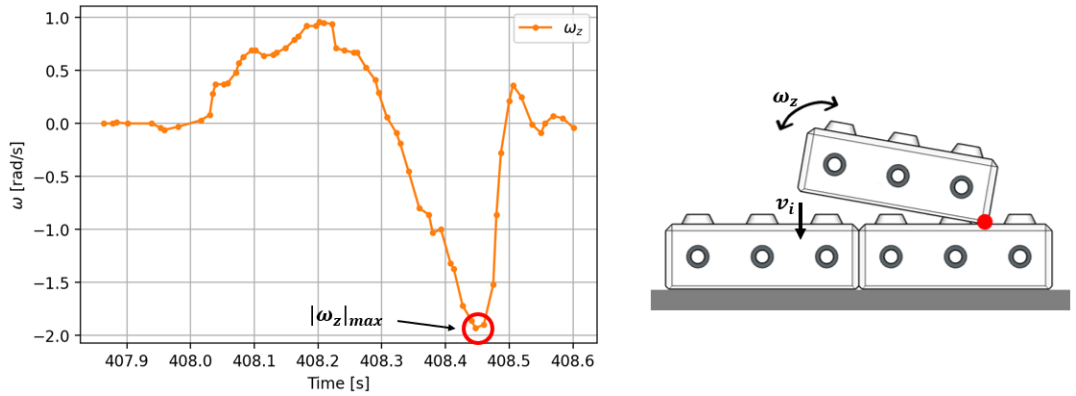

Figure 4.7: Determining the impact velocity of a rocking movement (test D10d47H12T2020s3IB, setup 17).

Sliding impact velocity

Sliding is a translational movement from which only the acceleration was measured. To get the sliding impact velocity, the acceleration up to the moment of impact is integrated over the time.

$$v_i = \int_{t_1}^{t_2} a_y \, dt \tag{4.2}$$

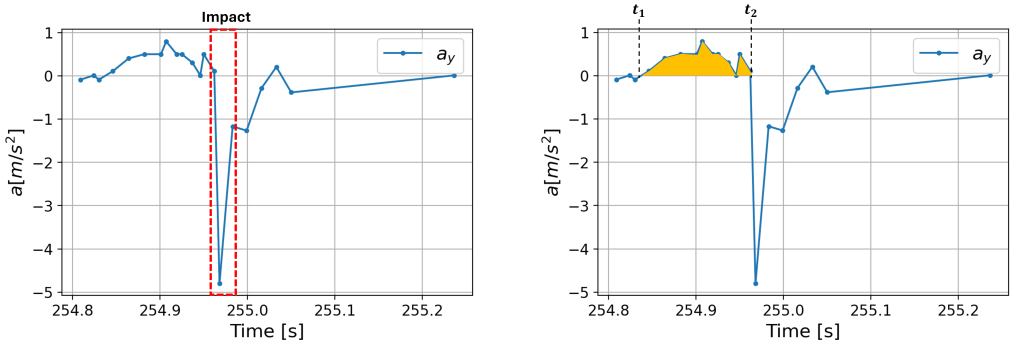

(a) Impact moment of a sliding collision.

(b) Part to be integrated (orange).

Figure 4.8: Determining the impact velocity of a sliding movement by integrating the acceleration before impact.

5 Test results and analysis

In this chapter, the outcomes of the wave flume experiments are presented and analysed. The results include the different types of movement for each setup, as well as the limit states and damage levels. Subsequently, an extensive analysis is performed on the sliding movements. Thereafter, the data of the mobility sensor is used to make a prediction on the structural performances of the ReefBlocks.

5.1 Waves

To get more insight into the waves that are used during the tests, the wave data collected from the wave gauges positioned in front of the structure is plotted into the Le Mehaute diagram (Figure 5.1). This diagram illustrates the applicability of different wave theories. From this diagram, it can be seen that the incoming waves near the structure fall outside the range of linear theory. This is a good representation of waves in the real world, which are non-linear as well. However, it should be noted that the used decomposition method is based on linear wave theory.

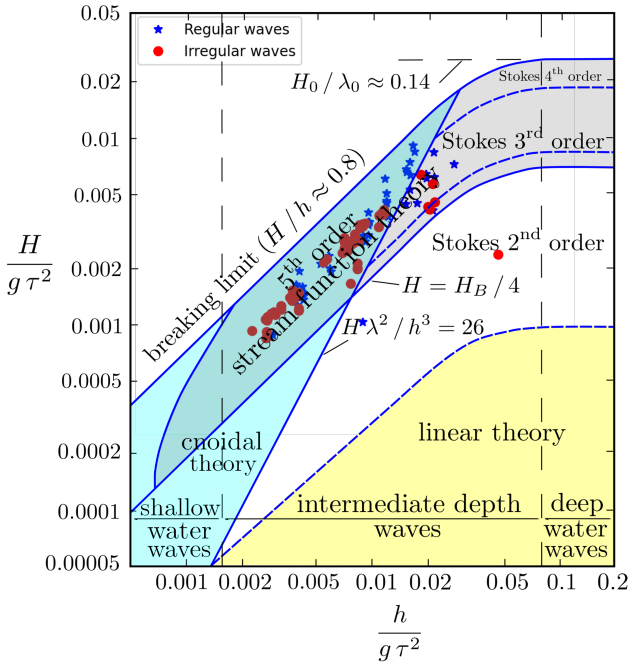

Figure 5.1: Wave data from wave gauge set 2 plotted in the Le Mehaute Diagram. (Le Mehaute, 1976). H_{m0} is used for H, d_s is used for h, T_p is used for T. For the tests on the alternative location, the wave data from wave gauge set 1 is used.

Furthermore, it can be seen that all waves in front of the structure are in intermediate water depths. This implies that their characteristics depend on both the water depth and the wave period.

Wave heights measured by wave gauge set 1, located in the offshore part of the flume, are often lower than the wave heights in the steering files. This could be caused by imperfections of the wave maker, human errors while operating the wave maker and damper, errors of the physical model setup, energy loss, measuring errors of the wave gauges, errors during the decomposition of the wave data.

5.2 Types of movements

This section presents the various types of movements that were observed during the tests and explains why those specific movements happened.

Sliding

The most common type of movement is sliding. It is a horizontal translation and occurs when the horizontal force caused by the wave motion exceeds the frictional resistance between the blocks. This occurred in both directions along the longitudinal axis. When the peak of a high wave reaches the structure, it exerts a horizontal force on the block, pushing it backward. When the trough of a wave reaches the structure, it exerts an opposing force, pulling the block forward.

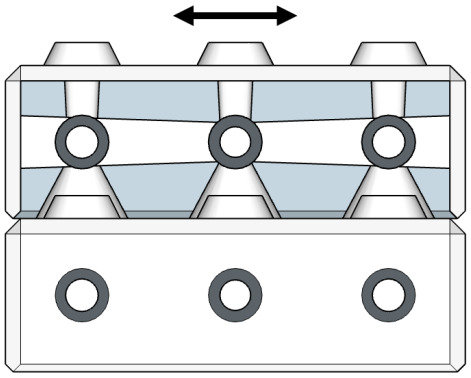

Figure 5.2: Sliding movement possible due to interlocking tolerance.

Sliding between two blocks is possible due to the difference in diameters of the holes and protrusions, which is 5 mm for the model blocks. Within this research, this is referred to as the interlocking tolerance. The sliding distances that were observed are equal to this tolerance.

Sliding was mainly observed in the top layer of the structure, which can be explained by the fact that the orbital wave motion in intermediate water depths is highest near the water surface (Figure 5.3). Given that the top layer of the REB is closest to the water surface, the horizontal forces are the largest in this layer. Apart from that, top blocks only have their own submerged weight acting as vertical pressure force, whereas the blocks in lower layers are loaded with the weight of those above them as well. As the horizontal resistance force is a fraction of this vertical component, the top blocks require less horizontal force to overcome this resistance and start sliding. Additionally, the top blocks are not sideways supported by other blocks, since the crest in most setups only consists of a single row of blocks.

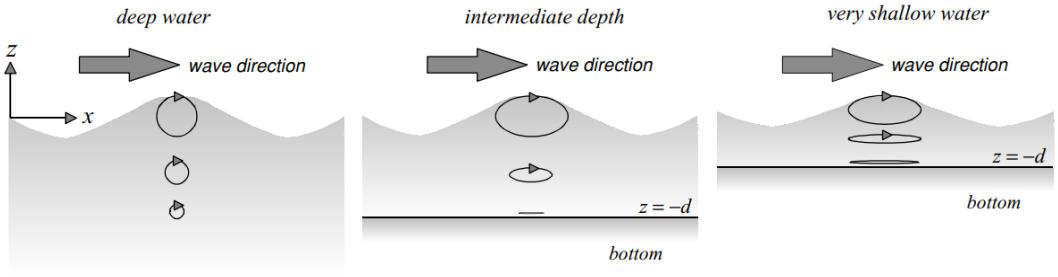

Figure 5.3: The orbital motion in deep water, intermediate-depth water and very shallow water. (Holthuijsen, 2007)

The fact that sliding was observed in nearly all setups emphasizes the importance of the interlocking system. Without interlocking, the blocks would start sliding, without being stopped, and slide off the structure. Therefore, it is crucial that the protrusions do not break. During the experiments none of the protrusions did, but as the model does not scale for structural performances, it is necessary to verify whether the protrusions of the prototype can handle these impacts. This is further analysed in Section 5.6.

Rocking

Based on visual observations, rocking was the second most occurring type of movement. Rocking is the rotational back and forth movement of one or multiple blocks. This mechanism is quite broad as the movement can occur in several directions and within different ranges. The direction and magnitude depend on the freedom of movement and the orientation of the block.

Rocking can be caused by a certain imperfection in the underlayer. This can result in a lack of support and the emergence of pivot points. Since the REB was placed on a gravel underlayer for all tests, there were imperfections in almost every setup, leading to rocking. Figure 5.4 illustrates different rocking movements observed during the experiments, caused by the unevenness of the underlayer.

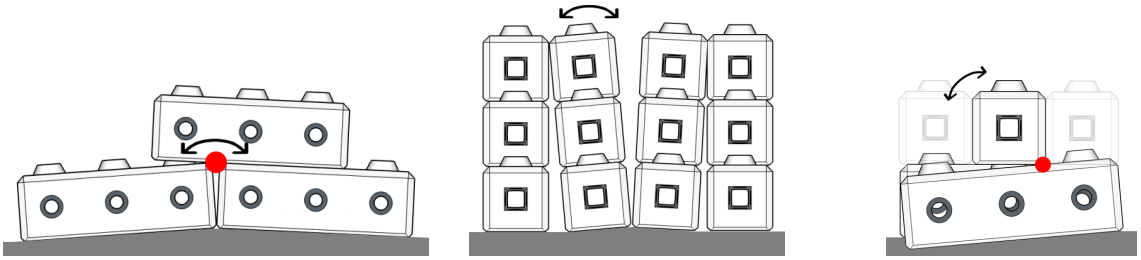

(a) Side view of the 2 level simple form REB.

(b) Front view of the 3 level simple form REB.

(c) Front view of the 2 level complex form REB.

Figure 5.4: Different types of rocking caused by an uneven underlayer. The red dots represent the pivot points.

Without these imperfections, rocking can still happen, but requires higher wave loads. This type of rocking can be confused with tilting, but the difference is that the block returns to its initial position, while a tilting block does not. This can happen for two different top block orientations.

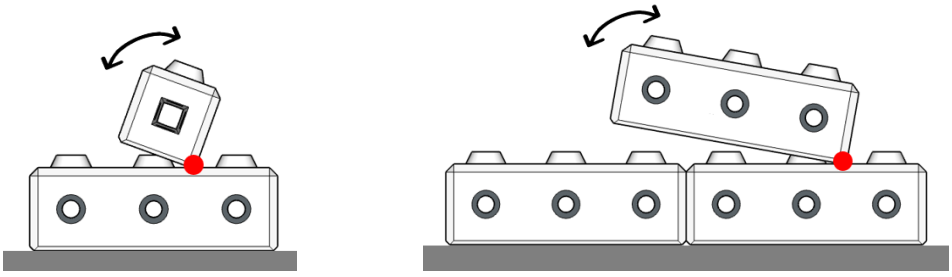

(a) Rocking of top block in unfavourable orientation (side view)

(b) Rocking of top block with smart orientation (side view).

Figure 5.5: Observed rocking types. The red dots represent the pivot points.

The rocking in Figure 5.5a was only observed in setup 1 because that setup was the only one with the unfavourable top block orientation. The rocking of Figure 5.5b was mainly observed during the tests with the structure on the alternative location. On the main location, this type of rocking was rare.

Shaking

Another observed movement was a combination of sliding and rocking. The base blocks are not able to properly transfer the forces from the top blocks to the underlayer and start acting as pivot points caused by their less stable orientation, perpendicular to the wave direction. This makes it possible for the top blocks to translate. This movement is defined as shaking. It can happen for the front block only, but also for the entire structure. There were no displacements caused by shaking and the structure always returned to its initial position.

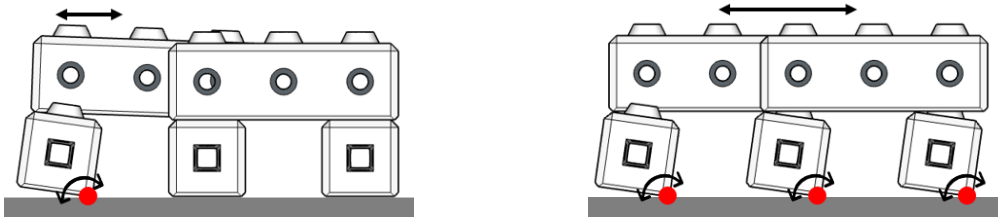

(a) Front part of the stack shaking (side view).

(b) Entire stack shaking (side view).

Figure 5.6: Two types of shaking. The red dots represent the pivot points.

Shaking was a rare movement, which only happened for the 2 level complex form configuration. The reason for this movement is the orientation of the base blocks, which have a small distance from gravity force component to the point of rotation. Although the base blocks of the 3 level complex form REB have the same orientation as those in the 2 level complex form, no shaking movements were observed for this configuration. This could be explained by the increased vertical pressure on these base blocks due to the weight of the extra layer on top.

Tilting

Tilting is the movement where a block rotates around a pivot point and, in contrast to rocking, not returns to its initial position.

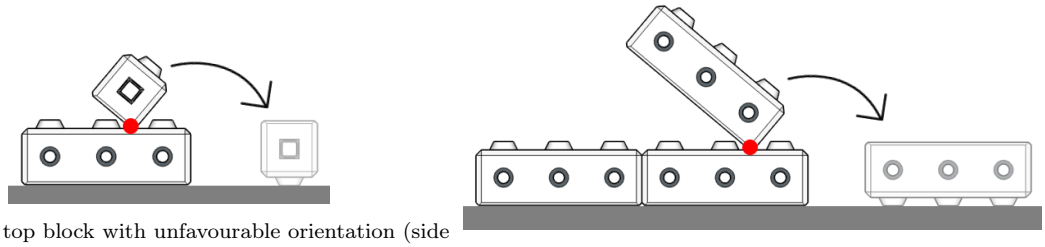

(a) Tilting top block with unfavourable orientation (side view).

(b) Tilting top block with smart orientation (side view).

Figure 5.7: Two types of tilting. The red dots represent the pivot points.

Figure 5.5 & 5.7 also clearly illustrate the reason for the favourable and unfavourable top block orientations. The distance from the centre of mass to the pivot point is larger for the smart orientation, which requires a much higher force to rotate it.

Beforehand it was known that it would be better to place the top blocks in the smart orientation and therefore all setups, except for setup 1, have this favourable top block orientation. Tilting of top blocks with the smart orientation was not observed for a structure at the main location of the structure. Only in the setups on the alternative location in the flume near the transition slope, the blocks tilted.

Lifting

The last type of movement that was observed is defined as lifting. This movement is the vertical translation of a block, often in combination with horizontal movement, such that it ends up in a different location. On the main location of the structure, the wave loads were insufficient for lifting to happen. It was only observed in setups 16, 17 and 18. On this alternative location, some of the blocks migrated backwards and interlocked itself again on the next protrusion. But for the higher wave loads, the blocks got lifted off the structure at once and ending up behind the structure.

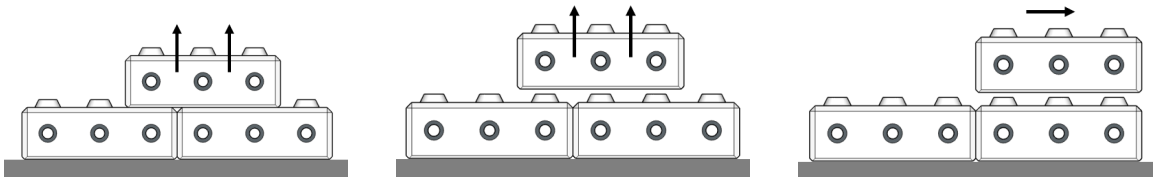

(a) **(b)** **(c)**

Figure 5.8: Block migrating backwards due to lifting.

5.3 Observations per setup

This section describes the visual observations for the various setups and is based on both the live observations during the experiments and the observations in the videos. First, this is done for the structure on the main location. Secondly, the observations of the REB on the alternative location are presented.

Main location

The main location of the structure is located on top of the foreshore between wave gauge sets 2 and 3, away from the slope. (see Figure 3.4a)

Top block orientation (Setup 1)

In setup 1, the two different top block orientations were tested using regular waves. The configuration included stacks with 1 top block in the unfavourable orientation, stacks with 2 top blocks behind one another in the unfavourable orientation, and some rows with smart top block orientation (Figure 5.9).

Figure 5.9: Setup 1.

There were no movements observed for the blocks with smart orientation. But in the other stacks, regular movements were observed, particularly in the stacks with 1 single top block. The blocks started rocking already during the first test with the lowest wave heights. The wave height was gradually increased, which led to more intense rocking motion like in Figure 5.5a. The wave period was tuned until resonance was reached. One top block started resonating, tilted and fell off the structure. The regular wave height during this particular test was 0.074 m and the steepness was 5.4%. The wave period of the test in which the block resonated and displaced, was equal to 1.07 seconds. This means that the natural frequency of the unfavourable orientated block is close to 0.93 Hz. For the full scale ReefBlocks (1x1x3 m) this would translate to 0.21 Hz. From the moment the block started rocking, it still took 12 waves before it finally fell off the structure.

There were no displacements in other stacks, which means that the stability can be somewhat improved by placing a second top block behind the other. The choice for the unfavourable top block orientation is depending on the conditions and can be an option in rivers for instance. This should be considered for each location, but the smart top block orientation is recommended.

2 level simple and complex (Setup 2)

Setup 2 consisted of a 2 level structure, partly in the complex form (see Figure 3.12a) and partly the simple form (see Figure 3.11a). This setup was tested using regular waves. Sliding and rocking was observed, mainly in the stacks with complex form. For a 2 level structure, the simple form seems to be more stable than the complex form.

Three different water levels were tested during this setup with corresponding freeboard values of -0.02 m, -0.07 m and -0.12 m. For the freeboard of -0.02 m, the highest waves did not result in movements. It should be noted that these waves are depth limited and therefore smaller than the waves that were tested for the other freeboards. Most movements were observed for a freeboard equal to -0.07 m. When the freeboard was decreased further to -0.12 m, the blocks were no longer moving. Even though the wave height was increased up to 0.137 m, not a single block moved for this water level. The structure is too submerged for instabilities to occur, because most of the wave energy passes over the structure. Based on these observations, it is likely that the structure will remain stable for even higher water levels as well. The influence of

the freeboard is further analysed in Section 5.5.

3 level simple and complex (Setups 3, 5, 6, 10)

A combination of the 3 level simple and complex form (see Figures 3.11b & 3.12b respectively) was tested in setups 3 and 10 using regular waves. There were no movements observed in the stacks with complex form, while the rows with simple form were constantly rocking and sliding.

In setups 5 & 6, a REB with simple form and a REB with complex form were tested for irregular waves. The setups were used to fill up the last testing hour of the day and were therefore only tested with one wave condition. Because the same wave condition was used during these tests, a clear comparison can be made. These tests show similar results compared to the regular wave tests: for a 3 level structure, the simple form is moving significantly more than the complex form. During these tests, the wave transmission was 2.8% higher for the complex form than for the simple form, indicating that the simple form leads to somewhat more intense wave breaking and thus somewhat more wave energy dissipation. This could be caused by the difference in permeability, which has been observed by Van Gent et al. (2023) to be an influencing factor for low-crested coastal structures. The difference in permeability can be explained by the number of blocks in the cross-section (per block width), which is equal to 4 and 6 for the complex and simple form respectively.

Contrary to expectations, it was found that for a 3 level REB the complex form is more stable than the simple form. This can be explained by the difference in support and connection with neighbouring blocks. The simple form is missing that support, resulting in more freedom of movement. The influence of small deviations at the base blocks increases towards the top layer, resulting in larger gaps between neighbouring blocks (Figure 5.4b). The rocking movements were predominantly concentrated around these gaps. Due to this outcome, it was decided already during the experiments not to proceed with extensive testing of the 3 level simple form, as this configuration lacks advantages when compared to the complex form. Its better performance in wave transmission was considered in this decision. However, this difference was deemed insufficiently important compared to other criteria such as stability and block efficiency.

2 level simple form (Setup 4)

In setup 4, only the 2 level simple form was tested with irregular waves. This configuration exhibited almost no movements, which is in line with the expectations. Sliding movements of top blocks were observed only sporadically. The structure is compact and all blocks are positioned in the same orientation. The blocks are not connected with neighbouring rows, which leaves room for movement in sideways direction. However, these sideways movements are not observed a lot. Apart from a few sliding events, the structure looked very stable.

2 level complex form (Setup 7 & 13)

The 2 level complex form was tested in setups 7 & 13 using irregular waves. Multiple movements were observed for this configuration. Top blocks were rocking like Figure 5.4c, induced by the exposure of the front top blocks. Due to lack of sideways support, the blocks have the freedom to start rocking. Furthermore sliding was observed. Horizontal wave forces pushing the blocks back and forth. During the highest waves, the base blocks encountered difficulty in transferring the forces generated by the sliding top blocks to the underlayer and started to act as pivot points. This resulted in a shaking structure as illustrated in Figure 5.6. The freeboard for which this happened was equal to -0.07 m. Despite the various movements, there were no displacements.

3 level complex form (Setup 12)

In setup 12, the 3 level complex REB was extensively tested using irregular waves. This configuration exhibited sliding movements in the top layer and frequent rocking motion in the middle and top layer. This configuration moves more than a 2 level structure, which can be explained by the increased structure height. An equal freeboard corresponds for the 3 level structure to a larger water depth, which can carry larger waves. Although the base blocks of the 3 level complex form REB have the same orientation as those in the 2 level complex form, no shaking movements were observed for this configuration. This could be explained by the increased pressure on these base blocks due to the weight of the extra layer. No displacements were observed during the tests of this configuration.

Four different water levels were tested during this setup with corresponding freeboard values of 0.03 m, -0.02 m, -0.07 m and -0.12 m. Most movements were observed for a freeboard of -0.02 m and -0.07 m. The influence of the freeboard is further analysed in Section 5.5.

Marine growth (Setup 8)

In setup 8, the 2 level complex REB from setup 7 was modified by adding miniature corals, stuffing some of the holes with clay and replacing some top blocks by ones with additional roughness. These adjustments increased the drag forces and resulted in more sliding movements. This setup did not lead to any damage.

Underlayer irregularity (Setup 14 & 15)

In setup 14 & 15 a 2 level simple and a 2 level complex structure were placed on top of a different underlayer. The increased irregularity of the underlayer was clearly visible through the skewed blocks. This caused some blocks to not properly interlock.

For the complex structure, this resulted in a displacement during the first wave condition. One block, resting on top of a protrusion, partially slid off the structure. Another loose block interlocked again after some waves. Once the structure settled a bit, it behaved similarly to the one on the less irregular underlayer. Despite increasing the wave height, there were no further displacements.

For the simple form REB the increased irregularity did not result in a lot of movements. Although there were more and larger gaps between blocks, it did not appear to have a notable influence on its stability.

Randomly placed blocks (Setup 9)

A randomly placed REB under regular wave loading was tested in setup 9. During the first test, one block settled into a new and more stable position. Another block was exposed and lacked direct support from neighbouring blocks, leading to constant rocking. The cross-section of the structure remained intact throughout the tests.

Alternative location

In setups 16, 17, 18 the structure was relocated closer towards the foreshore slope. This was done because the aim was to reach a failure, but that was not achieved on the main location. The combination of the foreshore slope, wave height and the water level caused

the waves to start plunging onto the structure. Plunging waves can cause far more damage compared to other waves, as they release the majority of their energy all at once, resulting in violent impacts. Similar to the setups on the main location, sliding and rocking movements were seen, but more intense. Other movement types were also observed, such as tilting and lifting.

In setup 16, the 2 level simple form was tested. The waves were not only plunging onto the REB, but also damaging the toe of the structure. Parts of the underlayer were washed away by the slamming waves, creating holes and leading to settlements of the frontmost base blocks. The settlements led to the formation of a large gap and exposed the bottom of the upper layer blocks, making them susceptible to uplift. While the frontmost base blocks are settling into the holes just in front of them, the other blocks are gradually pushed backwards, leading to a diverging structure. When a large plunging breaker eventually slammed into this gap, most of the top blocks were lifted and ended up behind the structure.

In setup 17 the same configuration was tested, but with an improved armour layer to prevent scouring like in the previous setup. The progression of damage was slower compared to setup 16. However, failure was still reached during the same wave condition with a significant wave height of 0.119 m. This wave height was measured with WG set 1, located in the offshore part of the flume. As the waves shoal due to the foreshore slope, the measured wave height is not representative for the wave height just in front of the structure. The height of the wave that led to the complete failure of the REB, was 0.186 m at WG set 1. The height at moment of breaking can be estimated from the videos and is about 5 times larger than the block height, corresponding to 0.25 m (Figure 5.10a). For a real scale ReefBlock of 3x1x1 m, this would be a 5 m high plunging wave. The measured shoaling factor for this particular wave is equal to 1.34. The theoretical shoaling factor was calculated with Equation 2.6 and is equal to 1.22.

(a) Before impact. **(b)** Moment of impact.

Figure 5.10: Plunging wave that led to failure of the structure.

The 2 level complex form was tested in setup 18 and also includes the improved toe structure. The damage progression in this setup was faster compared to the setups with complex form. This can be explained by the fact that the structure is less compact and the blocks are more exposed, making them more susceptible to wave impacts. Despite the fact that the structure was already severely damaged earlier, it only definitely failed for the same wave condition as the previous two setups.

Whether a wave plunges depends on the Iribarren number. According to Battjes (1974), the range for plunging breakers is approximately:

$0.5 < \xi_{0,p} < 3.3$ With $\xi_{0,p} = \frac{tan(\alpha)}{\sqrt{s_{0,p}}}$

For the tests at the alternative location, $\xi_{0,p}$ ranged between 1.10 - 1.45 (WG set1). These values of the Iribarren number confirm the emergence of plunging breakers. As described in section 2.3, the breaker type depends on the breaker index (γ_b) as well. A more conservative value of the Iribarren number, for which waves do not start plunging, can be derived from Figure 2.3 and is equal to 0.2.

Because plunging waves can lead to much more damage and even to failure of the REB, it should be examined per project area whether a plunging wave can occur at the location of the structure.

5.4 Limit states

In this chapter, the limit states and damage levels of the setups for which irregular waves were used, are determined. Again, the distinction is made between the main and alternative location.

Main location

An overview of the significant wave height ranges and corresponding stability numbers of the setups are listed in Table 5.1.

Setup	**Range of H_{m0} [m]**	**Range of N_s**
2 level simple	0.035 - 0.100	0.40 - 1.13
2 level complex	0.037 - 0.089	0.41 - 1.00
3 level complex	0.035 - 0.125	0.39 - 1.40
2 level complex (Marine growth)	0.036 - 0.085	0.40 - 0.96
2 level simple (Underlayer 2)	0.035 - 0.087	0.40 - 0.98
2 level complex (Underlayer 2)	0.058 - 0.088	0.65 - 0.99

Table 5.1: Ranges of the significant wave heights in front of the structure (WG set 2) and corresponding stability numbers of the setups on the main location (see Figure 3.4a).

The limit states are defined as:

- $N_{s,m}$ = Start of motion
- $N_{s,d}$ = Start of damage

The start of motion is equal to the moment at which one or multiple blocks within the structure move for the first time. This may be any type of movement. Damage is defined as the moment a block loses its interlocking with another block, also referred to as displacement. Start of damage is when this happens for the first time. Damage of corals and other epifauna are not considered within this research.

The precise values of the limit states are unclear due to the step size in wave heights. Therefore, the expected values are listed as well (Table 5.2). For example: if the structure did not move during the test in which $N_s = 0.5$, but it did move during the next test in which $N_s = 0.7$, the expected value for the start of movement ($E(N_{s,m})$) is equal to 0.6 with an uncertainty of 0.1.

Setup	$N_{s,nomovement}$	$N_{s,movement}$	$E(N_{s,m})$	Uncertainty
2 level simple	0.4	0.67	0.54	± 0.14
2 level complex	0.51	0.67	0.59	± 0.08
3 level complex	0.39	0.67	0.53	± 0.14
2 level complex (Marine growth)	0.4	0.66	0.53	± 0.13
2 level simple (Underlayer 2)	0.4	0.66	0.53	± 0.13
2 level complex (Underlayer 2)	0.65	0.87	0.76	± 0.11

Table 5.2: Expected values and uncertainties for the start of motion limit state (main location).

The expected value for the start of motion lies for most setups between 0.5 and 0.6. The complex REB on underlayer 2 falls outside this range. That can be explained by the limited number of wave conditions for which that setup was tested. Additionally, the wave height was stepwise decreased for this setup. By first testing the higher waves instead of the lower waves, time was saved as the water level had to be adjusted less often. This caused the structure to be better settled into a stable position compared to the other setups in which the water level was gradually increased. The limited number of wave conditions also contributed to the relatively high uncertainties. The wave height was mostly raised with steps of 2 or 3 cm. There was insufficient time to decrease the step size of the wave height, without being at the expense of other research objectives.

In a design, it is common to use the characteristic value instead of the expected value. The characteristic value can be determined by subtracting a part of the uncertainty from the expected value or by multiply the expected value by a safety factor. In this study, it is chosen to use the value of $N_{s,nomovement}$ as the characteristic value of the start of motion. Opting for the lower limit was deemed a safe decision as the available data was limited.

Damage level N_{od} can be calculated with Equation 2.13:

$$N_{od} = \frac{n_{dis} * D_n}{w}$$

In which:
n_{dis} = Number of displaced blocks
w = Width of the flume

Damage can also be expressed as a percentage:

$$Damage\ percentage = \frac{n_{dis}}{n_{tot}} * 100\%$$

In which:
n_{tot} = Total number of blocks in the flume

Setup	$N_{s,nodamage}$	$N_{s,damage}$	$E(N_{s,d})$	N_{od}	Damage [%]
2 level simple	1.13	Not obtained within the tested range	-	0	0
2 level complex	1.00	Not obtained within the tested range	-	0	0
3 level complex	1.40	Not obtained within the tested range	-	0	0
2 level complex (Marine growth)	0.96	Not obtained within the tested range	-	0	0
2 level simple (Underlayer 2)	0.98	Not obtained within the tested range	-	0	0
2 level complex (Underlayer 2)	0.65	0.87	0.76 (± 0.11)	0.067	3

Table 5.3: Values for the start of damage limit state and corresponding damage levels on the main location.

In Table 5.3 it can be seen that, except for the complex structure on underlayer 2, no damage occurred on the main location. Therefore, no expected value can be determined for the start of damage limit state. It is not likely that damage will occur for wave conditions outside the tested range of wave heights and freeboards of the submerged structure. Higher waves require larger water depths, and for these larger water depths the structure will be too submerged to result in damage.

The 2 level complex REB on underlayer 2 has equal values for the start of motion (Table 5.2) and the start of damage (Table 5.3). This may look strange, but it was the first movement that resulted in a displacement. The displaced block was not properly interlocked and partially slid off the structure.

The characteristic value of the start of damage limit state for the '2 level complex (Underlayer 2)' setup is chosen to be equal to the value of $N_{s,nodamage}$ and is equal to 0.65. For the other setups, no characteristic value can be determined, as no damage is expected at all.

Alternative location

Three setups were tested on the alternative location (see Figure 3.4b), in which the wave height was the only changing variable. An overview of the significant wave height ranges and corresponding stability numbers of the setups on the alternative location are listed in Table 5.4

Setup	Range of H_{m0} [m]	Range of N_s
2 level simple	0.068 - 0.119	0.76 - 1.34
2 level simple (improved toe)	0.084 - 0.119	0.94 - 1.34
2 level complex	0.084 - 0.119	0.94 - 1.34

Table 5.4: Ranges of the significant wave heights (WG set 1) and corresponding stability numbers of the setups on the alternative location.

Movements were already observed during the 'mildest' condition, so the start of movement limit state remains unknown. The damage levels and corresponding stability numbers are presented in Table 5.5

Setup	N_s	N_{od}	**Damage [%]**
Setup 16 (2 level simple)	0.76	0	0
	0.94	0	0
	1.12	0.73	19
	1.34	2.27	60
Setup 17 (2 level simple improved toe)	0.94	0	0
	1.11	0.20	5
	1.34	1.00	26
Setup 18 (2 level complex)	0.94	0	0
	1.11	0.40	15
	1.34	2.14	82

Table 5.5: Damage levels and corresponding stability numbers of the setups on the alternative location.

The influence of the improved toe structure is visible when setup 16 and 17 are compared. The damage levels of setup 17 are lower than that of setup 16. Comparing setup 17 and 18, it can be seen that the complex form suffers more damage than the simple form REB.

Setup	$N_{s,nodamage}$	$N_{s,damage}$	$E(N_{s,d})$
Setup 16 (2 level simple)	0.94	1.12	1.03
Setup 17 (2 level simple, improved toe)	0.94	1.11	1.03
Setup 18 (3 level complex)	0.94	1.11	1.03

Table 5.6: Values for the start of damage limit state and corresponding damage levels on the alternative location.

In this study, it is chosen to use the value of $N_{s,nodamage}$ as the characteristic value for the start of damage.

Failure

Failure corresponds to a certain damage level and can be defined in multiple ways and on different scales. Again, it is chosen to not include epifauna in the definition of failure, as this was not quantified. In this research, failure of the total structure is considered and is defined to be reached when a gap starts to appear in the cross-section. During the experiments, this corresponded to six displacements. This threshold is chosen because the formation of a gap adversely affects the breakwater's functionality in dissipating wave energy. The corresponding damage level is $N_{od} \geq 0.4$. This may sound as a lot, but a block is already counted as displaced when it is no longer in its initial position. This does not necessarily mean that it is removed from the structure. Blocks that migrate backwards and interlock on the next protrusion are counted as displacement as well. Using this threshold, a new limit state arises:

- $N_{s,f}$ = Failure

Failure was not reached for any of the structures on the main location, but only for the setups on the alternative location. The expected values of the corresponding stability numbers are listed in Table 5.7. The expected values are based on linear interpolation.

Setup	$N_{s,nofailure}$	$N_{s,failure}$	$E(N_{s,f})$	Uncertainty
2 level simple	0.94	1.12	1.04	± 0.1
2 level simple (improved toe)	1.11	1.34	1.17	± 0.17
2 level complex	0.94	1.11	1.11	± 0.17

Table 5.7: Expected values for the failure limit state of the setups on the alternative location.

The highest value is found for the simple form REB with the improved toe structure. Based on stability considerations, it is recommended that the 2 level simple form REB should be given preference on locations with plunging wave conditions.

In this study, it is chosen to use the value of $N_{s,nofailure}$ as the characteristic value of the failure limit state.

5.5 Sliding movements

Although it was tried to reach a failure, it appeared that this was not achievable on the main location. However, the structure did exhibit movements. To gain a better understanding of the stability and the influencing variables, the most common type of movement, sliding, is further analysed. The sliding movements of all irregular wave tests on the main location are quantified with the video method described in section 4.3, and compared with different variables.

Hydraulic variables

Wave height

One of the most important variables, when it comes to stability, is the wave height. In Figure 5.11, the significant wave height of the incident waves at the structure on the main location (derived from WG set 2) is plotted against the number of sliding movements. The main trend within this plot is that a higher significant wave height corresponds to more sliding movements. There are almost no sliding movements up to H_{m0} = 0.07 m. Until this value, the waves are not high enough to initiate movement. The tests with the most sliding events lie within the range H_{m0} = 0.08 - 0.12 m. For even higher waves, the number of sliding movements decreased again. The higher waves require larger water depths, leading to decreased freeboard values. When the structure gets more and more submerged, the waves start to feel the structure less and just pass over the structure. This was observed during the regular wave tests as well. This indicates that the freeboard is an important variable.

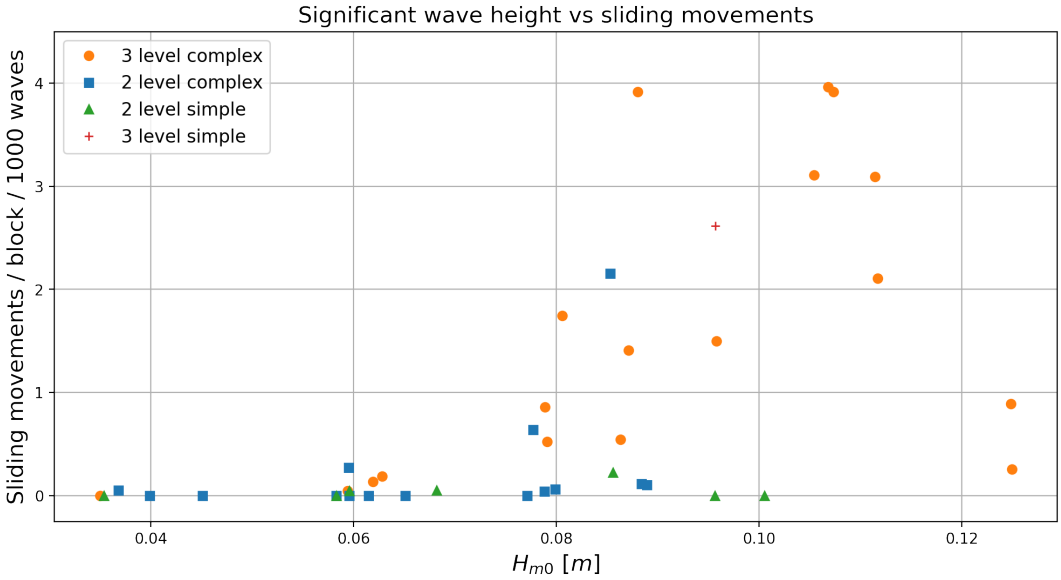

Figure 5.11: Significant wave heights (WG set 2) plotted against the number of sliding movements on the main location.

Dividing the significant wave height by the submerged density and the nominal diameter, results in the stability parameter $H_{m0}/\Delta D_n$ and makes the graph non-dimensional (Figure 5.12). The graph looks similar to the previous one, because ΔD_n was constant throughout the experiments. Furthermore it can be seen that the 3 level complex form REB exhibits more sliding movements compared to the 2 level structures and that most sliding movements happen for $H_{m0}/\Delta D_n > 0.8$.

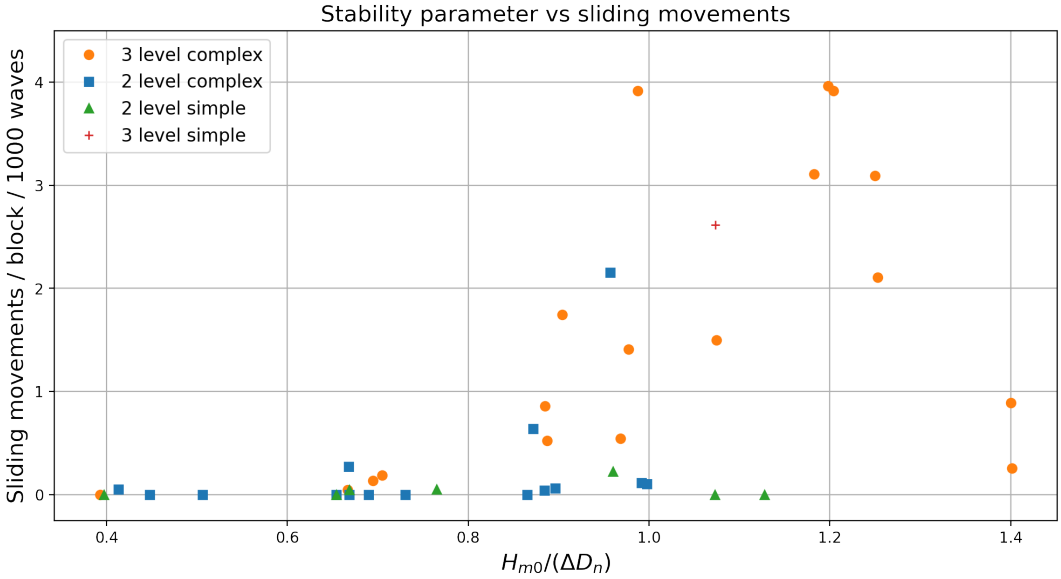

Figure 5.12: Stability parameter ($H_{m0}/\Delta D_n$) plotted against the number of sliding movements on the main location. H_{m0} of WG set 2 is used.

Relative freeboard

To further analyse the influence of submergence, the relative freeboard is plotted against the number of sliding movements (Figure 5.13). Note that a negative value of the freeboard (left side of graph) corresponds to the submerged state and the positive values (right side of graph)

correspond to the emerged state. For each of the four tested values of the freeboard, the tests with the most sliding movements are plotted. This is done for the three main configurations. The maxima correspond to the highest possible significant waves for that specific freeboard. Dividing these significant waves heights by the local water depths results in values close to 0.4. In Section 2.3 it was mentioned that waves start breaking when this ratio is in the range of 0.4 - 0.5. This confirms that the waves, corresponding to those maxima, are indeed the highest for that particular freeboard. Higher waves would break before reaching the structure. This was also checked during the experiments. Through the maximum values, a curve is fitted, which estimates the intermediate values.

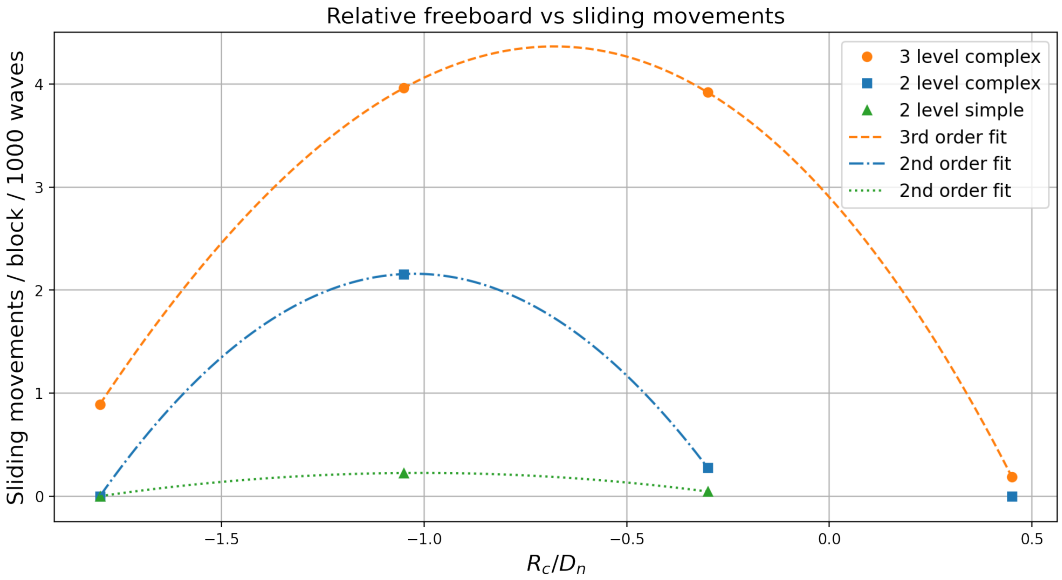

Figure 5.13: Maximum number of sliding movements on the main location per freeboard (indicated with the markers) within the range $-1.8 < R_c/D_n < 0.45$. For each configuration, a curve is fitted through the data points.

For the 3 level complex REB, the peak of the curve lies around $R_c/D_n = -0.7$, while for the 2 level structures, the peak is narrower and closer to $R_c/D_n = -1.0$. This can be explained by the difference in structure height. For equal values of the freeboard, the local water depth is larger for the 3 level structure than for the 2 level structure. A larger water depth also means larger waves and therefore more movements. The maximum wave height at $R_c/D_n = -0.35$ is equal to 0.06 m and 0.088 m for the 2 and 3 level structure respectively. Looking at Figure 5.11 again, it can be seen that a significant wave height of 0.06 m is not sufficient to cause many sliding movements, while a significant wave height of 0.088 m can.

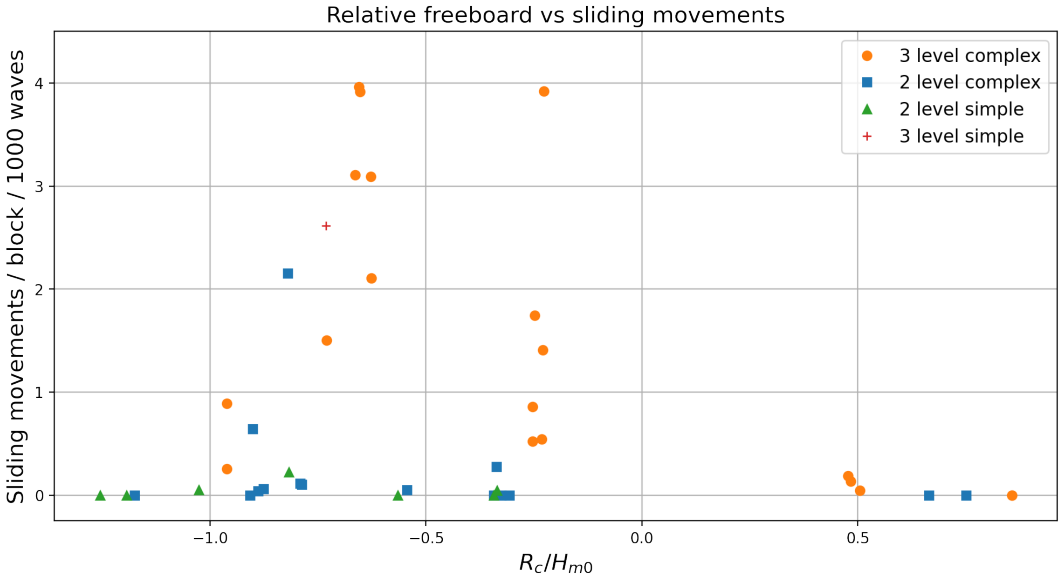

Figure 5.14: Relative freeboard (R_c/H_{m0}) plotted against the number of sliding movements on the main location. H_{m0} of WG set 2 is used.

Figure 5.14 shows a different relative freeboard, based on the significant wave height instead of the nominal diameter. Waves only lead to sliding moments, when the significant wave height is larger than the submergence.

Wave steepness

In Figure 5.15, the wave steepness s_p, calculated from the local water depth and peak period, is plotted against the number of movements. Similar wave conditions, in which only the steepness was changed, are connected by the dashed lines. Within the tested range, which is about 2% - 4%, a lower wave steepness leads to more sliding movements. This is in line with literature and can be explained by the fact that longer waves contain more energy.

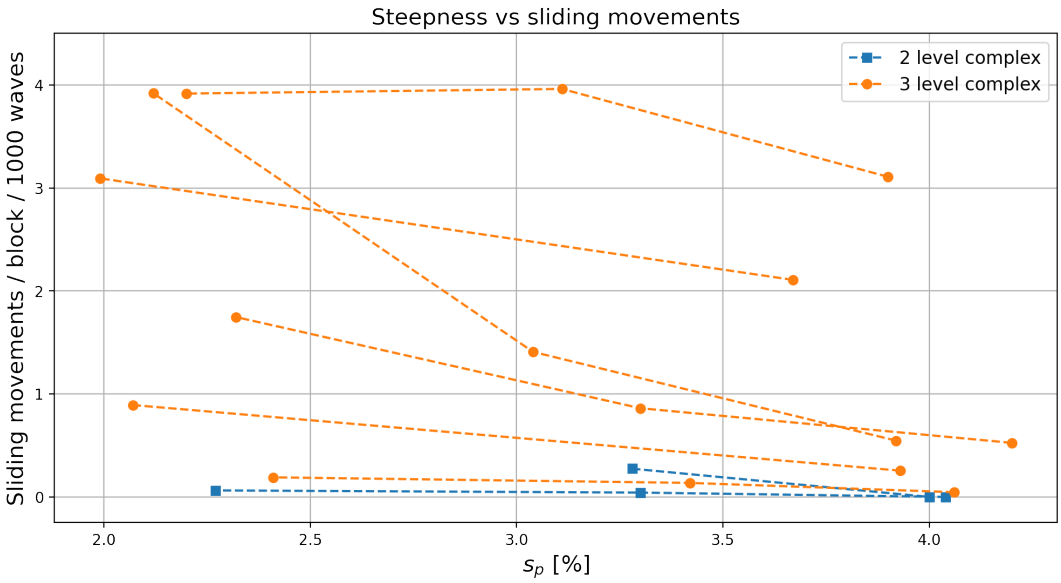

Figure 5.15: Wave steepness (WG set 2) plotted against the number of sliding movements on the main location.

Structural variables

Underlayer irregularity

Two underlayers with different irregularities were used on the main location. Underlayer 1 with a standard deviation of 4.0 mm, and underlayer 2 with a standard deviation of 5.8 mm. The 2 level simple and 2 level complex form have been tested on both these underlayers to examine its influence on the stability. In Figure 5.16, the sliding movements of the simple form are plotted for both underlayers. Unfortunately, the used wave conditions for the two different underlayers were not identical. However, that does not seem to matter because in both situations there were hardly any sliding movements. The increased irregularity does not seem to affect the number of sliding movements for the 2 level simple form.

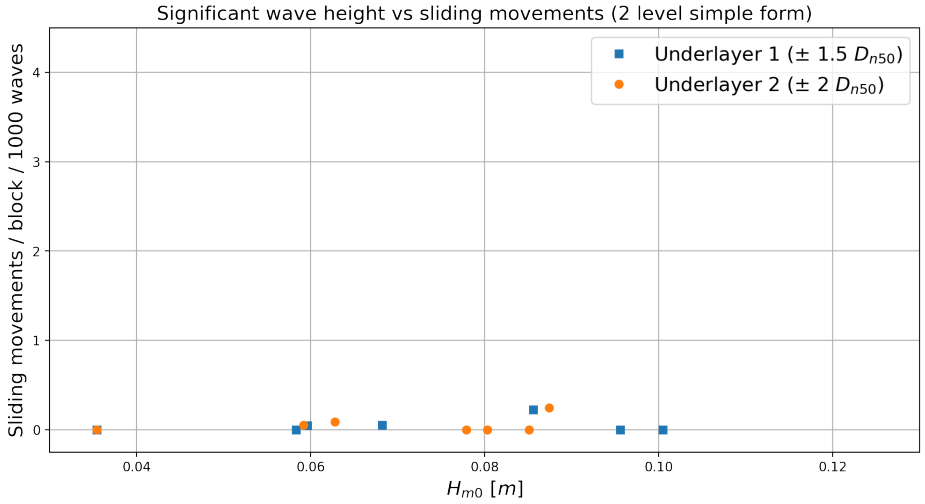

Figure 5.16: Influence of the underlayer irregularity for the 2 level simple REB on the main location. Significant wave heights of WG set 2 are used.

For the complex form, it is slightly different. There were more sliding movements in the tests with underlayer 2 (Figure 5.17). This is in line with the visual observations. Identical wave conditions were used, which allow for a good comparison.

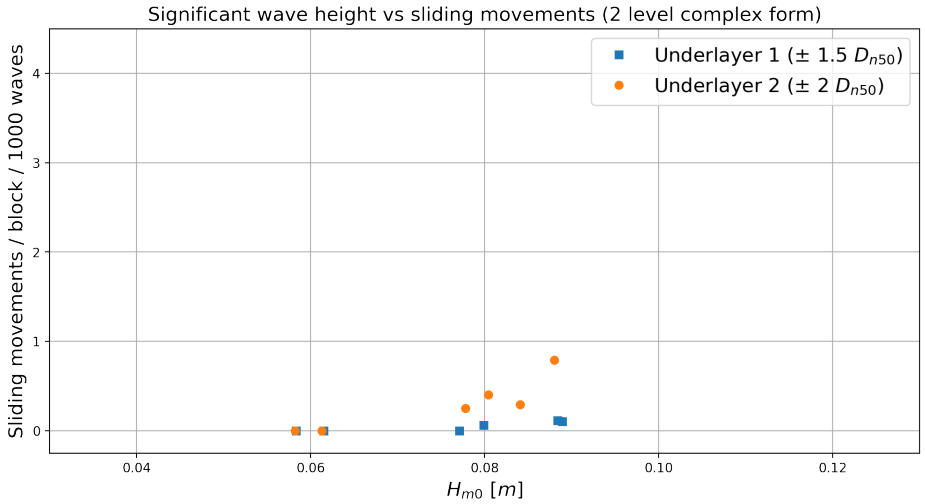

Figure 5.17: Influence of the underlayer irregularity for the 2 level complex REB on the main location. Significant wave heights of WG set 2 are used.

Marine growth

The influence of marine growth on the number of sliding movements is presented in Figure 5.18. Only the tests with identical wave conditions are plotted, which makes the number of data points limited. Still, it can be seen that there were more movements for the setup in which the epifauna added than for the setup without.

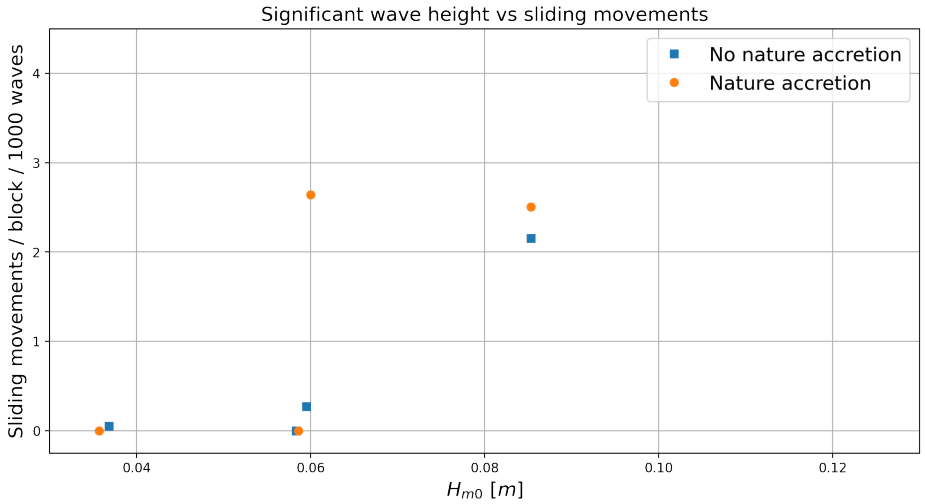

Figure 5.18: Influence of marine growth on the number of sliding movements on the main location. Significant wave heights of WG set 2 are used.

5.6 Block impacts

This section presents the impact velocities of two extreme sliding and rocking events. The structural performance of the protrusions is checked by making a conservative estimation of the sliding induced tensile stresses.

Impact velocity

Sliding

The impact velocity of the extreme sliding event is calculated with Equation 4.2 and equal to 0.044 m/s. Velocity scales to the power 0.5, implying that the impact velocity of the model needs to be multiplied by a factor $20^{0.5}$ to obtain the impact velocities of the full-scale ReefBlock (3x1x1 m). This results in: 0.197 m/s

Rocking

The impact velocity of the extreme rocking event is calculated with Equation 4.1 and equal to 0.3 m/s. Scaling this to a full-scale ReefBlock (3x1x1 m) results in: 1.34 m/s. On the main location, maximum rocking impact velocities in the order of 0.2 m/s were found.

The impact velocity of the extreme rocking event is higher than the impact velocity of the extreme sliding event. The difference can be explained by the fact that this extreme rocking event happened during the plunging wave tests on the alternative location, while the used sliding event happened on the main location. Also, a sliding movement is limited by the relatively small distance between the holes and the protrusions and therefore it only has a limited time to

accelerate before the impact. A rocking movement has much more space for movement, which allows it to reach a higher velocity.

The test during which the extreme rocking event happened, already led to damage of the structure. The impact on the structural performance is not checked in this research.

Sliding induced stresses

Whether the protrusions can withstand an impact velocity of 0.197 m/s, depends on the resulting tensile stresses in the concrete. This section presents a conservative approach to get a first estimate of the maximum tensile stresses in the protrusions.

Concrete strength

The strength of concrete depends on the class. For concrete class C55/67, which was previously used for a Reefy project, the static tensile strength is 4.21 N/mm^2 (Eurocode 2, 2004). However, concrete is stronger during short term loading. The exact strength depends on multiple variables, therefore Goud (2020) estimated a reasonable value for the impact strength based on CUR (1989):

$$f_{c,impact} = 2 * f_c = 8.42\ N/mm^2 \tag{5.1}$$

Because the timescale of sliding movements is in the order of tenths of a second, a tensile strength of 8.42 N/mm^2 is used. To determine the maximum stresses in the concrete, an impact force must be deducted from the velocity.

Impact force

In his study on rocking induced stresses, Goud (2020) schematized concrete armour units as a mass spring system in which the kinetic energy of the moving unit is absorbed by the elastic deformation of the protrusion. Based on the energy balance, the following formula for the impact force is deducted:

$$F = \sqrt{m * v_i^2 * k} \tag{5.2}$$

In which:

m = Mass of the block (5716 kg)
v_i = Impact velocity
k = Spring stiffness of the protrusion

The same approach is applied to protrusions of the ReefBlock. The assumption is made that one side of the protrusion takes on all the force. The system is schematized as a cantilever beam with a perpendicular force acting at the top (Figure 5.19 & 5.20).

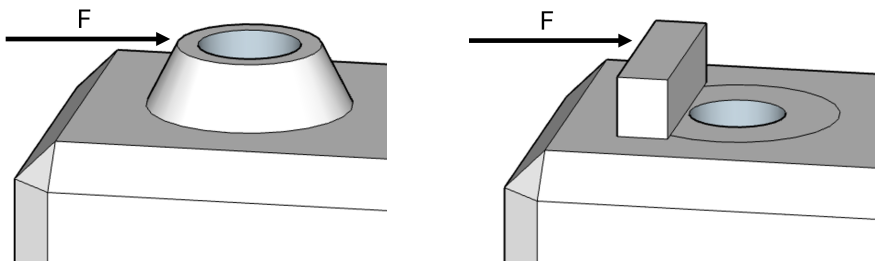

(a) Actual protrusion. **(b)** Assumed protrusion.

Figure 5.19: Simplification of the protrusion.

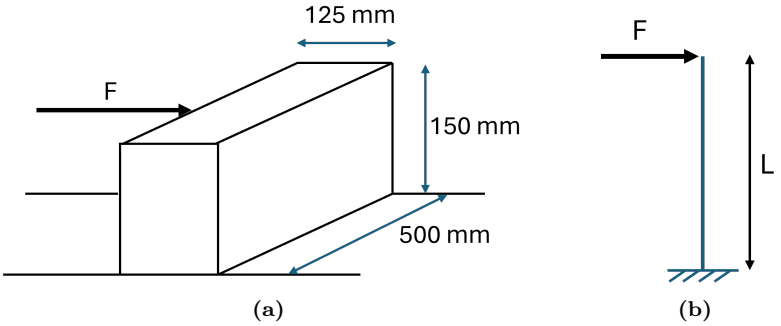

Figure 5.20: Schematization of the assumed protrusion.

Compared to the normal protrusion, the surface area of the rectangular shaped protrusion (125 x 500 mm) is a factor 2.44 smaller.

Some additional assumptions are made:

- The block does not move due to the collision.
- The stiffness of the system only consists of the bending stiffness of the protrusion.
- Only elastic deformation occurs.

The spring stiffness is deducted from the equation for the deflection (δ) of a cantilever:

$$\delta = \frac{FL^3}{3EI} \tag{5.3}$$

In which:
E = Young's modulus (38214 MPa for concrete class C55/67)
I = Moment of inertia ($= \frac{1}{12}bh^3$ for rectangular cross-section)
L = Length of the cantilever

The relation between force, spring stiffness and deflection is:

$$F = k * \delta \tag{5.4}$$

Combining 5.3 & 5.4 results in:

$$k = \frac{3EI}{L^3} \tag{5.5}$$

Filling in the equations results in:

$$k = \frac{3 * 38214 * \frac{1}{12} * 500 * 125^3}{150^3} = 2.76 * 10^6 \ N/mm$$

And

$$F = \sqrt{5716 * 0.197^2 * 2.76 * 10^9} = 7.82 * 10^5 \ N$$

The assumed failure mechanism is rupture. This could be caused by either shearing or bending.

Rupture due to shearing

The shear stress is calculated by dividing the force by the cross-sectional area:

$$\sigma_{shear} = \frac{F}{A} = \frac{7.82 * 10^5}{500 * 125} = 12.51 \ N/mm^2 \tag{5.6}$$

A unity check is performed to compare the stress to the strength of the concrete. The maximum shear stress in the concrete exceeds the strength with 49%.

$$u.c. : \frac{12.51}{8.42} = 1.49$$

Rupture due to bending

Rupture may also be caused by the bending moment. The maximum stresses induced by the bending moment can be calculated with:

$$\sigma_{max} = \frac{M}{W} \tag{5.7}$$

In which:
M = Bending moment
W = Moment of resistance ($= \frac{1}{6}bh^2$ for rectangular cross-section)

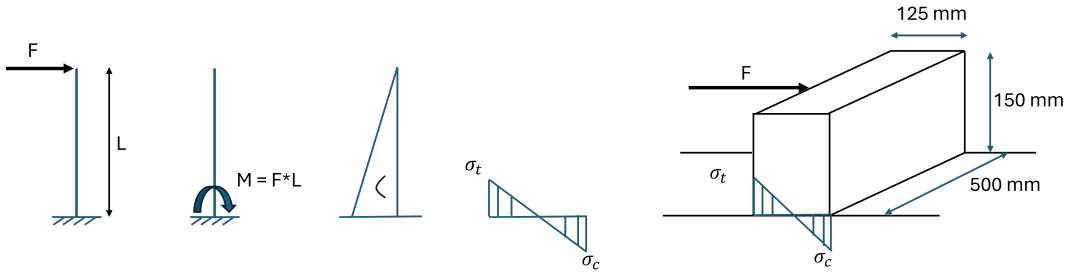

Figure 5.21: Stresses induced by the bending moment.

The maximum stress in the cross-section are:

$$\sigma_{max} = \frac{7.82 * 10^5 * 150}{\frac{1}{6} * 500 * 125^2} = 90.1 \ N/mm^2$$

A unity check is performed to compare the stress to the strength of the concrete. The maximum tensile stress in the concrete is much higher than the strength of the concrete.

$$u.c. : \frac{90.1}{8.42} = 10.7$$

6
Discussion

Conducting experiments is accompanied by uncertainties. The outcomes should therefore be properly interpreted. This chapter discusses various limitations and uncertainties of the study.

Physical model

In this research, a 1:20 scale model is used. The differences between the model and the prototype are discussed in this section.

Block weight

Stability is influenced by the weight of a block. A lighter block will move sooner than a heavier block, given an equal volume. There are deviations in the weight of the model blocks that were used for the experiments (Table 3.1). After removing the largest outliers, the standard deviation of the block weight is equal to 8.8 grams, corresponding to 1.3% of the mean block weight. This deviation is considered to be realistic, as the block have a certain weight deviation in reality as well.

Due to the pores in the concrete, water is able to penetrate the block and increase the weight. This results in a difference between the dry and the saturated weight. When a block is placed underwater, it can take up to 1 hour before it is fully saturated. During the first tests of each testing day, the blocks were put in the flume and might not have been fully saturated. However, wave conditions were gradually increased for each setup, meaning that at the start of each day the conditions were relatively mild. During the milder conditions, no movements were observed at all and the weight difference did not affect the results. It is expected that the effect is negligible, but if it did affect the results, it would lead to a conservative value.

Angle of repose

The model blocks and real ReefBlocks are not made of the same materials and therefore have different properties. To compare the difference in friction between the two, a test is conducted to determine the angle of repose of the model blocks. Two blocks are stacked on top of each other and tilted until the upper block starts sliding. Note that the block only slides a small distance until it bumps into the protrusions. The angle at which the block starts sliding represents the angle of repose (Figure 6.1). The test is repeated several times as the quality of the PLA printed blocks varies. This test was also performed with concrete blocks.

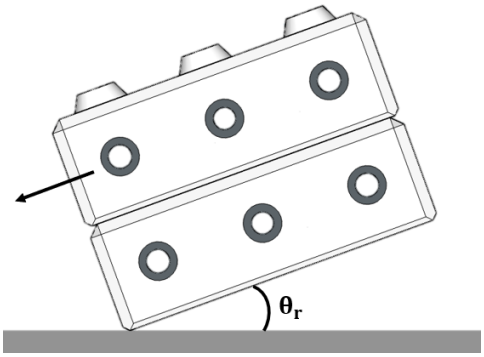

Figure 6.1: Angle of repose of the model blocks.

An average angle of roughly 20 degrees is found for the PLA blocks and 30 degrees for the concrete blocks (see Figure 6.2). The friction coefficient can be calculated by taking the tangent of this angle and results in values of 0.36 and 0.58 for the PLA and concrete blocks respectively. This is in line with Eurocode 2 (2004), which states that smooth concrete has a friction coefficient of 0.6. This indicates that the model is conservative for sliding movements, since the PLA model blocks start sliding for smaller horizontal force components than the concrete blocks would. The additional friction caused by natural deposits and marine growth has also not been taken into account.

(a) **(b)**

Figure 6.2: Maximum achievable angle of repose for PLA (a) and concrete (b) blocks.

Wave incidence

All waves were normal incident, attacking the structure in shore normal direction. In reality, the waves are obliquely incident as well, approaching the structure from different directions.

Obliquely incident waves can be decomposed into two components: a shore normal component and a perpendicular component. This perpendicular component might cause more sideways rocking movements on places with gaps between the blocks. The number of sliding movements will probably decrease for obliquely incident waves as the shore normal component of the waves, which corresponds to the sliding direction, is smaller when waves approach the structure under an angle.

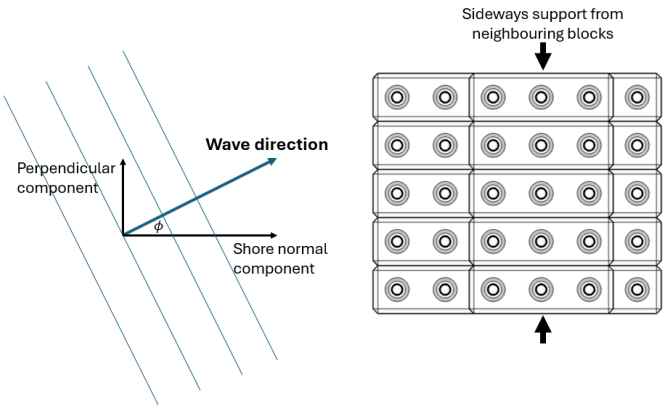

Figure 6.3: Top view of a 2 level simple form REB with obliquely incident waves.

Oblique waves may cause that the blocks do not fall back into their original position. This is especially relevant for the breakwater head, where the blocks are not supported by neighbouring blocks.

Underlayer thickness

The total structure height consists of the underlayer thickness and the height of the REB. With a thin underlayer, this total structure height is lower compared to a thick underlayer. For equal freeboard values, the maximum depth-limited waves that can reach the structure are lower for a smaller structure height than for a larger one (Figure 6.4). This implies that a thick underlayer can lead to more instabilities than a thin underlayer, as they have different crest levels. It also means that there is no critical freeboard for a particular configuration, this depends on the underlayer thickness as well.

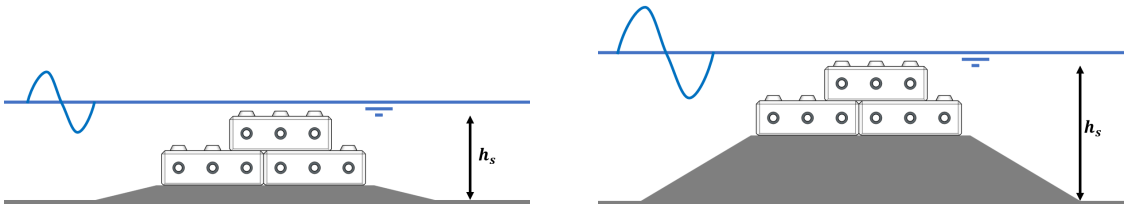

Figure 6.4: Difference in maximum depth limited wave height for thin (a) and thick (b) underlayers. Higher waves can reach the structure for a thicker underlayer.

In this research, the underlayer thickness of the scale model was 0.05 m and is equal to the height of a block. Therefore, the results of this research only hold for underlayers that extend up to 1 block height above the bed level. For designs with thicker underlayers, the stability behaviour is unknown.

Epifauna

It was tried to determine the influence of marine growth on the structure's stability by stuffing the holes, adding roughness and miniature corals. Consequently, there was an increase in sliding movements due to the increased drag. However, the true effect of epifauna on stability remains uncertain. Although the increased drag has a negative effect on the stability, there are other factors, such as increased weight, that positively affect the stability. Additionally, marine growth

can have a cementitious effect, bonding the blocks together. Moreover, the presence of epifauna might reduce the spaces between the holes and protrusions and hinder sliding movements.

When the ecological value of the REB were to be considered, the limit states might be more strict. There is a possibility that corals could break when the ReefBlocks themselves are still stable. However, this was not investigated during this study.

Test program

Due to time restrictions, the test program was limited. The number of wave conditions is sufficient to see trends, but leads to high uncertainties when quantifying the limit states. Also, it is plausible that the most critical scenario is not tested, as the step sizes of water level and wave height were over 2 cm. However, based on all observations and the damage levels, it is deemed unlikely that the structure at the main location will fail.

Mobility sensor

The mobility sensors have a sampling frequency of 100 Hz and the signal contains noise, leading to errors between the measured values and the exact values. This mainly applies to narrow peaks. The peaks of the acceleration, induced by the sliding collisions, only consists of a single data point (see Figure 4.8a). Therefore, the actual peak values might be higher and would underestimate the impact force. Instead, the acceleration of the moment before impact is integrated to obtain the impact velocity and use this value to calculate the impact force. The moment before impact contains about 10 data points and is therefore more reliable.

Nevertheless, using stand-alone motion sensors in breakwater experiments is a state-of-the-art method and can give more insight into the stability of breakwaters. In this research it was managed to measure movements and that is already a big achievement.

Processing errors

There is a relatively high uncertainty in the number of sliding movements. This is caused by the used counting method, which is sensitive for multiple consecutive movements. Also, the poor visibility, caused by blocked sight or by the waves could have resulted in an underestimation of the movements.

The Z&S method is based on linear wave theory, but the waves were non-linear (see Figure 5.1). Non-linear decomposition was performed for several tests and the differences between the obtained incident wave heights were minor ($<$1mm).

Sliding induced concrete stresses

For the determination of the structural performance of the protrusions, multiple conservative assumptions were made, resulting in stresses that exceed the concrete strength. It is likely that the tensile stresses are actually lower than the calculated values.

Based on the unity checks, it seems that the protrusions are more likely to fail due to bending than due to shearing, but that is not necessarily the case. The used method to calculate the

stresses is not valid for this model. The protrusions have a large thickness to height ratio and should therefore be treated as deep beams. Patel et al. (2014) investigated stress distributions in deep beams and found that, compared to regular beams, the bending stresses are lower and the shear stresses are higher.

According to the scaling rules, the material stiffness of the model should be 20 times smaller than that of the prototype. The Young's modulus of PLA is 9.3 times smaller than that of concrete. The model is therefore stiffer than it should be, leading to conservative impact forces.

In the used approach, only one side of the protrusion is considered and simplified as rectangular shape, while in reality the forces are handled by the entire protrusion. The circular shape of the actual protrusion can transfer the forces better, leading to more compressive and less tensile stresses. Also, the surface area of the cross-section is 2.44 times larger than for the rectangular shape, which decreases the shear stress significantly. Dividing the impact force by the surface area of the circular protrusion results in a shear stress that is lower than the concrete strength.

The stresses are calculated for the case of one single protrusion. In reality, a sliding block can be countered by at least two protrusions. If two protrusions are blocking the sliding block at exactly the same moment in time, the forces are then divided between the protrusions, resulting in lower stresses.

The calculated impact force is quite high because only the bending stiffness of the protrusion is taken into account. In reality, the sliding block would deform as well, leading to a lower combined stiffness as it can be schematized as two springs in series (Goud, 2020). Moreover, the obtained formula for the impact force (Equation 5.2) assumes no movement of the lower block. However, as a consequence of the impact, the lower block might start moving and transfers the energy partly into kinetic energy. This reduces the energy that is taken on by the protrusion and would give a lower impact force.

Another way to calculate the impact force is with the Newton's second law of motion, which states that the net force is equal to mass times acceleration. Even though the peak acceleration might be an underestimation of the actual value, it can give insight in the order of magnitude.

$$F = m * a = 5716 * 5 = 2.858 * 10^4 \ N \tag{6.1}$$

This force is about 27 times lower than the calculated force in Section 5.6. Even if the actual value of the peak acceleration were twice as high as measured by the sensor, then it would still result in maximum tensile stresses that are lower than the concrete strength. That would imply that the protrusion is strong enough to endure sliding impacts

The only considered failure mechanism is rupture. However, other failure mechanisms such as chipping and crushing are likely as well. Especially because the force acts as a point load.

7
Conclusions

This study aims to provide insight into the hydraulic stability of the Reef Enhancing Breakwater under wave loading. Four research questions are answered to achieve this.

1. What type of movements occur within the REB?

Both 2 and 3 layer configurations with simple and complex forms (Figures 3.11 & 3.12) have been tested on two different locations in the flume (Figures 3.4a & 3.4b). There are 5 main type of movements observed during the experiments in the wave flume.

Sliding: Translational movement in horizontal direction (Figure 5.2). The movement is possible due to the difference in diameters between the holes and protrusions. It is the most common type of movement, observed in all configurations, and happens mainly in the top layer. The maximum number of observed sliding events in one test was equal to 4 movements/block/1000 waves.

Rocking: Rotational back and forth movement in an arbitrary direction. The movement is often enabled by an imperfection in the underlayer, resulting in lack of support and the emergence of pivot points (Figure 5.4 & 5.5). Especially the 3 level simple form structure exhibited more rocking than the other configurations, caused by its lack of interconnected rows.

Shaking: Combination of rotating base blocks and translating top blocks (Figure 5.6). This movement was rare and only observed sporadically in the 2 level complex configuration.

Tilting: Rotational movement around a pivot point, such that the block does not return to its initial position (Figure 5.7). It can happen for both top block orientations. Tilting of a top block with the smart orientation (Figure 3.10) only happened at the alternative location (see Figure 3.4b), where the structure was exposed to plunging waves.

Lifting: Vertical translation of a block in combination with a horizontal displacement, such that the block ends up in a different location (Figure 5.8). This movement requires large wave impacts and was only observed at the alternative location, where plunging waves attacked the structure.

2. What are the limit states of the REB?

Three limit states are distinguished:

- Start of motion
- Start of damage
- Failure

The expected values and characteristic values of the limit states are presented in Tables 7.1 & 7.2. Damage is defined as a block that loses its interlocking with another block. Failure is defined to be reached for a damage level of $N_{od} = 0.4$.

	Start of motion ($N_{s,m}$)		Start of damage ($N_{s,d}$)	
Setup	**Expected value**	**Characteristic value**	**Expected value**	**Characteristic value**
2 level simple	0.54	0.4	-	-
2 level complex	0.59	0.51	-	-
3 level complex	0.53	0.39	-	-
2 level complex (Marine growth)	0.53	0.4	-	-
2 level simple (Rougher underlayer)	0.53	0.4	-	-
2 level complex (Rougher underlayer)	0.76	0.65	0.76	0.65

Table 7.1: Expected and characteristic values for the start of motion and start of damage limit state on the main location. A dash implies that this state was not reached.

	Start of damage ($N_{s,d}$)		Failure ($N_{s,f}$)	
Setup	**Expected value**	**Characteristic value**	**Expected value**	**Characteristic value**
2 level simple	1.03	0.94	1.04	0.94
2 level simple (improved toe)	1.03	0.94	1.17	1.11
2 level complex	1.03	0.94	1.11	0.94

Table 7.2: Expected and characteristic values for the start of damage and failure limit state on the alternative location.

This study shows contrasting outcomes between the main location on the flat foreshore and the alternative location close to the transition slope. On the flat foreshore, damage was only observed for the 2 level complex setup on the rougher underlayer. No failures were reached on this main location. This means that the 2 level simple, 2 level complex and 3 level complex form structures will be stable for bed slopes that do not allow for plunging waves, given that the protrusions do not fail and that the thickness of the underlayer does not exceed 1 block height. Conversely, on the alternative location close to the transition slope, plunging breakers led to significant damage and failure of the structure. This underscores the vulnerability of the REB when the conditions are such that plunging waves can emerge. So, it is crucial to check for the potential of plunging waves, as it results in critical differences.

3. How do hydraulic and structural variables influence the number of sliding movements within the structure?

Sliding was the most common type of movement and was further analysed by quantifying the movements and comparing with hydraulic and structural variables.

Wave height

An increase in the wave height leads to an increase in sliding movements. However, it should be noted that the wave height is often limited by the depth. Most sliding movements happen for $H_{m0}/\Delta D_n > 0.8$ (Figure 5.12).

Relative freeboard

The relation between the relative freeboard and the number of sliding movements is depicted in Figure 5.13. The main trend is that for higher values of the freeboard, the water depth limits the waves such that no instabilities can occur. For decreasing values of the freeboard, the number of sliding movements increases. When the freeboard decreases even further, such that $R_c/H_{m0} < -1$, the structure becomes too submerged for sliding movements to occur (Figure 5.14).

Wave steepness

Within the tested range, which is about 2% - 4%, a lower wave steepness (s_p) leads to more sliding movements as longer waves contain more energy when the wave heights are equal.

Configuration

The 2 level structures are more stable than the 3 level structures, because of the difference in structure height. For a 2 level REB, the simple form is more stable than the complex form due to its compactness.

Underlayer irregularity

Two underlayers with different bed irregularities ($\pm$ 1.5 D_{n50} & $\pm$ 2 D_{n50}) are tested. The rougher underlayer, resulted in more sliding movements for the 2 level complex form configuration. For the 2 level simple form configuration, there was no significant difference in sliding movements between the two underlayers.

Marine growth

Mimicking epifauna on the blocks by stuffing the holes and adding roughness and miniature corals, resulted in more sliding movements due to the increased drag. However, things like additional weight and the cementitious effect were not considered.

4. Can the sliding induced stresses lead to rupture of a protrusion?

The maximum shear and bending induced stresses in the protrusion, caused by a sliding impact, were estimated. It appears that the shear stress exceeds the concrete strength by a factor 1.49 and the bending induced stress exceeds the concrete strength by a factor 10.7. However, it is questionable to what extent this approach is representative for the actual protrusion, as multiple conservative assumptions were made. Another method was listed, which uses an underestimation of the acceleration and resulted in concrete stresses below the critical rupture limit. Whether the protrusions can withstand the sliding impact remains uncertain and requires additional research that also looks at other failure mechanisms than rupture.

8
Recommendations

Based on the limitations and uncertainties of this study, recommendations for further research and for the design of the REB are made and presented in this final chapter.

Research

There is room for improvement in the physical model setup. Using concrete model blocks instead of PLA will give a more accurate representation of the sliding movements. Testing more configurations allows investigating a wider range of structural variables. Also, the influence of the underlayer thickness, which influence the crest height of the structure, should be investigated by making it a variable. Using more conditions and smaller step sizes in the test program will increase both the accuracy and the precision of the results. Also, the effect of oblique incident waves should be investigated. If more mobility sensors are used, the quantity of various movements can be determined much more accurately. Finding a relation between wave transmission and damage level is necessary to improve the understanding of what failure is. Since the options with physical model tests are endless and the tests are time-consuming, it is hard to achieve accurate results in a relatively short time that apply to all possibilities. Ideally, a physical model validation for a proposed design is conducted prior to the project, using the site specific conditions.

Assessing the structural performance of the ReefBlock requires additional research. Combinations of different failure mechanisms and impacts should be considered and the focus should not solely be on the extreme events. A computer model with the finite element method can be used to determine the stresses in the block more accurately. Eventually, the obtained values and their deviations should be integrated into a probabilistic model. With that information it can be determined whether the structural performance might be a limiting factor for the stability of the REB.

Design

During the design and installation phase of the REB, there are some important points of interest regarding the stability. It starts with a proper site investigation. It is important to check whether plunging waves can emerge, as these can cause significantly more damage. Furthermore, it must be ensured that the blocks are placed accurately, such that they interlock. The tests have shown the importance of the interlocking feature. It is recommended that the blocks in the top layer have the smart orientation. This orientation prevents them from tilting and gives sideways support in the case of obliquely incident waves. The outer ends of the structure do not have this sideways support and asks for a special design. Based on stability, it is recommended to use the simple form for a 2 level REB and the complex form for a 3 level REB.

During the experiments, sliding was the most common type of movement. Sliding can be prevented by eliminating the interlocking tolerance. However, this difference between the diameters of the protrusion and the hole of the block is desirable due to placement considerations. Therefore, this problem should be tackled just after the installation. It could be an option to fill the spaces between the blocks with material such as concrete. The material can be placed by inserting a pipe through the upper tubes (Figure 8.1). The feasibility of this technique should be further investigated.

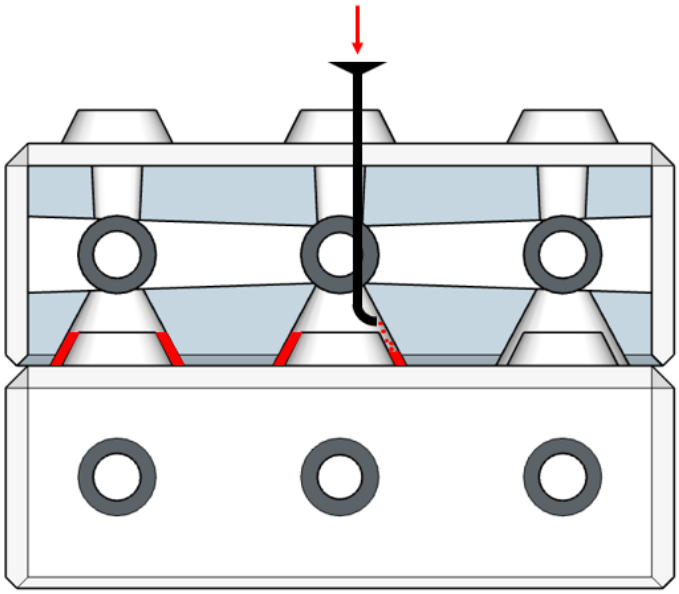

Figure 8.1: Fill the space between the protrusions and holes with material.

References

Ahrens, J. P. (1987). *Characteristics of reef breakwaters* (tech. rep.). Coastal Engineering Research Center, US Army Corps of Engineers.

Ahrens, J. P., & Cox, J. (1990). *Rational Design of Mound Structures* (tech. rep. No. 7). https://about.jstor.org/terms

Ahrens, J. P., & Member, A. (1989). *Stability of reef breakwaters* (tech. rep.).

Baine, M. (2001). *Artificial reefs: a review of their design, application, management and performance* (tech. rep.).

Battjes, J. A. (1974). SURF SIMILARITY. *Coastal Engineering Proceedings*, *1*(14), 26. https://doi.org/10.9753/icce.v14.26

Bosboom, J., & Stive, M. J. F. (2022). *Coastal Dynamics*. TU Delft Open.

Burcharth, H. (1997). Reliability-Based Design of Coastal Structures.

Burgess, C. P. (2021). *Stability of Low Crested and Submerged Breakwaters: A Stability of Low Crested and Submerged Breakwaters: A Reanalysis and Model Development Reanalysis and Model Development* (Doctoral dissertation). https://doi.org/10.25777/d7g8-c212

Caldera, H. P. G. M. (2019). *Rocking of Single Layer Armour Units Rocking Revisited III* (tech. rep.). Delft University of Technology. https://repository.tudelft.nl/

Camenen, B., & Larson, M. (2007). Predictive Formulas for Breaker Depth Index and Breaker Type. *2007*(234), 1028–1041. https://doi.org/10.2112/05-0566.1

CUR. (1989). *Golfbrekers. Sterkte Betonnen Afdekelementen.* (tech. rep.). Integratie van Fasen 1-3. Verslag werkgroep 1. Civiel Centrum Uitvoering Research en Regelgeving. In Dutch.

Deltares. (n.d.). Scaling and Measurements.

Douglas, A. E. (2003). *Coral bleaching-how and why?* (Tech. rep.). https://doi.org/10.1016/S0025-326X(03)00037-7

Dronen, N. (2018). How technology is helping professionals manage coastal erosion successfully.

Dwito Armono, H. (2016). *Artificial Reefs as Shoreline Protection Structures* (tech. rep.).

Eurocode 2. (2004). *EN 1992-1-1: Eurocode 2: Design of concrete structures - Part 1-1: General rules and rules for buildings* (tech. rep.).

EurOtop. (2018). Manual on wave overtopping of sea defences and related structures (J. W. van der Meer, N. W. H. Allsop, T. Bruce, J. de Rouck, A. Kortenhaus, T. Pullen, H. Schüttrumpf, P. Troch, & B. Zanuttigh, Eds.). www.overtopping-manual.com

Ferrario, F., Beck, M. W., Storlazzi, C. D., Micheli, F., Shepard, C. C., & Airoldi, L. (2014). The effectiveness of coral reefs for coastal hazard risk reduction and adaptation. *Nature Communications*. https://doi.org/10.1038/ncomms4794

Firth, L. B., Mieszkowska, N., Thompson, R. C., & Hawkins, S. J. (2013). Climate change and adaptational impacts in coastal systems: the case of sea defences. https://doi.org/10.1039/c3em00313b

Goud, T. (2020). *Rocking revisited 4 Analysis of rocking-induced stresses for concrete breakwater armour units* (tech. rep.). Delft University of Technology. https://repository.tudelft.nl/

Greshko, M. (2018). Window to Save World's Coral Reefs Closing Rapidly.

Heller, V. (2011). Scale effects in physical hydraulic engineering models. *Journal of Hydraulic Research*, *49*(3), 293–306. https://doi.org/10.1080/00221686.2011.578914

Hofland, B., Antonini, A., Houtzager, D., Caldera, G., Van Gent, M., Bakker, P., & Van Der Lem, C. (2023). Rocking of single layer armour units measured by embedded sensors. *Journal of Coastal and Hydraulic Structures*, *3*, 28. https://doi.org/10.59490/jchs.2023.0028

Hofland, B., Arefin, S. S., Van Der Lem, C., & Van Gent, M. R. A. (2018). Smart Rocking Armour Units. *In Proceedings of the 7th International Conference on the Application of Physical Modelling in Coastal and Port Engineering and Science (Coastlab18): Santander, Spain, May 22-26, 2018*.

Holthuijsen, L. (2007). *Waves in Oceanic and Coastal Waters*. Cambridge University Press.

Houtzager, D. (2020). *Experimental investigation of the spatial and temporal variation of rocking armour units Rocking revisited V* (tech. rep.). Delft University of Technology. https://repository.tudelft.nl/

Houtzager, D., Hofland, B., Caldera, G., van der Lem, C., van Gent, M. R. A., Bakker, P., & Antonini, A. (2023). Embedded rocking measurement of single layer armour units: Development and first results. *Procedings ICE Breakwaters conference 25-27 April 2023, Portsmouth*. https://repository.tudelft.nl/islandora/object/uuid%3A88317cb3-aa42-4bce-9bd3-c9e1b3d3f8d7

Hughes, S. (1993). *Physical Models and Laboratory Techniques in Coastal Engineering* (Vol. 7). World Scientific Publishing Co. Pte. Ltd.

IPCC. (2021). *Climate Change 2021: The Physical Science Basis. Contribution of Working Group I to the Sixth Assessment Report of the Intergovernmental Panel on Climate Change* (tech. rep.). IPCC.

Islam, M., Jahra, F., & Hiscock, S. (2016). Data analysis methodologies for hydrodynamic experiments in waves. *Journal of Naval Architecture and Marine Engineering*, *13*(1), 1–15. https://doi.org/10.3329/jname.v13i1.25347

Kadoglou, K. (2023). *Numerical modeling of wave transmission over a living breakwater* (tech. rep.). Delft University of Technology. https://repository.tudelft.nl/

Knowlton, N., Brainard, R. E., Fisher, R., Moews, M., Plaisance, L., & Caley, M. J. (2010). Coral Reef Biodiversity, Chapter 4.

Le Mehaute, B. (1976). An introduction to hydrodynamics and water waves. https://doi.org/10.1007/978-3-642-85567-2/COVER

Lobo, P. (2020). The impending destruction of the great barrier reef.

Mazzaretto, O. M., Menéndez, M., & Lobeto, H. (2022). A global evaluation of the JONSWAP spectra suitability on coastal areas. *Ocean Engineering*, *266*, 112756. https://doi.org/10.1016/J.OCEANENG.2022.112756

Mohamad, M. E., Ibrahim, I. S., Abdullah, R., Abd Rahman, A. B., Kueh, A. B. H., & Usman, J. (2014). Friction and cohesion coefficients of composite concrete-to-concrete bond. https://doi.org/10.1016/j.cemconcomp.2014.10.003

Molenkamp, A. (2022). *Hydraulic performance of CoastaLock armour units* (tech. rep.). Delft University of Technology. https://repository.tudelft.nl/

Na'Im, I. I., Shahrizal, A. R. M., & Safari, M. D. (2018). A Short Review of Submerged Breakwaters. *MATEC Web of Conferences*, *203*, 01005. https://doi.org/10.1051/MATECCONF/201820301005

Neumann, B., Vafeidis, A. T., Zimmermann, J., & Nicholls, R. J. (2015). Future Coastal Population Growth and Exposure to Sea-Level Rise and Coastal Flooding - A Global Assessment. https://doi.org/10.1371/journal.pone.0118571

Patel, R., Dubey, S. K., & Pathak, K. K. (2014). Effect of depth span ratio on the behaviour of beams. *International Journal of Advanced Structural Engineering*, *6*(2). https://doi.org/10.1007/S40091-014-0056-3

Perry, C. T., Smithers, S. G., Gulliver, P., & Browne, N. K. (2012). *Evidence of very rapid reef accretion and reef growth under high turbidity and terrigenous sedimentation* (tech. rep. No. 8). GeoScienceWorld. https://doi.org/10.1130/G33261.1

Pörtner, H.-O., Roberts, D., Tignor, M., Poloczanska, E., Mintenbeck, K., Alegría, A., Craig, M., Langsdorf, S., Löschke, S., Möller, V., Okem, A., & Rama, B. (2022). *Climate Change 2022: Impacts, Adaptation, and Vulnerability. Contribution of Working Group II to the Sixth Assessment Report of the Intergovernmental Panel on Climate Change* (tech. rep.). IPCC.

Rock Manual. (2007). *The Rock Manual. Use of rock in hydraulic engineering.* C683, CIRIA, London. https://www.researchgate.net/publication/295855125_CIRIA_CUR_CETMEF_2007_The_Rock_Manual_The_use_of_rock_in_hydraulic_engineering_2nd_edition_C683_CIRIA_London_ISBN_978-0-86017-683-1

Saengsupavanich, C., Helmy Ariffin, E., Yun, L. S., & Pereira, D. A. (2022). Environmental impact of submerged and emerged breakwaters. https://doi.org/10.1016/j.heliyon.2022.e12626

Schiereck, G. (2019). *Introduction to bed, bank and shore protection* (H. Verhagen, Ed.; 2nd). Delft Academic Press / VSSD.

Shirlal, K. G., Rao, S., & Ganesh, V. (2004). *Stability of breakwater defenced by a seaward submerged reef* (tech. rep.). https://doi.org/10.1016/j.oceaneng.2004.11.017

Small, C., & Nicholls, R. J. (2003). *A Global Analysis of Human Settlement in Coastal Zones* (tech. rep. No. 3).

Speth, F. (2023). *Physical Modeling of 3D-Printed Artificial Reefs with Complex Shapes in the Wave Flume* (tech. rep.). Delft University of Technology. https://repository.tudelft.nl/

Sylvan, J. (2006). Sustainable Development Law & Policy How to Protect A Coral Reef: The Public Trust Doctrine and the Law of the Sea Recommended Citation. http://digitalcommons.wcl.american.edu/sdlp

Taveira-Pinto, F. (2005). *Analysis of submerged breakwaters stability design* (tech. rep.). www.witpress.com,

Thierry, J.-M. (1988). *Artificial Reefs in Japan-A General Outline* (tech. rep.).

Toth, L. T., Storlazzi, C. D., Kuffner, I. B., Quataert, E., Reyns, J., McCall, R., Stathakopoulos, A., Hillis-Starr, Z., Holloway, N. H., Ewen, K. A., Pollock, C. G., Code, T., & Aronson, R. B. (2023). The potential for coral reef restoration to mitigate coastal flooding as sea levels rise. *Nature communications*, *14*(1), 2313. https://doi.org/10.1038/s41467-023-37858-2

Tschirky, P., Brashear, P., Sella, I., & Manson, T. (2018). Living breakwaters: designing for resiliency. *Coastal Engineering Proceedings*, *1*(36), risk.50. https://doi.org/10.9753/icce.v36.risk.50

UNEP & WWF. (2003). *Fourteen Multilateral Environmental Agreements, Programmes, Partnerships and Networks Relevant to the Protection and Conservation of Coral Reefs, and the World Summit on Sustainable Development Plan of Implementation* (tech. rep.).

USACE. (2002). *Coastal Engineering Manual - Part VI* (tech. rep.).

Van den Bos, J. P., & Verhagen, H. J. (2018). *Breakwater design Lecture notes CIE5308* (tech. rep.).

Van den Brekel, E. R. I. (2021). *Hydrodynamic and ecological performance of a new modular unit for living breakwaters Wave flume experiments and results* (tech. rep.). Delft University of Technology. http://repository.tudelft.nl/.

Van der Meer, J. (1988). *Deterministic and Probabilistic Design of Breakwater Armor Layers* (tech. rep.).

Van der Meer, J., & Daemen, I. (1994). *Stability- and wave transmission at low-crested rubble-mound structures* (tech. rep.).

Van der Meer, J., & Pilarczyk, K. (1990). *Stability of low-crested and reef breakwaters* (tech. rep.).

Van der Meer, J., Tutuarima, W., & Burger, G. (1996). Influence of rock shape and grading on stability of low-crested structures.

Van Gent, M. R. A., Buis, L., Van den Bos, J. P., & Wüthrich, D. (2023). Wave transmission at submerged coastal structures and artificial reefs. *Coastal Engineering*, 104344. https://doi.org/10.1016/j.coastaleng.2023.104344

Verhagen, H. J., & d'Angremond, K. (2009). *Breakwaters and closure dams* (2nd).

Vidal, C., Losada, M. A., Medina, R., Mansard, E. P., & Gomez-Pina, G. (1992). A Universal Analysis for the Stability of Both Low-Crested and Submerged Breakwaters. *Proceedings of the Coastal Engineering Conference*. https://doi.org/10.1061/9780872629332.127

Vidal, C., Losada, M. A., & Mansard, E. P. D. (1995). Stability of Low-Crested Rubble-Mound Breakwater Heads. *Journal of Waterway, Port, Coastal, and Ocean Engineering*, *121*(2), 114–122. https://doi.org/10.1061/(ASCE)0733-950X(1995)121:2(114)

Vittal Hegde, A. (2010). *Coastal erosion and mitigation methods-Global state of art* (tech. rep. No. 4). National Institute of Technology Karnataka.

Wolters, G., Van Gent, M., Allsop, W., Hamm, L., & Mühlestein, D. (2010). HYDRALAB III: Guidelines for physical model testing of rubble mound breakwaters. *Coasts, Marine Structures and Breakwaters: Adapting to Change - Proceedings of the 9th International Conference*, *2*, 659–670. https://doi.org/10.1680/cmsb.41318.0062

Yalin, M. (1971). *Theory of Hydraulic Models* (tech. rep.).

Zelt, J. A., & Skjelbreia, J. E. (1992). Estimating incident and reflected wave fields using an arbitrary number of wave gauges. *Coastal Engineering Proceedings*, *1*(23). https://doi.org/10.9753/icce.v23.{\%}p

List of Figures

List of Tables

Appendix A: Block production

For the experiments, a total of 120 blocks were made. The block production starts with plastic moulds that are 3D printed from PLA. The mould contains an opening on one of its two ends through which a concrete mixture can be poured.

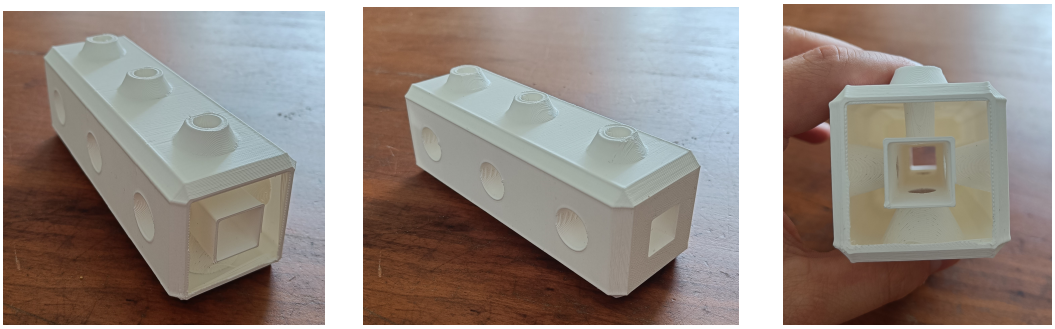

(a) Side with opening. **(b)** Side without opening. **(c)** Opening.

Figure 2: 3D printed mould.

The objective density of the blocks is 2340 kg/m3. However, the density of the PLA is only 1240 kg/m3 and that of the used concrete mix is about 2100 kg/m3. This means that additional ballast material is needed to obtain the desired density. Therefore, steel flakes (ponsdoppen) are added to increase the density of the mixture.

Figure 3: Steel flakes.

A suitable ratio between concrete mix, water and steel was found that resulted in a good workable mixture with the right density. The three components are combined into a concrete tub and properly mixed using a hand drill with mixing rod.

(a) Hand drill with mixing rod.

(b) Mixture in concrete tub.

Figure 4: Concrete mixing.

To make the pouring process easier, a special funnel was designed that properly fits onto the blocks. This funnel is made from 3D printed PLA as well. There was hardly any spillage and the speed of the process increased significantly. During and after the pouring, the blocks were gently vibrated to get all the air out and fill the moulds completely with the mixture.

(a) Without funnel.

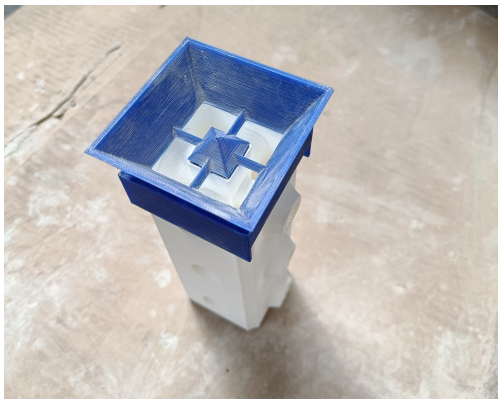

(b) With funnel.

Figure 5: Funnel to simplify filling process.

After being filled, the blocks must dry for at least one day. After that, the blocks are weighed.

(a) Drying of the blocks. **(b)** Weighing of the blocks.

Figure 6: Post-processing of the blocks.

As the concrete dries further over the days, the weight of the blocks decreases a bit. And when the blocks are placed in the water, they get heavier again. Therefore, the blocks had to be weighed again after the tests.

Appendix B: Sensor block production

The mobility sensor consists of 3 ultra-compact Arduino compatible boards:

- Processor board with integrated micro-USB port
- 9-Axis inertial measurement unit board
- Micro SD board

The boards can be connected by stacking them together. The size of the stack is about 20x20x15 mm. The boards are powered by a lithium-ion polymer battery (3.7V, 150mAh). A micro SD card 32GB type V30 is placed in the micro SD board.

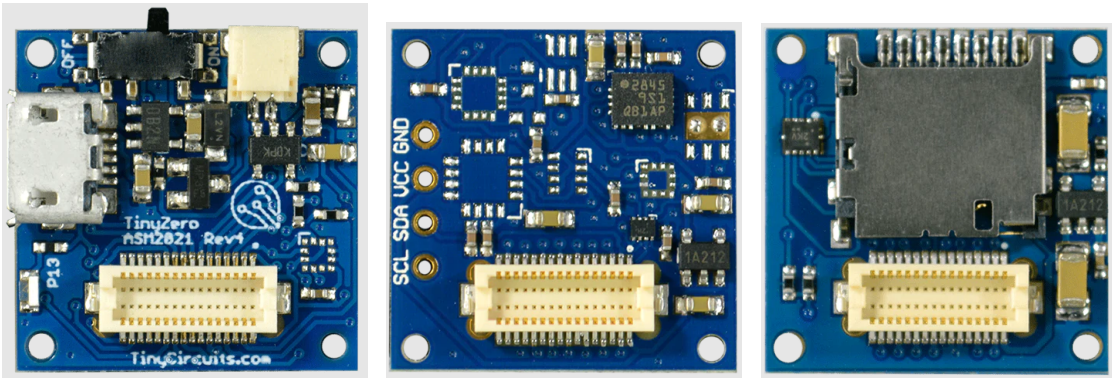

(a) Tinyzero processor board (ASM2021-R).

(b) 9-axis IMU tinyshield (ASD2511-R-N).

(c) MicroSD shield (ASD2201-R).

Figure 7: 3 modular component boards of the mobility sensor.

Because the sensor is used in the water, it had to be made waterproof. An electric circuit was designed, in which the sensor is soldered to a waterproof micro-USB connector. Reed switches were integrated so the power and the USB connections could be controlled with magnets. A reed switch opens or closes when a magnet is hold near it. The switches are placed such that magnets are only required for connecting it to a laptop or to recharge the battery, but not during a test.

(a) Micro-USB plug.

(b) Waterproof micro-USB connector.

(c) Reed switches.

Figure 8: Used electronic parts.

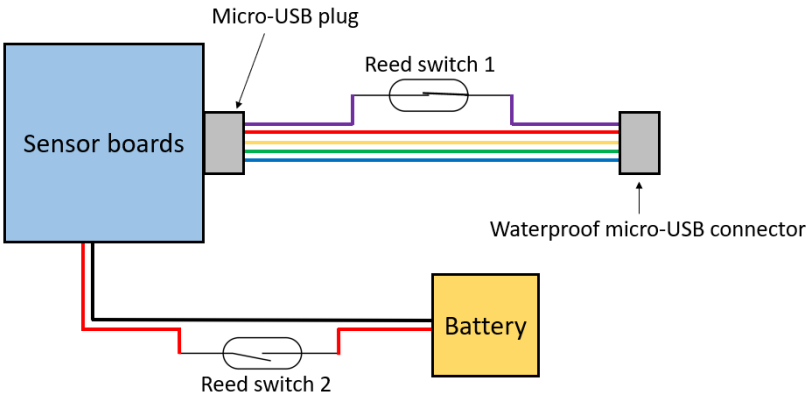

Figure 9: Electric circuit of the mobility sensor.

When all the components are soldered together, the entire circuit was placed into a 3D printed compartment. This compartment has one hole in it, intended for the waterproof micro-USB connector. The two reed switches are positioned away from one another and directly against the wall. In this way the switches can be controlled individually. Finally, the entire compartment was filled with non-conductive epoxy. 'Wilsor Polyurethaan giethars 500ml' was used for this.

(a) Internal structure of the sensor compartment. **(b)** Filling compartment with epoxy.

Figure 10: Sensor compartment.

A special ReefBlock was designed, into which the sensor compartment can be placed. After combining the two parts, it matches the shape of a standard ReefBlock. To give this sensor block also the same weight as the standard ReefBlocks, some extra steel flakes were added to the concrete mixture. The compartment clamps itself into the block, which makes it easy to take it out again.

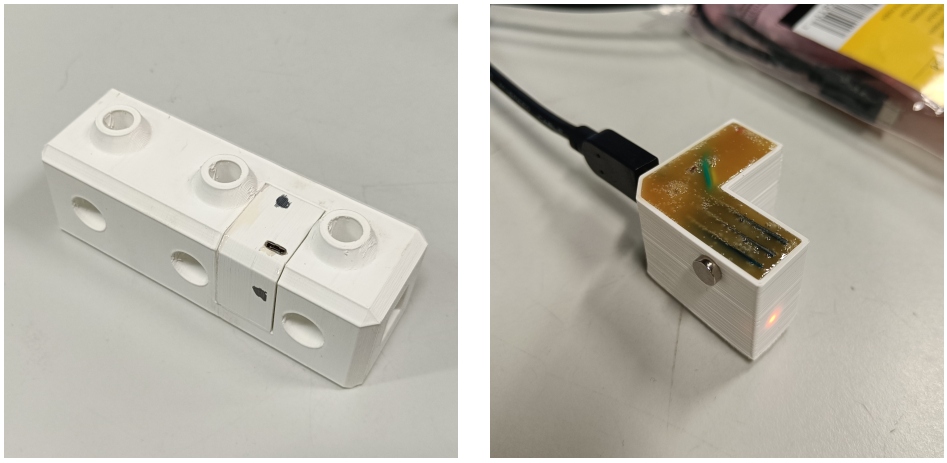

(a) Compartment placed into special ReefBlock. **(b)** Sensor compartment wired to laptop.

Figure 11: ReefBlock including sensor compartment. The locations of the reed switches are marked with black dots. The orange light means that the battery is charging

For convenience, black dots are added to locations where the magnets should be placed to turn the switch on or off.

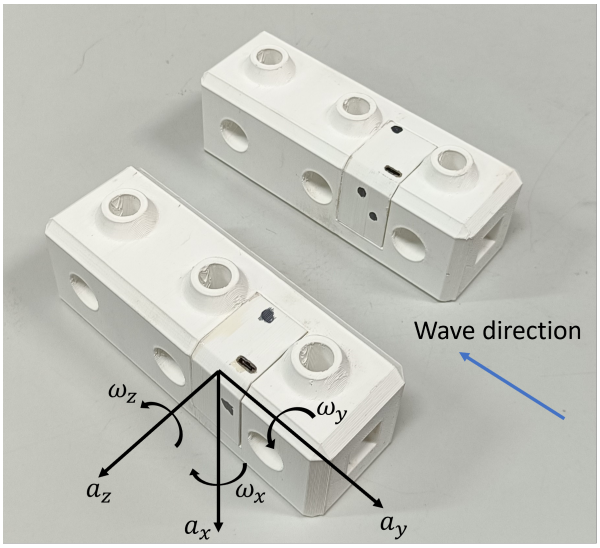

Figure 12: Directions of the accelerations and angular velocity.

Appendix C: Overview all setups

Setup 1

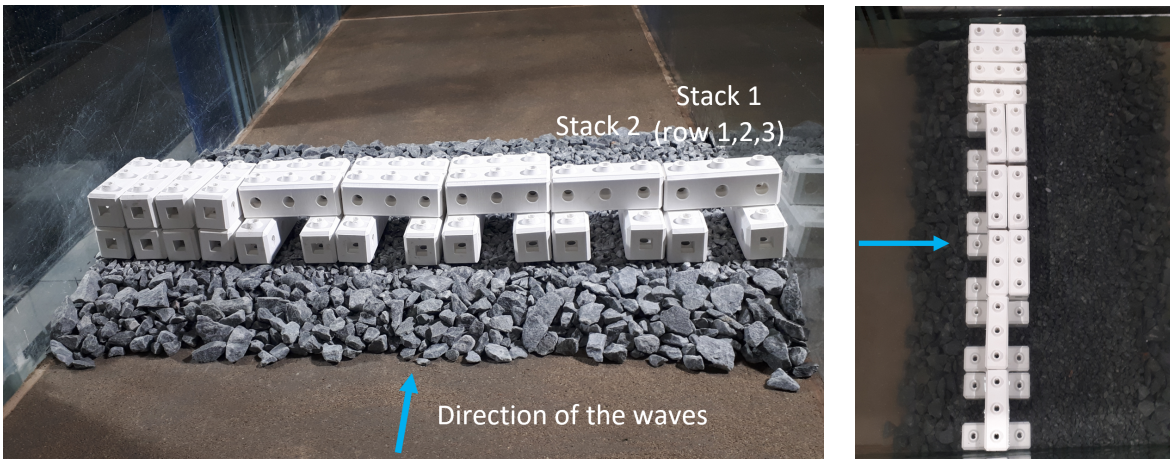

(a) (b)

Figure 13: Setup 1.

Setup 2

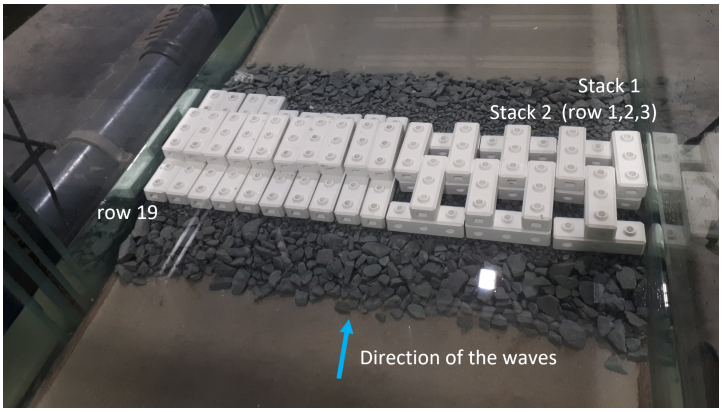

Figure 14: Setup 2.

Setup 3

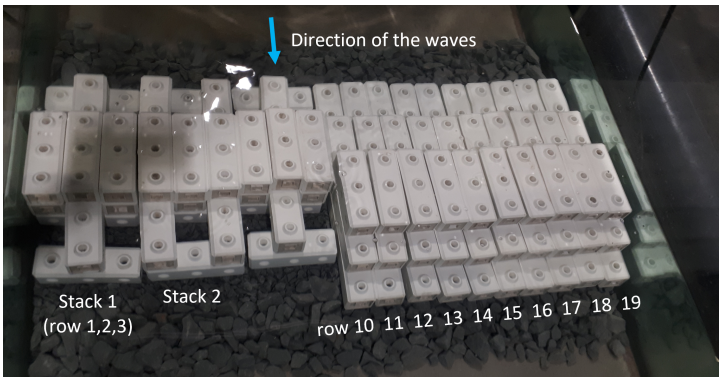

Figure 15: Setup 3.

Setup 4

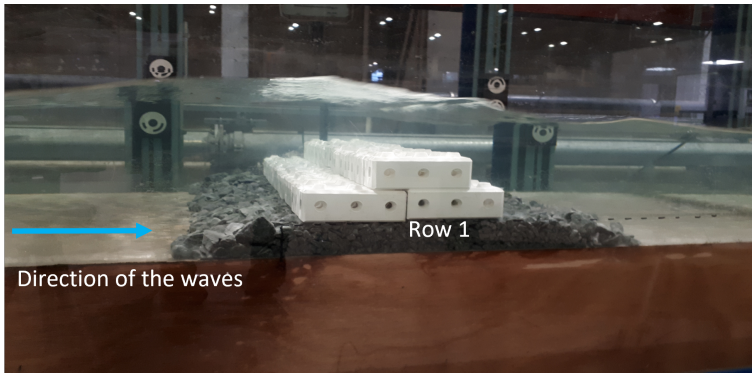

(a)

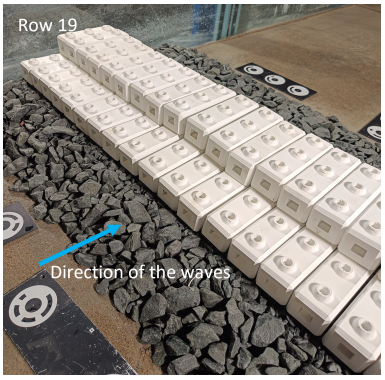

(b)

Figure 16: Setup 4.

Setup 5

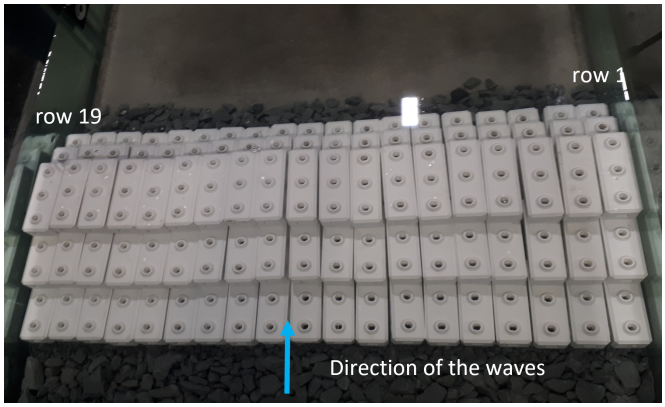

(a)

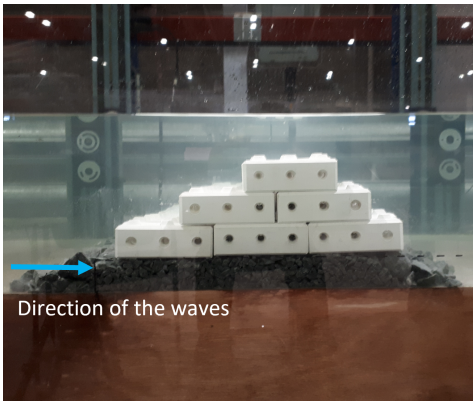

(b)

Figure 17: Setup 5.

Setup 6

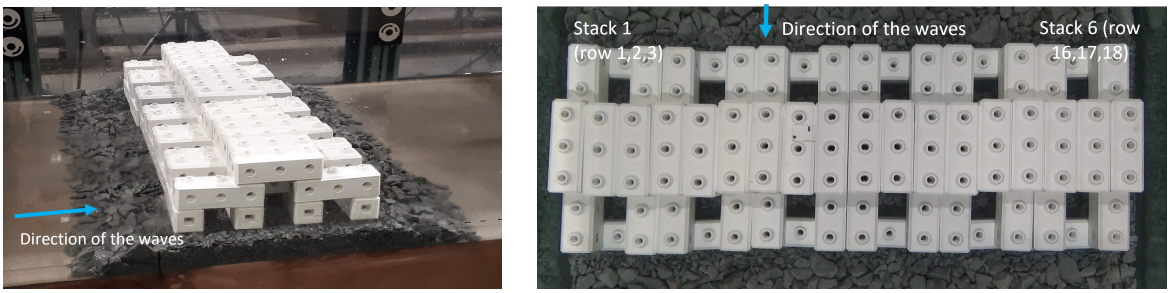

(a) **(b)**

Figure 18: Setup 6.

Setup 7

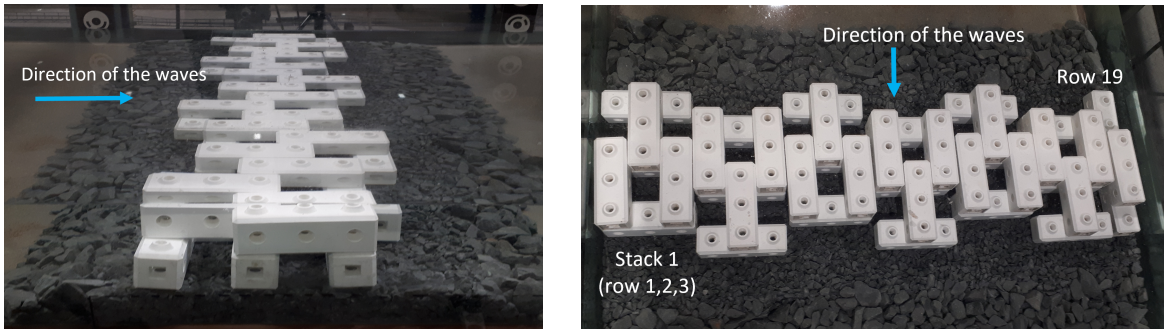

(a) **(b)**

Figure 19: Setup 7.

Setup 8

(a) **(b)**

Figure 20: Setup 8.

Setup 9

(a) **(b)**

Figure 21: Setup 9.

Setup 10

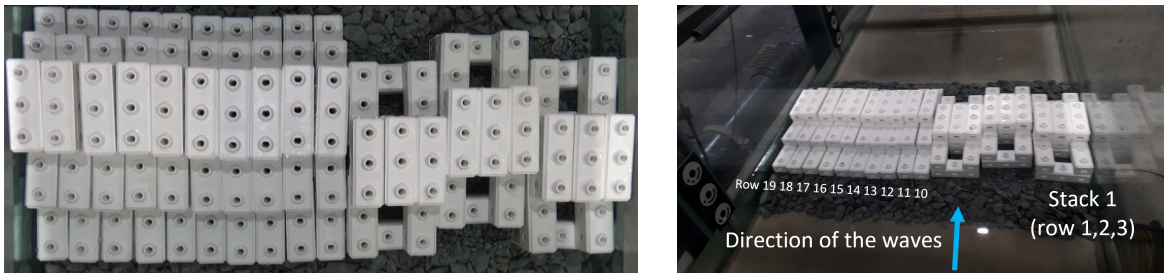

(a) **(b)**

Figure 22: Setup 10.

Setup 12

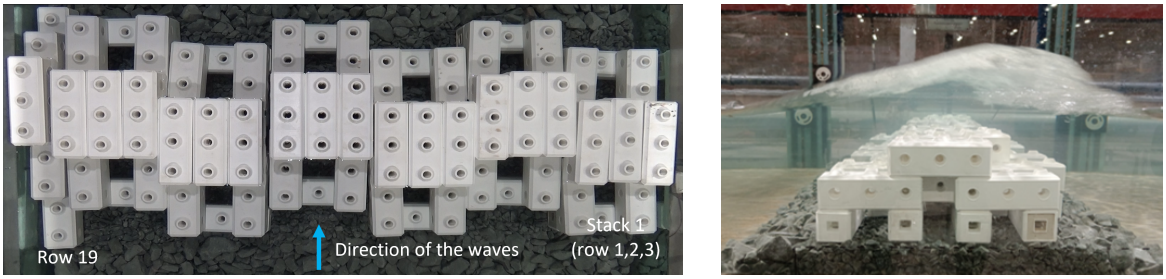

(a) **(b)**

Figure 23: Setup 12.

Setup 13

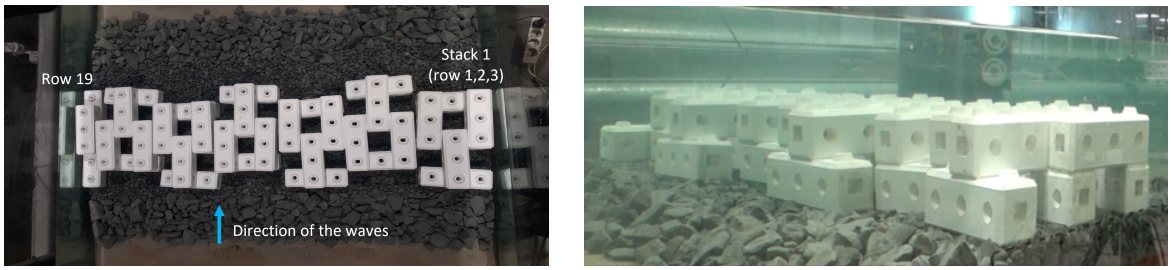

(a) **(b)**

Figure 24: Setup 13.

Setup 14

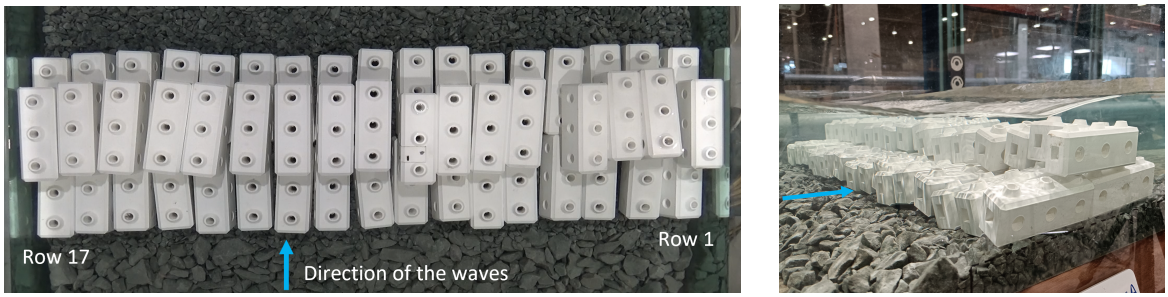

(a) **(b)**

Figure 25: Setup 14.

Setup 15

(a) **(b)**

Figure 26: Setup 15.

Setup 16

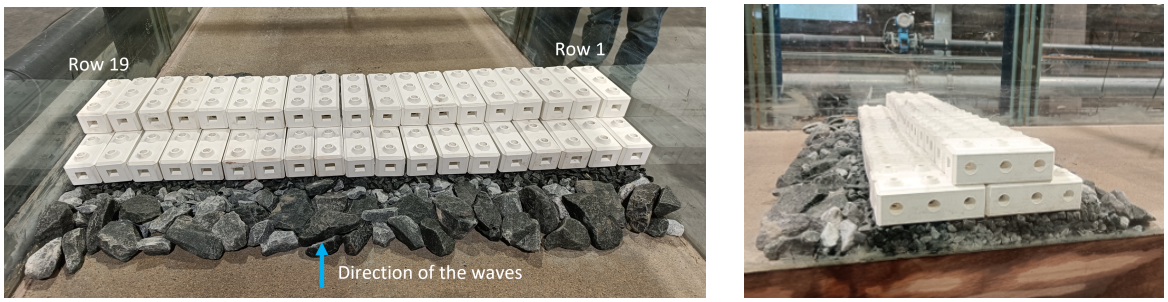

(a) **(b)**

Figure 27: Setup 16.

Setup 17

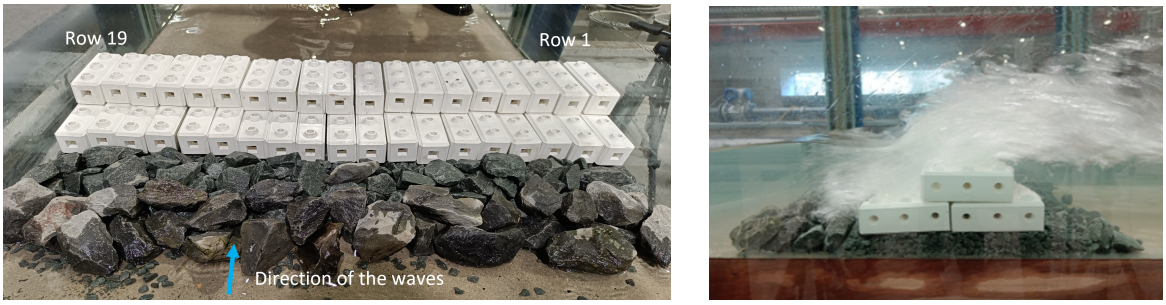

(a) **(b)**

Figure 28: Setup 17.

Setup 18

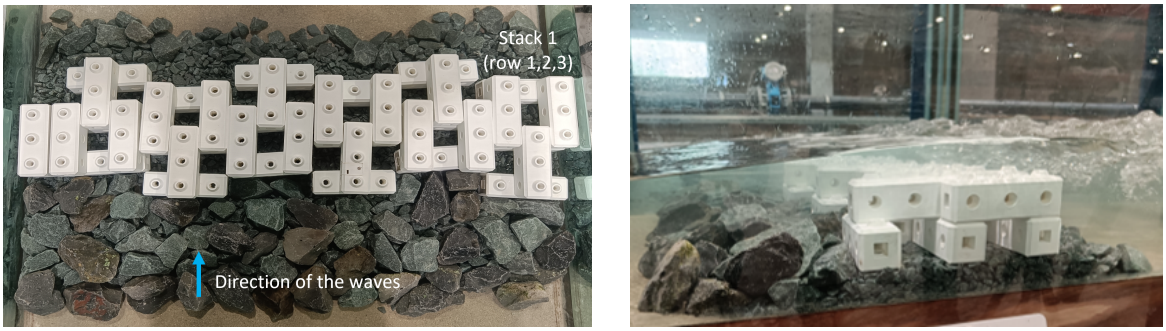

(a) **(b)**

Figure 29: Setup 18.